

**UNCLASSIFIED**

CENTRAL RESEARCH LIBRARY  
DOCUMENT COLLECTION

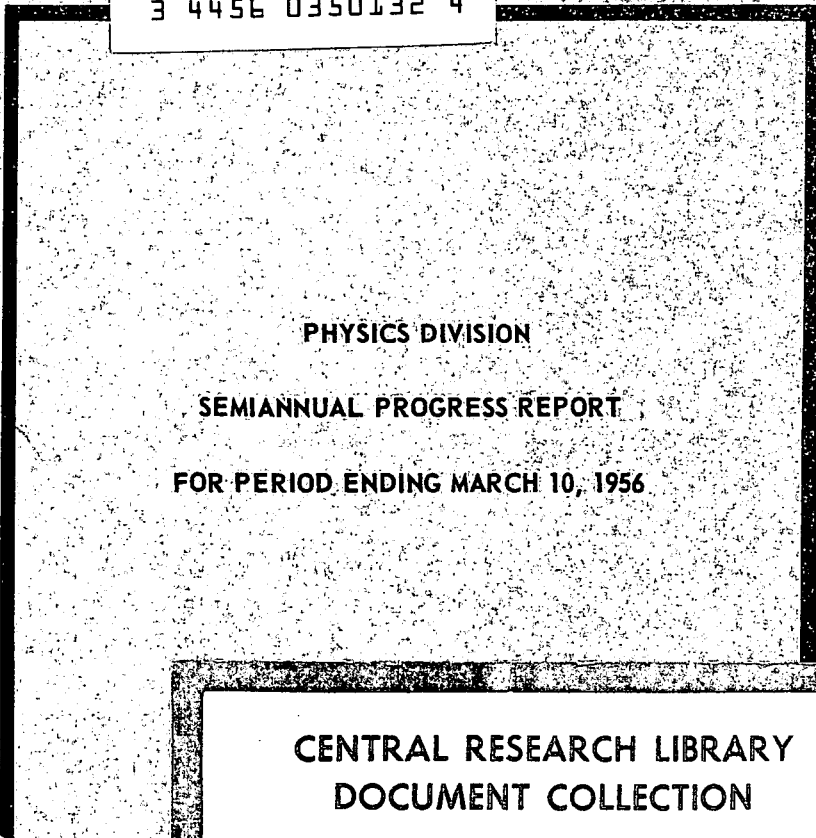
MARTIN MARIETTA ENERGY SYSTEMS LIBRARIES



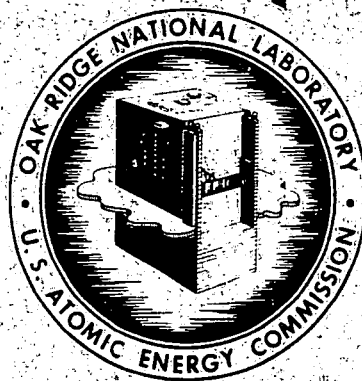
3 4456 0350132 4

ORNL-2076  
Progress

*cy. 5*



PHYSICS DIVISION  
SEMIANNUAL PROGRESS REPORT  
FOR PERIOD ENDING MARCH 10, 1956



CENTRAL RESEARCH LIBRARY  
DOCUMENT COLLECTION

**LIBRARY LOAN COPY**

DO NOT TRANSFER TO ANOTHER PERSON

If you wish someone else to see this document,  
send in name with document and the library will  
arrange a loan.

**OAK RIDGE NATIONAL LABORATORY**  
OPERATED BY  
**UNION CARBIDE NUCLEAR COMPANY**  
A Division of Union Carbide and Carbon Corporation



POST OFFICE BOX P • OAK RIDGE, TENNESSEE

**UNCLASSIFIED**

#### LEGAL NOTICE

This report was prepared as an account of Government sponsored work. Neither the United States, nor the Commission, nor any person acting on behalf of the Commission:

- A. Makes any warranty or representation, express or implied, with respect to the accuracy, completeness, or usefulness of the information contained in this report, or that the use of any information, apparatus, method, or process disclosed in this report may not infringe privately owned rights; or
- B. Assumes any liabilities with respect to the use of, or for damages resulting from the use of, any information, apparatus, method, or process disclosed in this report.

As used in the above, "person acting on behalf of the Commission" includes any employee or contractor of the Commission to the extent that such employee or contractor prepares, handles or distributes, or provides access to, any information pursuant to his employment or contract with the Commission.

**UNCLASSIFIED**

ORNL-2076

Contract No. W-7405-eng-26

**PHYSICS DIVISION  
SEMIANNUAL PROGRESS REPORT  
for Period Ending March 10, 1956**

A. H. Snell, Director

Edited by  
J. L. Fowler and E. O. Wollan  
Associate Directors

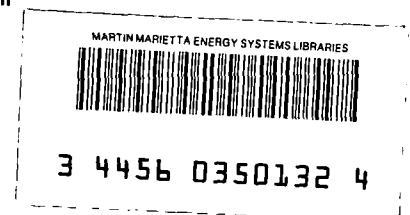
DATE ISSUED

**JUN 14 1956**

---

OAK RIDGE NATIONAL LABORATORY  
Operated by  
UNION CARBIDE NUCLEAR COMPANY  
A Division of Union Carbide and Carbon Corporation  
Post Office Box P  
Oak Ridge, Tennessee

**UNCLASSIFIED**



# UNCLASSIFIED

Physics Division progress reports previously issued in this series are as follows:

ORNL-325 Supplement	December, January, and February, 1948-1949
ORNL-366	Period Ending June 15, 1949
ORNL-481	Period Ending September 25, 1949
ORNL-577	Period Ending December 15, 1949
ORNL-694	Period Ending March 15, 1950
ORNL-782	Period Ending June 15, 1950
ORNL-865	Period Ending September 20, 1950
ORNL-940	Period Ending December 20, 1950
ORNL-1005	Period Ending March 20, 1951
ORNL-1092	Period Ending June 20, 1951
ORNL-1164	Period Ending September 20, 1951
ORNL-1278	Period Ending December 20, 1951
ORNL-1289	Period Ending March 20, 1952
ORNL-1365	Period Ending June 20, 1952
ORNL-1415	Period Ending September 20, 1952
ORNL-1496	Period Ending December 20, 1952
ORNL-1620	Period Ending September 10, 1953
ORNL-1705	Period Ending March 10, 1954
ORNL-1798	Period Ending September 10, 1954
ORNL-1879	Period Ending March 20, 1955
ORNL-1975	Period Ending September 10, 1955

UNCLASSIFIED

# UNCLASSIFIED

ORNL-2076  
Progress

## INTERNAL DISTRIBUTION

1. C. E. Center
2. Biology Library
3. Health Physics Library
- 4-6. Central Research Library
7. Reactor Experimental Engineering Library
- 8-19. Laboratory Records Department
20. Laboratory Records, ORNL R.C.
21. A. M. Weinberg
22. L. B. Emler (K-25)
23. J. P. Murray (Y-12)
24. J. A. Swartout
25. E. H. Taylor
26. E. D. Shipley
27. E. J. Murphy
28. M. L. Nelson
29. A. H. Snell
30. A. Hollaender
31. K. Z. Morgan
32. F. L. Culler
33. M. T. Kelley
34. E. M. King
35. E. O. Wollan
36. D. W. Cardwell
37. A. S. Householder
38. L. D. Roberts
39. R. B. Briggs
40. R. N. Lyon
41. W. C. Koehler
42. E. P. Blizard
43. M. E. Rose
44. G. E. Boyd
45. W. H. Sullivan
46. R. W. Stoughton
47. C. E. Winters
48. W. H. Jordan
49. E. C. Campbell
50. D. S. Billington
51. M. A. Bredig
52. R. S. Livingston
53. C. P. Keim
54. F. C. Maienschein
55. C. E. Clifford
56. G. H. Clewett
57. C. D. Susano
58. C. J. Borkowski
59. M. J. Skinner
60. M. K. Wilkinson
61. S. Bernstein
62. P. M. Reyling
63. D. D. Cowen
64. W. M. Good
65. G. C. Williams
66. J. L. Fowler
67. R. W. Johnson
68. J. R. McNally, Jr.
69. J. L. Gabbard
70. R. A. Charpie
71. E. P. Wigner (consultant)
72. H. A. Bethe (consultant)
73. K. Lark-Horovitz (consultant)
74. Eugene Guth
75. R. W. Peelle
76. W. M. Breazeale (consultant)
77. E. C. Smith
78. C. G. Shull
79. P. R. Bell
80. G. G. Kelley
81. C. C. Harris
82. H. G. MacPherson (consultant)
83. P. H. Stelson
84. J. E. Sherwood
85. U. H. Bents
86. W. Zobel
87. R. B. Murray
88. H. B. Willard
89. J. Schenck
90. J. H. Neiler
91. E. D. Klema
92. C. F. Barnett
93. N. H. Lazar
94. R. R. Dickison
95. A. Simon
96. J. H. Gibbons
97. J. J. Pinajian
98. ORNL - Y-12 Technical Library,  
Document Reference Section

UNCLASSIFIED

# UNCLASSIFIED

## EXTERNAL DISTRIBUTION

99. W. G. Pollard, ORINS
100. W. K. H. Panofsky, Stanford University
101. L. C. Biedenharn, Rice Institute
102. R. F. Bacher, California Institute of Technology
103. John Dunning, Columbia University
104. Phillips Petroleum Co., Attn: Librarian
105. R. L. Heath, Phillips Petroleum Company
106. S. DeBenedetti, Carnegie Institute of Technology
107. Massachusetts Institute of Technology, Department of Electrical Engineering
108. A. von Hippel, Laboratory for Insulation Research, MIT
109. M. Goodrich, Louisiana State University
110. Truman S. Grey, Massachusetts Institute of Technology
111. V. C. Wilson, General Electric Co., Schenectady
112. D. S. Hughes, University of Texas
113. E. A. Rollor, ANP Project Office, Fort Worth
114. S. Frankel, Physics Dept., University of Pennsylvania
115. G. Griffith, Westinghouse Research Laboratory, E. Pittsburgh, Pennsylvania
116. F. Allison, Emory and Henry University, Emory, Virginia
117. J. A. Sauer, Physics Dept., Pennsylvania State University
118. J. E. Goldman, Dept. of Physics, Carnegie Institute of Technology
119. R. Stephenson, Dept. of Chemical Engineering, New York University
120. M. Goldhaber, Brookhaven National Laboratory
121. M. N. Saha, c/o Library, Institute of Nuclear Physics, 92 Upper Circular Road, Calcutta, India
122. J. A. Wheeler, Palmer Physical Laboratory, Princeton University
123. R. S. Christy, California Institute of Technology
124. T. J. Turner, Wake Forrest College
125. T. Lauritsen, California Institute of Technology
126. N. F. Ramsey, Harvard University
127. University of Notre Dame (Attention: Library)
128. J. H. Van Vleck, Harvard University
129. A. Glassgold, University of Minnesota
130. P. M. Steir, National Carbon Research Laboratories, P. O. Box 6087, Cleveland, Ohio
131. Boeing Airplane Company
132. Division of Research and Development, AEC, ORO
- 133-535. Given distribution as shown in TID-4500 under Physics Category

DISTRIBUTION PAGE TO BE REMOVED IF REPORT IS GIVEN PUBLIC DISTRIBUTION

UNCLASSIFIED

# UNCLASSIFIED

## INDEX AND SUMMARY

### **THEORY OF ALPHA-PARTICLE EMISSION FROM ALIGNED NUCLEI**

M. E. Rose . . . . . 1

The theory of alpha-particle emission for aligned nuclei is presented, with particular emphasis on the role played by nuclear structure and barrier penetrability. The results, in agreement with observations, show that existing ideas on this subject have to be modified.

### **ANISOTROPY OF ALPHA-PARTICLE EMISSION FROM ORIENTED $Np^{237}$ AND $U^{233}$ NUCLEI**

L. D. Roberts, J. W. T. Dabbs, and G. W. Parker . . . . . 3

Angular-distribution measurements on alpha particles emitted by partially oriented  $Np^{237}$  and  $U^{233}$  nuclei have been obtained. Determination of the direction of the nuclear alignment in the  $Np^{237}$  is in progress.

### **THE ALPHA-PARTICLE MODEL OF $C^{12}$**

A. E. Glassgold and A. Galonsky . . . . . 6

The energy levels predicted by the alpha-particle model of  $C^{12}$  have been obtained by fixing the parameters of the model with the first three known excited states of  $C^{12}$ .

### **ENERGY LEVELS OF $C^{12}$**

C. D. Moak and A. Galonsky . . . . . 7

The energy levels of  $C^{12}$  are being studied through the  $C^{10}(He^3,p)C^{12}$  reaction. No new levels below 10 Mev have yet been observed.

### **AN EMPIRICAL KINEMATICAL NUCLEAR MODEL**

E. D. Klema and R. K. Osborn . . . . . 8

The model discussed previously has been applied to the problem of determining nuclear shape factors from the energies of first excited states of even-even nuclei and from the measured cross sections for  $E2$  coulomb excitation of these levels. In this work an empirical parameter has been found which allows one to calculate the fractional nuclear mass taking part in the collective core rotation.

### **GAMMA-RAY YIELDS FROM COULOMB EXCITATION**

P. H. Stelson and F. K. McGowan . . . . . 9

The yields of gamma rays resulting from coulomb excitation have been measured for the even-even isotopes of ruthenium. Values for the reduced transition probability for electric quadrupole transitions,  $B(E2)_{ex}$ , have been obtained. A summary of information on level positions and values of  $B(E2)_{ex}$  for the even-even isotopes of Mo, Ru, Pd, Cd, and Te is given.

### **POLARIZATION OF GAMMA RAYS FOLLOWING COULOMB EXCITATION**

F. K. McGowan and P. H. Stelson . . . . . 12

A polarimeter based on the Compton scattering mechanism has been constructed, and its effectiveness has been determined by measurements of known polarization of gamma rays from excitation of  $2^+$  levels in even-even nuclei. Polarization-direction measurements of five transitions of the type  $\frac{3}{2}(E2 + M1)\frac{1}{2}$  have resolved the ambiguity in the values of  $(E2/M1)^{1/2}$ .

### **POLARIZATION OF GAMMA RAYS IN $Ta^{181}$**

F. K. McGowan and P. H. Stelson . . . . . 15

The polarization-direction correlation for the 132-480-kev gamma-ray cascade in  $Ta^{181}$  has been determined. It is concluded that the correct spin assignment is  $\frac{1}{2}(E2)\frac{5}{2}(E2 + M1)\frac{7}{2}$ .

UNCLASSIFIED

# UNCLASSIFIED

## **DIRECTIONAL ANGULAR CORRELATIONS OF GAMMA RAYS IN CASCADE**

E. D. Klema . . . . . 17

Directional angular correlations of gamma rays in cascade have been measured for certain excited states in  $\text{Sr}^{88}$ ,  $\text{Lu}^{175}$ , and  $\text{Hf}^{177}$ . Spins have been assigned to some of the levels, and some of the transitions have been classified.

## **DECAY OF $\text{Sb}^{125}$**

N. H. Lazar . . . . . 19

Eleven gamma rays between 0.100 and 0.637 Mev have been identified in the decay of  $\text{Sb}^{125}$ . From their relative intensities as measured with a 3-in.-dia, 3-in.-high sodium iodide crystal and with the assistance of coincidence spectrometry, a decay scheme may be constructed which is consistent with all the data. The half life for  $\text{Sb}^{125}$  was determined as  $2.0 \pm 0.2$  years

## **THE 2.07-Mev RESONANCE IN THE $\text{C}^{12}(n,n)\text{C}^{12}$ REACTION**

J. E. Wills, Jr. . . . . 22

Total cross-section and angular-distribution measurements were made with the object of removing uncertainties in the assignment of level parameters for the 2.07-Mev resonance in the scattering of neutrons from carbon. Measurements indicate a  $D_{3/2}$  level.

## **DIFFERENTIAL ELASTIC SCATTERING AT 1.62- AND 1.68-Mev NEUTRON RESONANCE IN NEON**

J. L. Fowler and H. O. Cohn . . . . . 26

The technique of measuring coincidences between nuclear recoils and scattered neutrons has been used to investigate the elastic scattering at the 1.62- and 1.68-Mev resonances in neon. The angular distributions indicate that the 1.62-Mev level has odd parity and the 1.68-Mev level has even parity.

## **NEUTRON ACTIVATION OF IODINE NEAR 25 keV**

R. L. Macklin . . . . . 27

A value of  $0.82 \pm 0.06$  barns was found for the  $^{127}(n,\gamma)^{128}$  cross section near 25 keV with the use of an antimony-beryllium neutron source.

## **MILLIMICROSECOND TIME-OF-FLIGHT NEUTRON SPECTROMETRY**

H. E. Banta, J. H. Gibbons, W. M. Good, and J. H. Neiler . . . . . 29

Millimicrosecond time-of-flight neutron spectrometry has progressed so that new levels have been observed in transmission spectra between 2 and 30 keV, and well resolved groups of neutrons have been observed from  $\text{Be}^9(d,n)$ ,  $\text{F}^{19}(d,n)$ , and other reactions.

## **EXPERIMENTS WITH PULSED-NEUTRON SOURCE**

E. C. Campbell and P. H. Stelson . . . . . 32

A square-wave-modulated fast-neutron source and synchronized multichannel time analyzer have been used for decay measurements of the nuclear isomers  $\text{Ta}^{181m}$  and  $\text{As}^{75m}$  and to measure thermal-neutron diffusion parameters in  $\text{H}_2\text{O}$  and beryllium.

## **REACTOR PARAMETERS OF A SMALL ENRICHED SUBCRITICAL REACTOR BY PULSED-NEUTRON TECHNIQUES**

E. C. Campbell and P. H. Stelson . . . . . 37

Measurements of the decay rate of a subcritical reactor following exposure to bursts of fast neutrons provide a new means for investigation of multiplying systems.

UNCLASSIFIED

# UNCLASSIFIED

## RECOIL SPECTROMETRY

A. H. Snell and F. Pleasonton ..... 39

Internal conversion accompanying the decay of  $Xe^{131m}$  gives rise to cascades in the Auger effect, leaving the atoms in high states of multiple ionization. A "shakeoff" of electrons originating from the change in nuclear charge follows the beta decay of  $Kr^{85}$  as well as rare Auger cascades. The resulting distributions in charge of the product atoms are given.

## ANTIFERROMAGNETIC STRUCTURES OF ANHYDROUS $CoCl_2$ AND $FeCl_2$

M. K. Wilkinson and J. W. Cable ..... 44

Antiferromagnetic structures have been determined for anhydrous  $CoCl_2$  and  $FeCl_2$  at temperatures below their Néel transitions.

## INVESTIGATIONS OF CRITICAL MAGNETIC SCATTERING

M. K. Wilkinson and C. G. Shull ..... 46

Experiments have been performed with iron, nickel, and magnetite to determine the characteristics of the critical magnetic scattering which occurs at small angles in the temperature range of Curie transitions.

## NEUTRON-DIFFRACTION OBSERVATIONS ON HOLMIUM OXIDE

W. C. Koehler, E. O. Wollan, M. K. Wilkinson, and J. W. Cable ..... 48

Neutron-diffraction data on  $Ho_2O_3$  give  $\sigma_{coh}(Ho) = 9.1$  barns with positive phase, and analysis of the transmission data gives about 12 barns for the total nuclear scattering cross section. Preliminary measurements of the paramagnetic scattering and observations indicating antiferromagnetic ordering at low temperatures are also reported.

## RAPID SEPARATION BY ION-EXCHANGE. YIELD FOR ANION-EXCHANGE SEPARATION OF $Pb^{207m}$ FROM $Bi^{207}$

E. C. Campbell and F. Nelson ..... 52

Measurements on the elution rate of lead from ion-exchange resin indicate a diffusion constant of  $7.8 \times 10^{-8}$   $cm^2/sec$ . A comparison is made with the measured yield of  $Pb^{207m}$  (0.8 sec) separated from  $Bi^{207}$ .

## EXTENSION OF PEAK EFFICIENCY OF $3 \times 3$ in. $NaI(Tl)$ TO HIGH ENERGIES

N. H. Lazar and H. B. Willard ..... 55

The peak efficiency of  $3 \times 3$  in.  $NaI(Tl)$  crystals has been extended to 7.5 Mev. Essentially single gamma rays with energies from 1.78 to 7.48 Mev have been produced by reactions of various nuclei with protons, and the ratios of peak area to total area have been determined from their pulse-height distributions.

## TRANSMISSION CHARACTERISTICS OF LIGHT PIPERS

C. C. Harris and P. R. Bell ..... 58

Experimentation has been begun with the objective of improving the transmission of long, thin light pipers. Certain comparative results on piper reflectors are given.

## ELECTROSTATIC LENS FOR THE 3-Mv VAN DE GRAAFF

C. H. Johnson and J. P. Judish ..... 61

A compound electrostatic lens incorporating a unipotential lens was installed in the 3-Mv Van de Graaff to reduce magnification and aberration. This lens (which is lined with beryllium to reduce x rays) produces a good beam focus in general agreement with its theoretical design.

## LIFE TESTS OF FILAMENTARY SUBMINIATURE TUBES

C. C. Harris and P. R. Bell ..... 64

Continuing life tests on filamentary subminiature tubes show life to 15,000 hr, with expectancy of much longer life. Tests also indicate the filament voltage for longest life in one emission-current condition.

# UNCLASSIFIED

# UNCLASSIFIED

## PUBLICATIONS

J. K. Bair, J. D. Kington, and H. B. Willard, "Gamma-Ray and Neutron Yields from the Proton Bombardment of Boron," *Phys. Rev.* **100**, 21 (1955).

S. Bernstein, W. K. Ergen, F. L. Talbott, J. K. Leslie, and C. P. Stanford, "Yield of Photoneutrons from  $U^{235}$  Fission Products in Beryllium and Deuterium," *J. Appl. Phys.* **27**, 18 (1956).

S. Bernstein, J. K. Leslie, C. R. McKinney, and H. K. Jackson, "Photoneutrons from  $U^{235}$  and  $Pu^{249}$  Fission Products in Heavy Water," *J. Appl. Phys.* **27**, 23-24 (1956).

J. E. Francis, P. R. Bell, and C. C. Harris, "Medical Scintillation Spectrometer," *Nucleonics* **13**, 82 (1955).

A. Galonsky and J. P. Judish, "Angular Distribution of  $n-p$  Scattering at 17.9 Mev," *Phys. Rev.* **100**, 121 (1955).

A. I. Galonsky, C. H. Johnson, and C. D. Moak, "Energy Response of Csl to Protons," *Rev. Sci. Instr.* **27**, 58 (1956).

J. H. Gibbons, R. L. Macklin, and H. W. Schmitt, "The  $V^{51}(p,n)Cr^{51}$  Reaction as a 5-120 keV Neutron Source," *Phys. Rev.* **100**, 167 (1955).

W. M. Good and E. O. Wollan, "Range and Range Dispersion of Specific Fission Fragments," *Phys. Rev.* **101**, 249 (1956).

E. D. Klema, "Gamma-Gamma Angular Correlation in  $Ba^{134}$ ," *Phys. Rev.* **100**, 66 (1955).

R. W. Lamphere and R. E. Greene, "The Neutron-Induced Fission Cross Sections of U-234 and U-236," *Phys. Rev.* **100**, 763-770 (1955).

N. H. Lazar, E. Eichler, and G. D. O'Kelley, "Nuclear Levels in  $Sr^{88}$  from the Disintegration of  $Rb^{88}$  and  $Y^{88}$ ," *Phys. Rev.* **101**, 727 (1956).

R. B. Murray and L. D. Roberts, "Magnetic and Thermal Properties of  $MnCl_2$  at Liquid Helium Temperatures: I. Magnetic Susceptibility," *Phys. Rev.* **100**, 1067 (1955).

R. B. Murray, "Magnetic and Thermal Properties of  $MnCl_2$  at Liquid Helium Temperatures: II. Specific Heat," *Phys. Rev.* **100**, 1071 (1955).

G. D. O'Kelley, N. H. Lazar, and E. Eichler, "The Decay Chain  $Ca^{49}$ - $Sc^{49}$ - $Ti^{49}$ ," *Phys. Rev.* **101**, 1059 (1956).

R. K. Osborn and E. D. Klema, "Empirical Correlation of Nuclear Magnetic Moments," *Phys. Rev.* **100**, 822-834 (1955).

L. D. Roberts and R. B. Murray, "The Magnetic and Thermal Properties of  $U_3$  at Liquid Helium Temperatures," *Phys. Rev.* **100**, 650 (1955).

L. D. Roberts, R. B. Murray, and J. W. T. Dabbs, "The Influence of Crystalline Electric Fields on Antiferromagnetic Transitions," *Phys. Rev.* **100**, 1100 (1955).

M. E. Rose, book review ("Mathematical Foundations of Quantum Mechanics," by John von Neumann, Princeton Univ. Press, Princeton, N. J., 1955) *Physics Today* **8**, 21 (1955).

A. H. Snell and F. Pleasonton, "Spectrometry of the Neutrino Recoils of Argon-37," *Phys. Rev.* **100**, 1396 (1955).

A. H. Snell, book review ("Nuclear Physics," by Alex E. S. Green, McGraw-Hill, 1955) *Am. Scientist* **44**, 62A (1956).

H. B. Willard, J. K. Bair, J. D. Kington, and H. O. Cohn, "Elastic Scattering of Neutrons by  $Li^6$  and  $Li^7$ ," *Phys. Rev.* **101**, 765 (1956).

E. O. Wollan and W. C. Koehler, "Neutron Diffraction Study of the Magnetic Properties of the Series of Perovskite Type Compounds  $[(1-x)La, xCa]MnO_3^*$ ," *Phys. Rev.* **100**, 545 (1955).

C. E. Holley, Jr., R. N. R. Mulford, F. H. Ellinger, W. C. Koehler, and W. A. Zachariasen, "The Crystal Structure of Some Rare Earth Hydrides," *J. Phys. Chem.* **59**, 1226 (1955).

C. D. Moak and W. R. Wisseman, "The Energy Levels of  $Be^8$ ," *Phys. Rev.* **101**, 1326 (1956).

UNCLASSIFIED

# UNCLASSIFIED

## PAPERS PRESENTED AT SCIENTIFIC MEETINGS

*Diffraction Conference, Pittsburgh, Pennsylvania, November 1955*

J. E. Worsham, Jr., C. G. Shull, and M. K. Wilkinson, "Neutron Diffraction Observations on the Palladium-Hydrogen System."

W. C. Koehler and E. O. Wollan, "Antiferromagnetic Structures of  $\text{MnBr}_2$  and  $\text{FeBr}_2$ ."

U. H. Bents, W. C. Koehler, and E. O. Wollan, "Magnetic-Neutron Diffraction Study of the Perovskite Systems  $\text{La}(\text{Mn}, \text{Cr})\text{O}_3$ ."

*American Institute of Electrical Engineers—Institute of Radio Engineers 8th Annual Conference on Electrical Techniques in Medicine and Biology, Washington, D. C., November 14–16, 1955*

J. E. Francis and P. R. Bell, "Sharp Localization of Radiation Sources *in vivo*."

C. C. Harris, J. E. Francis, P. R. Bell, and G. G. Kelley, "A Surgical Scintillation Probe."

*American Physical Society Meeting, Chicago, Illinois, November 25–26, 1955*

C. H. Johnson and A. I. Galonsky, "The  $\text{T}(d,n)\text{He}^4$  Reaction, 1.5 Mev."

C. F. Barnett and P. M. Stier, "The Electron Loss Cross Section for Fast Helium Atoms."

*Low Temperature Conference, Baton Rouge, Louisiana, December 1955*

L. D. Roberts, J. W. T. Dabbs, G. W. Parker, and R. D. Ellison, "Alpha Particle Emission from Oriented  $\text{Np}^{237}$  Nuclei and the Spheroidal Shape of this Nucleus."

J. W. T. Dabbs, L. D. Roberts, and S. Bernstein, "'Brute Force' Polarization of  $\text{In}^{115}$  Nuclei."

*Atlanta Meeting of the American Association for the Advancement of Science, Atlanta, Georgia, December 27, 1955*

J. E. Francis and P. R. Bell, "The Medical Spectrometer."

*American Physical Society Meeting, New York, N. Y., January 30–February 3, 1956*

R. C. Block and H. W. Newson, "Neutron Resonance Scattering at 180 and 90 Degrees."

W. Haerberli and R. C. Block, "Anisotropy in the Scattering of 55 to 105 kev Neutrons from Intermediate Weight Elements."

D. A. Geffen, "Some Properties of Solutions of the Bethe-Salpeter Equation."

R. L. Macklin, H. W. Schmitt, and J. H. Gibbons, "Neutron Absorption by Fissionable Materials in the 5 to 50 kev Energy Range."

A. H. Snell and F. Pleasonton, "The Auger Cascade in Xenon."

T. A. Welton, "A Subtraction Prescription for Closed-Loop Divergences."

T. A. Welton, "Phase Stability in Fixed-Frequency Cyclotrons."

D. S. Falk and T. A. Welton, "Orbit Calculations for Fixed-Frequency Cyclotrons."

H. B. Willard, J. K. Bair, H. O. Cohn, and J. D. Kington, "Elastic Neutron Scattering by  $\text{Li}^7$  as a Polarization Analyzer."

J. H. Neiler, G. G. Kelley, and P. R. Bell, "Millimicrosecond Neutron Spectrometry, I. Multi-channel Time Analyzer."

V. E. Parker and R. F. King, "Millimicrosecond Neutron Spectrometry, II. Pulsed Ion Source."

H. E. Banta, R. F. King, and J. P. Jewish, "Millimicrosecond Neutron Spectrometry, III. Pulsed Van de Graaff."

E. C. Smith, J. H. Gibbons, W. M. Good, J. H. Neiler, and H. E. Banta, "Millimicrosecond Neutron Spectrometry, IV. Kilovolt Neutron Cross Sections."

W. M. Good, J. H. Neiler, and J. H. Gibbons, "Millimicrosecond Neutron Spectrometry, V.  $\text{Be}^9(d,n)\text{B}^{10}$  Neutron Spectrum."

# UNCLASSIFIED

# UNCLASSIFIED

*American Physical Society Meeting, Houston, Texas, February 24-25, 1956*

E. D. Klema, "Gamma-Gamma Angular Correlation in  $\text{Sr}^{88}$ ."

W. M. Good (invited paper), "Millimicrosecond Neutron Time-of-Flight Spectrometry."

J. A. Harvey, "Neutron Resonance Parameters of  $\text{U}^{235}$ ."

*Scintillation Counter Symposium, Washington, D. C., February 28-29, 1956*

R. C. Davis, P. R. Bell, G. G. Kelley, and N. H. Lazar, "Response of 'Total Absorption' Spectrometer to  $\gamma$ -Rays."

R. C. Davis, P. R. Bell, J. H. Neiler, and C. C. Harris, "Sodium Iodide Crystal Canning Techniques."

N. H. Lazar and H. B. Willard, "Response of 3"  $\times$  3" NaI(Tl) Crystals to High Energy Gamma Rays."

N. H. Lazar, R. C. Davis, and P. R. Bell, "An Improved Coincidence Spectrometer."

N. H. Lazar, R. C. Davis, and P. R. Bell, "Peak Efficiency of NaI(Tl) Crystals for Gamma Rays from 0.150 to 7.5 Mev."

G. G. Kelley, P. R. Bell, R. C. Davis, and N. H. Lazar, "Intrinsic Scintillator Resolution."

C. C. Harris and P. R. Bell, "Transmission Characteristics of Light Pipes."

J. H. Neiler, G. G. Kelley, and P. R. Bell, "Time-of-Flight Spectrometry for 2 kev to 10 Mev Neutrons."

J. E. Francis and P. R. Bell, "Medical Type Collimators."

P. R. Bell, R. C. Davis, and N. H. Lazar, "Characterization of Photomultipliers by Photosensitivity and Light Pulser Response."

J. Schenck, " $\text{Li}^6\text{I}(\text{Eu})$  as a Neutron Detector and Spectrometer."

---

## ANNOUNCEMENTS

Additions to the Physics Division staff during this period were as follows: J. A. Harvey and R. C. Block (Neutron Velocity Selector), and H. R. Child (Neutron Diffraction).

J. D. Kington (High Voltage) transferred to the Applied Nuclear Physics Division.

UNCLASSIFIED

# UNCLASSIFIED

## PHYSICS DIVISION SEMIANNUAL PROGRESS REPORT

### THEORY OF ALPHA-PARTICLE EMISSION FROM ALIGNED NUCLEI

M. E. Rose

The recent experiments of Roberts *et al.*,<sup>1</sup> in which they observed the anisotropic angular distribution of alpha particles emitted by aligned U<sup>233</sup> and Np<sup>237</sup> nuclei, provide an opportunity for obtaining important nuclear information. These experiments and their analysis have not yet been completed, and it is premature to discuss the question of possible conclusions to be drawn from them. However, it is pertinent to discuss the theoretical basis on which the analysis of these experiments would be made.

At one time it was believed that with nuclei having a prolate charge distribution, aligned along their symmetry axis, the alpha particles would emerge preferentially in this direction because of the greater penetrability of the coulomb barrier which this entails. However, the actual situation is somewhat different. The experiments, in the cases studied, showed preferential emission in the equatorial plane.

The role of barrier penetrability, as well as intrinsic alpha-particle formation probability, may be clarified as follows. First consider a transition in which the final-state angular momentum is either 0 or  $\frac{1}{2}$  depending on whether the mass is even or odd. The case of even mass is probably academic, but the following argument is presented for the purpose of exposition of the ideas involved. In the case envisaged, the alpha particles can have only one value of  $L$ , orbital angular momentum. This will be  $L = j_i$  (initial angular momentum) for  $j_f = 0$  and  $L = j_i \pm \frac{1}{2}$ , depending on the parity change, when  $j_f = \frac{1}{2}$ . Of course, for alignment  $j_i \geq 1$  is necessary.

Now, as has been emphasized by others,<sup>2</sup> the wave function of the system can contain the propagation vector of the alpha particle only in the form  $Y_L^M(k)$ . The rest of the wave function can depend on the radial coordinate of the alpha

particle and on all internal coordinates, and the manner in which these are expressed depends on the model. Thus, for a given  $L$ , we would write for the total wave function

$$(1) \quad \Psi = R_L(r) \sum_M Y_L^M(k) \chi_L^{M*}(x),$$

where  $x$  stands for internal coordinates. For example, Rasmussen and Segall write  $\chi_L^M$  as a product of a particle structure state vector and a rotation matrix element (wave function of symmetric top) describing the rigid body motion of a core. In a way, it does not matter for us whether the propagation vector relative to body- or space-fixed axes is meant, although we eventually need to express the  $Y_L^M$  in terms of the space-fixed axes, since this is the reference frame in which the observations are made. However, the transformation between these is made as usual with a rotation matrix, and the form of Eq. 1 is not thereby changed. In any event this transformation is a geometrical one, and it does not change the role played by the radial function  $R_L$ , which still appears as a multiplicative factor. All details of barrier penetrability are contained in  $R_L$ . The entire mechanism of alpha-particle formation must be contained in the function  $\chi_L^M(x)$  if it is expressed at all.

Now in calculating the angular distribution we can proceed as if perturbation theory were used and write down a matrix element of some interaction energy  $H'$  between initial and final states. In a self-explanatory notation this would be

$$(2) \quad \langle j_f m_f | H' | j_i m_i \rangle.$$

In addition  $H'$  is invariant and for a fixed  $L$  must have the form

$$H' = \sum_M Y_L^M T_L^{M*},$$

where  $T_L^M$  depends on radial functions and possibly

<sup>1</sup>L. D. Roberts, J. W. T. Dabbs, and G. W. Parker, the following paper, this report.

<sup>2</sup>J. Rasmussen and B. Segall, *Alpha Decay of Spheroidal Nuclei*, UCRL-3040 (Oct. 7, 1955).

# UNCLASSIFIED

on internal coordinances. Then Eq. 2 becomes

$$(3) \quad (j_f m_f | H' | j_i m_i) \\ = C_{m_i^{-M}}^{j_i L j_f} \delta_{m_f, m_i - M} (j_f || T_L || j_i) .$$

The last factor is called a reduced matrix element, and we make no attempt to evaluate it. For a single  $L$  it appears as a multiplicative factor and controls the total intensity. The rest of the calculation involves the evaluation of

$$\sum_M \sum_{m_i} \sum_{m_f} P_{m_i} |Y_L^M|^2 \left( C_{m_i^{-M}}^{j_i L j_f} \right)^2 \delta_{m_f, m_i - M} ,$$

where  $P_{m_i}$  is the population of the initial substrate  $m_i$ . Note that the  $M$  sum is incoherent instead of coherent, because of the conservation rule expressed by the Kronecker delta.

The summation over  $m_f$  or  $M$ , is trivial and gives an angular distribution

$$(4) \quad W_{LL}(\theta) \\ = \sum_{\nu} G_{\nu} C_{00}^{LL \nu} W(j_i j_i LL; \nu j_f) P_{\nu}(\cos \theta) ,$$

and  $0 \leq \nu \leq \nu_{\max}$ , where  $\nu_{\max}$  is the smaller of  $2L$  and  $2j_i$ . Also  $\nu$  is even.

The parameter  $G_{\nu}$  contains the spin properties of the initial state. These are called statistical tensors and are given by

$$(5) \quad G_{\nu} = \sum_{m_i} (-)^{j_i - m_i} P_{m_i} C_{m_i^{-m_i}}^{j_i j_i \nu} .$$

When the nuclear spin is coupled to that of the surrounding electrons, as in Bleaney alignment, it is necessary to adjoin a sum over the magnetic quantum numbers of the electrons to Eq. 5. Then Eq. 5 is more correctly

$$(6) \quad G_{\nu} = \frac{\text{Tr} \mathfrak{J}_{\nu}^0 e^{-H/kT}}{\text{Tr} e^{-H/kT}} ,$$

where  $H$  is the spin Hamiltonian. The tensor components  $\mathfrak{J}_{\nu}^0$  are easy to identify.<sup>3</sup> For instance

for  $\nu = 2$

$$\mathfrak{J}_2^0 = \sqrt{\frac{180(2j_i - 1)!}{(2j_i + 3)!}} \left[ j_i^2 - \frac{1}{3} j_i(j_i + 1) \right] .$$

Now we are in a position to generalize the result to the case that more than one value of  $L$  is permitted. First we define a mixed angular distribution

$$(7) \quad W_{LL'} \\ = \sum_{\nu} G_{\nu} C_{00}^{LL' \nu} W(j_i j_i LL'; \nu j_f) P_{\nu}(\cos \theta) ,$$

and now the lower limit on  $\nu$  is  $|L - L'|$ . Since  $\nu$  is still even and  $|L - L'|$  must be even for parity reasons  $\nu_{\min} = 2$  for  $L \neq L'$ . Then it is easy to see, from symmetry reasons, that the angular distribution is

$$(8) \quad W = \sum_{LL'} C_{LL'} W_{LL'} ,$$

where  $C_{LL'}$  are intensity parameters for  $L = L'$  and measure the strength of interference patterns for  $L \neq L'$ . In fact, we can show that

$$C_{LL'} = (j_f || T_L || j_i)^* (j_f || T_{L'} || j_i) \cos(\sigma_L - \sigma_{L'})$$

and is real.  $\sigma_L = \arg \Gamma(L + 1 + ie^2 Z z_{\alpha} / \hbar \nu)$  is introduced by the coulomb field. This then is where the barrier penetrability enters.

Consider a transition  $j_i = \frac{5}{2} \rightarrow j_f = \frac{5}{2}$ . Then possible  $L$  values are  $L = 0, 2, 4$ .  $G$  waves are cut down in strength by the centrifugal barrier to the point where they need not be considered. Then we have

$$(9) \quad W = W_S + \delta^2 W_D + 2\delta \cos(\sigma_2 - \sigma_0) W_{SD} ,$$

where  $W_S$  is the (isotropic) distribution for  $S$ -wave alphas and  $W_D$  that for  $D$ -wave alphas. If we normalize both of these to 1, then  $\delta^2$  is the ratio of  $D$ -wave to  $S$ -wave intensities.  $W_{SD}$  is the interference term, and, since the sign of  $\delta$  is not known a priori, the emission can be preferentially polar or equatorial. The distribution (Eq. 9) will have the form

$$W = 1 + A_2 P_2(\cos \theta) + A_4 P_4(\cos \theta) .$$

The coefficient  $A_4$  is small unless  $kT$  is comparable to the coupling energy which aligns the nucleus.

<sup>3</sup>For further details consult M. E. Rose, *Theory of Angular Momentum*, unpublished.

The coefficient  $A_2$  will have the form

$$A_2 = \frac{G_2}{1 + \delta^2} [\delta^2 A_2(D) + 2\delta \cos(\sigma_2 - \sigma_0) A_2(SD)] ,$$

where  $A_2(D)$  and  $A_2(SD)$  are the coefficients of  $P_2$  in  $W_D$  and  $W_{SD}$ . For  $-\infty < \delta < \infty$ ,  $A_2$  can take on

both signs, in general. Note that the shape of  $A_2$  as a function of temperature is independent of the unknown nuclear factors containing  $\delta$ . If one can measure  $A_2$  as a function of  $1/T$ , normalizing in an arbitrary way, then some information about the coupling parameters can be obtained no matter how complicated (or unknown) the decay scheme may be. For this purpose the shape of the  $A_2 - 1/T$  curve is essential, and hence it is necessary to go to temperatures low enough so that curvature develops.

### ANISOTROPY OF ALPHA-PARTICLE EMISSION FROM ORIENTED $Np^{237}$ AND $U^{233}$ NUCLEI

L. D. Roberts      J. W. T. Dabbs      G. W. Parker

In the last semiannual report, preliminary experiments on the emission of alpha particles from oriented  $Np^{237}$  nuclei were described.<sup>1</sup> In this work a single crystal of  $NpO_2 \cdot Rb(NO_3)_3$  was cooled to liquid-helium temperatures, and the ratio of intensities  $W(0^\circ)/W(90^\circ)$  was measured. It was found that, as the temperature was reduced, the intensity parallel to the  $c$ -axis of the rhombohedral crystal ( $\theta = 0^\circ$ ) decreased relative to that perpendicular to the  $c$ -axis ( $\theta = 90^\circ$ ). In these experiments, the counting rates were quite low, because of the good geometry used, in which the ZnS detector was placed in a room-temperature region at the top of the cryostat.

The apparatus has since been improved by placing the ZnS (Ag activated) detector in the liquid-helium temperature region of the cryostat and piping the light flashes produced to an external photomultiplier. Figure 1 displays the new arrangement, in which the ZnS is coated on the lower end of a truncated paraboloid of revolution which was cut off normal to the axis and through the focal point. The outer surface was aluminized, and the upper end was inserted into a pyrex glass tube, silvered on the outside, through which the light was conducted to the photomultiplier at the upper end of the cryostat. Both Lucite and pyrex

strongly absorb infrared radiation; thus room-temperature radiation ( $\sim 10 \mu$ ) is not piped downward to the sample, while visible light from the

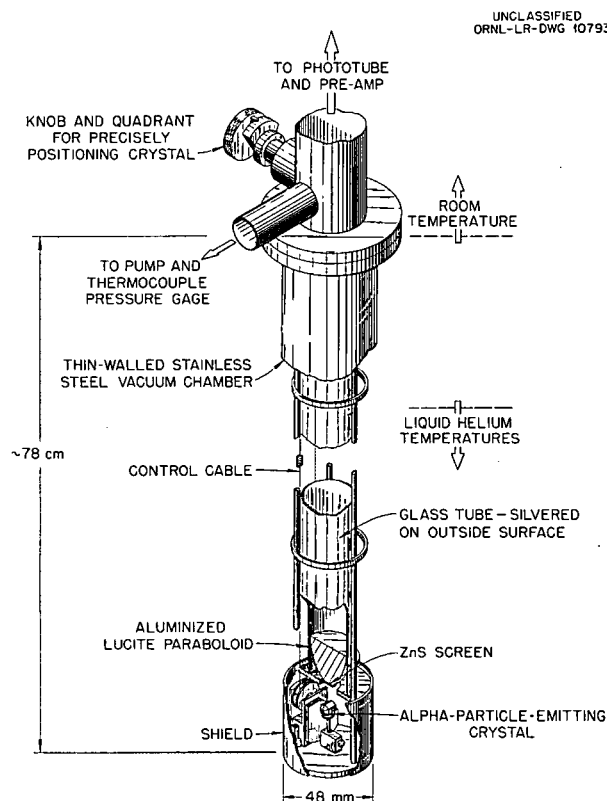


Fig. 1. Apparatus for Observing Anisotropic Alpha-Particle Emission.

<sup>1</sup>L. D. Roberts et al., *Phys. Semiann. Prog. Rep.* Sept. 10, 1955, ORNL-1975, p 45-47.

ZnS is transmitted upward to the photomultiplier. In this arrangement, counting rates of approximately 2500 per minute were obtained with negligible background. This is about 30 times greater than before. A device for remote rotation of the crystal was incorporated, by means of which the angular distribution of alpha-particle emission,  $W(\theta)$ , could be measured.

Figure 2 gives results on the angular distribution of alpha-particle emission obtained at a temperature of 1.16°K for  $\text{Np}^{237}$  nuclei. Other data taken in this apparatus confirmed the results reported earlier<sup>1</sup> and show that the angular distribution is approximately given by

$$(1) \quad W(\theta) = 1 + A_2 P_2(\cos \theta) ,$$

where  $A_2$  is negative and proportional to the calculated nuclear alignment (i.e., approximately proportional to  $1/T$ ) within experimental error. The value of  $A_2$  is  $-0.068$  at the lowest temperature (1.16°K). Both sets of data were obtained with the same crystal; however, preliminary work with another crystal shows agreement with the earlier results.

The following ideas<sup>2</sup> are probably correct in connection with the electronic structure of the

uranyl and neptunyl ions. The uranium valence orbitals in the  $\text{UO}_2^{++}$  group are very likely  $5f$ ,  $6d$ , and  $7s$ , or linear combinations of these, and must accommodate four electrons of the six originally associated with the uranium. Bonding orbitals of  $\sigma$  type can be formed by linear combinations of  $\sigma$  substates (i.e., those for which  $m_l = 0$ ), which may be denoted by  $5f_{\sigma}$ ,  $6d_{\sigma}$ , and  $7s$ . Two strongly directed hybrid orbitals can be formed in this way, one pointing toward each oxygen position in the linear group, giving rise to bonding by overlapping with  $2s2p_{z(\sigma)}$  hybrid orbitals on the two oxygens. These covalent bonds can accommodate the four electrons required. In the  $\text{NpO}_2^{++}$  ion, there is one extra  $5f$  electron, which is thought to be repelled by the charge cloud of the shared electrons, thus having a lowest energy state  $5f_{\phi}$  ( $m_l = \pm 3$ ) and a distribution largely in the plane perpendicular to the  $c$  axis, along which the  $\text{NpO}_2^{++}$  (or  $\text{UO}_2^{++}$ ) groups lie. Thus the major bonding orbitals are thought to form a "column" of negative charge along the  $c$ -axis direction in both  $\text{UO}_2^{++}$  and  $\text{NpO}_2^{++}$ , and the extra  $5f$  electron in  $\text{NpO}_2^{++}$  is thought to go into a more planar distribution around the Np position. The "planar"  $5f_{\phi}$  orbital in  $\text{NpO}_2^{++}$  has been estimated<sup>2</sup> to have a smaller effect on the nuclear quadrupole coupling than do the  $\sigma$  bonding orbitals, so that, for a positive nuclear quadrupole moment, one would expect the nucleus to orient along the  $c$  axis of the crystal in both  $\text{UO}_2^{++}$  and  $\text{NpO}_2^{++}$  when it is cooled to sufficiently low temperatures.

Whether the above estimate is correct – that is, whether the quadrupole coupling constant,  $Q$ , is positive or negative – was not resolved by microwave measurements in the  $\text{NpO}_2^{++}$  case,<sup>3</sup> and the sign of  $Q$  cannot be measured by such techniques in the case of  $\text{UO}_2^{++}$ . It is possible, however, to determine the sign of  $Q$ , at least in the  $\text{NpO}_2^{++}$  case, by alpha-particle anisotropy measurements below 1°K, and an experiment to answer this question is in progress.

In view of the above ideas on the electronic structure of the  $\text{UO}_2^{++}$  and  $\text{NpO}_2^{++}$  ions in the rubidium nitrate salts, it was postulated that  $\text{U}^{233}$  nuclei could probably be aligned in the isomorphous salt  $\text{UO}_2\text{Rb}(\text{NO}_3)_3$ , since  $\text{U}^{233}$  is thought<sup>4</sup> to have

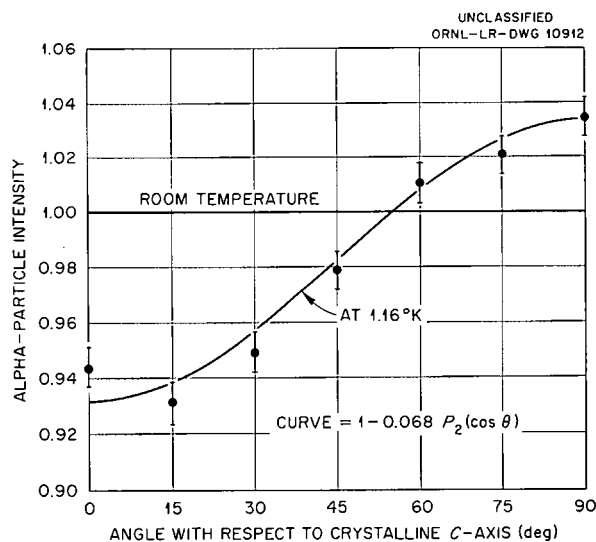


Fig. 2. Angular Distribution of Alpha-Particle Emission from Aligned  $\text{Np}^{237}$  in  $\text{NpO}_2\text{Rb}(\text{NO}_3)_3$ .

<sup>3</sup>B. Bleaney, et al., *Phil. Mag.* 45, 992 (1954).

<sup>4</sup>K. L. Vander Sluis and J. R. McNally, Jr., *J. Opt. Soc. Amer.* 44, 87 (1954).

a large nuclear electric quadrupole moment. In this case the quadrupole coupling term is the only important term in the spin Hamiltonian; that is,

$$(2) \quad \mathcal{H} = Q \left[ I_z^2 - \frac{1}{3} I(I+1) \right],$$

and the alignment is thus a pure Pound<sup>5</sup> alignment. Accordingly, preliminary experiments on  $U^{233}$  alpha-particle anisotropy have been carried out in the apparatus of Fig. 1. The data of Fig. 3, which shows  $W(0^\circ)/W(90^\circ)$  as a function of  $1/T$ , indicate that this expectation has been confirmed, and preliminary angular-distribution measurements indicate that the distribution has predominantly a  $P_2(\cos \theta)$  departure from isotropy, with a coefficient of approximately  $-0.05$  at  $1.15^\circ\text{K}$ . A small amount (0.2%) of the  $NpO_2$  salt was added to the  $UO_2$  salt to provide an additional relaxation mechanism so that the nuclear alignment could take place more rapidly.

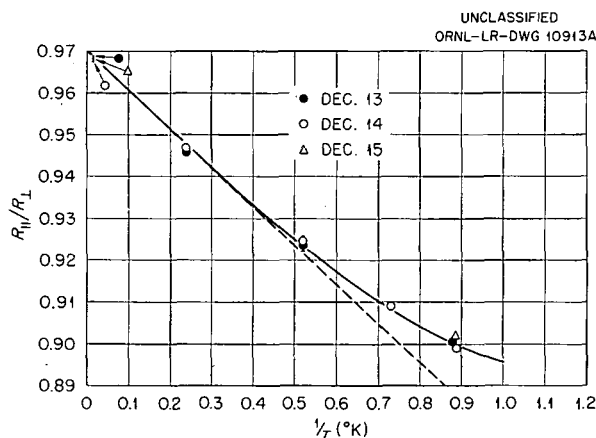


Fig. 3. Nuclear Alignment of  $U^{233}$  in  $UO_2Rb(NO_3)_3$ .

The behavior of the alpha-particle anisotropy is thus rather similar to that in  $Np^{237}$ , although the details are somewhat different. For example, it is now thought that the upward curvature in the data of Fig. 3 possibly has some validity, since certain subsidiary gas heat-transfer experiments have indicated reasonably small ( $\sim 0.008^\circ\text{K}$ ) temperature

differences between sample and helium bath at heat inputs similar to the alpha-particle heating produced in the  $U^{233}$  sample. If this is true, the curvature then corresponds to the onset of saturation of the nuclear alignment and indicates an extremely large quadrupole coupling in this salt ( $\sim 2 \text{ cm}^{-1}$ ); if not true, the present data set a lower limit of about  $0.04 \text{ cm}^{-1}$ . It should be noted that no microwave data on the magnitude of this coupling have been obtained. Further experiments designed to establish the angular distribution more accurately and to verify the presence or absence of curvature in measurements of the type shown in Fig. 3 are in progress.

M. E. Rose has shown<sup>6</sup> that, for an alpha-particle decay from a state of angular momentum  $j\hbar$  to a state  $j'\hbar$  in which the alpha particle carries off  $L$  units of angular momentum, the angular alpha-particle intensity distribution is given by

$$(3) \quad W_{LL}(\theta) = (-)^{j-j'} (2L + 1) \sum_{\nu} C_{00}^{LL\nu} W(jjLL; \nu j') G_{\nu} P_{\nu}(\cos \theta),$$

where a pure (one  $L$  value) transition occurs. This expression is the same as that for the case of gamma-ray emission from oriented nuclei except that the Clebsch-Gordan subscripts  $(0, 0)$  replace those in the gamma-ray theory  $(1, -1)$ .  $G_{\nu}$  in the above expression corresponds to the degree of nuclear alignment relative to a spatial axis; that is,

$$(4) \quad G_{\nu} = \sum_m (-)^{j-m} p_m C_{m-m}^{jj\nu},$$

where  $p_m$  is the probability of finding the nucleus in the magnetic substate  $m$ ; thus  $G_{\nu}$  is the temperature-dependent parameter in Eq. 3.

In the list below, the angular distribution to be expected [in terms of  $A_2$ , the coefficient of  $P_2(\cos \theta)$ ] is given for the calculated amount of alignment in  $Np^{237}O_2Rb(NO_3)_3$  at  $1.16^\circ\text{K}$ . All entries are

<sup>5</sup>R. V. Pound, *Phys. Rev.* **76**, 1410 (1949).

<sup>6</sup>In the preceding paper, this report.

based on an initial  $j = \frac{5}{2}$ , and the signs for  $A_2$  are for  $Q < 0$ .

$j'$	$L$	$A_2 (1.16^\circ\text{K})$
$\frac{3}{2}$	1	-0.0802
$\frac{5}{2}$	1	+0.0917
$\frac{7}{2}$	1	-0.0287
$\frac{3}{2}$	2	-0.0409
$\frac{5}{2}$	2	+0.0409
$\frac{7}{2}$	2	+0.0696
$\frac{9}{2}$	2	-0.0409
$\frac{5}{2}$	0,2	-0.0652

The last line of the list corresponds to the particular admixture of  $L = 0$  and  $L = 2$  which produces the largest negative value for  $A_2$ . There are nine known alpha-particle groups in the decay

of  $\text{Np}^{237}$ ; a tentative assignment of a decay scheme in which the rotational level scheme of Bohr and Mottelson was used as a criterion gave a maximum negative value for the over-all value of  $A_2$  at  $1.16^\circ\text{K}$  of  $-0.043$  for one parity assignment and  $-0.0576$  for a less likely parity assignment. These are to be compared with the observed value of  $-0.068$ . Both these calculations utilized the maximum possible interference value in the last line of the list for one term in the weighted sum of  $A_2$ ; it is, therefore, possible that the quadrupole and hyperfine structure couplings in the relatively concentrated (30%  $\text{NpO}_2$  in  $\text{U}^{238}\text{O}_2$ ) salts used are somewhat larger than in the dilute salt (1%  $\text{NpO}_2$ ) used in the microwave measurements of Bleaney *et al.*<sup>3</sup>

The decay scheme for  $\text{U}^{233}$  alpha emission is much simpler; only three important groups have been found, and it should be possible to analyze the situation when an accurate angular distribution is obtained. A new apparatus for this measurement has been constructed.

### THE ALPHA-PARTICLE MODEL OF $\text{C}^{12}$

A. E. Glassgold<sup>1</sup>

A. Galonsky

The alpha-particle model of  $\text{C}^{12}$  has been re-examined in the same spirit as Dennison's analysis<sup>2</sup> of  $\text{O}^{16}$ . For  $\text{C}^{12}$  the alpha particles are considered to be at the vertices of an equilateral triangle and permitted to undergo small vibrations as well as rigid-body rotations. The allowed states are restricted to those satisfying Bose statistics for the alpha particles. The excitation energy of a state is the sum of a rotational and a vibrational energy and depends upon the quantum numbers of the state and the values of three parameters - the size of the triangle (for the rotational energy) and the two force constants of the vibrational potential. The three constants have been chosen by fitting three alpha-particle-model states to the first three excited states of  $\text{C}^{12}$ :  $2^+$  at 4.43 Mev,  $0^+$  at 7.65

Mev, and a state of unknown spin and parity at 9.61 Mev. If there are not to be predicted many unobserved, low-lying levels of  $\text{C}^{12}$ , the 9.61-Mev state must be either  $1^-$  or  $2^+$ . The energy levels predicted by each of these two possibilities are indicated in Fig. 1, along with the observed levels in  $\text{C}^{12}$  below 15 Mev.

The  $2^+$  level at 4.43 Mev is a pure rotational state and determines the radius of an "equivalent" spherical nucleus to be  $(1.3 \times 10^{-13} \text{ cm}) (12)^{1/3}$ . This is in agreement with the size determined<sup>3</sup> by electron elastic scattering from  $\text{C}^{12}$ . The  $3^-$  level predicted to be at 5.53 Mev is also a pure rotational level, and there has as yet been no evidence for its existence. This is a serious objection to the validity of the model.

<sup>1</sup>Now at the University of Minnesota.

<sup>2</sup>D. M. Dennison, *Phys. Rev.* 96, 378 (1954).

<sup>3</sup>J. H. Fregeau and R. Hofstadter, *Phys. Rev.* 99, 1503 (1955).

UNCLASSIFIED  
ORNL-LR-DWG 13951

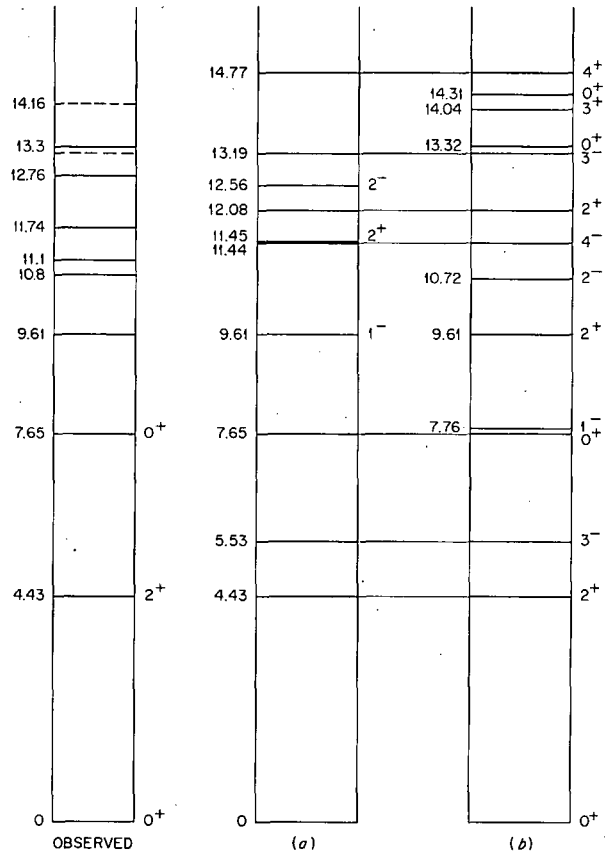


Fig. 1. Observed Levels of  $C^{12}$  and the Two Alternative Correlations with the Alpha-Particle Model.

### ENERGY LEVELS OF $C^{12}$

C. D. Moak

A. Galonsky

The energy-level structure of  $C^{12}$  is being studied through an examination of the proton spectrum produced in the reaction  $B^{10}(He^3, p)C^{12}$ . Since that spectrum has been examined before,<sup>1</sup> the major effort in this work is being directed toward a search for previously undisclosed levels. Under particular scrutiny is the region corresponding to excitations in  $C^{12}$  near 5.53 Mev. A  $3^-$

level at 5.53 Mev has been predicted<sup>2</sup> with the alpha-particle model of  $C^{12}$ .

Doubly charged  $He^3$  ions of 1.25 Mev from the 625-kv cascade accelerator are being used to bombard targets of metallic boron enriched to 97.1%  $B^{10}$ . The boron was obtained from the Stable Isotopes Division through the much-appreciated cooperation of P. S. Baker. Although some targets were made by painting Borag (a suspension in

<sup>1</sup>C. B. Bigham, K. W. Allen, and E. Almquist, *Phys. Rev.* 99, 631 (1955).

<sup>2</sup>A. E. Glassgold and A. Galonsky, the preceding paper, this report.

water of colloidal boron) on tantalum, for a set of more stable and uniform targets the authors are grateful to B. J. Massey and J. C. Smith of the Radioisotope Department, who made vacuum evaporations of the boron from a graphite crucible. Except for minor changes the proton spectrometer is that described by Moak and Wisseman in the last semiannual report.<sup>3</sup>

The proton spectrum in Fig. 1 reveals excitations in  $C^{12}$  up to approximately 17 Mev. Only the rather obvious identifications of the first few firmly established levels are given at this time. Note the striking difference in intensity of the 4.43- and 7.65-Mev groups. The small group between these two is probably not to be associated with the predicted 5.53-Mev level, but more likely, as indicated in the figure, with the ground state of  $C^{13}$ . More highly enriched  $B^{10}$  is being sought. With the aid of absorbers placed between target and detector, the well-known "stretching" technique is being applied to this spectrum so that it may be examined in more detail.

<sup>3</sup>C. D. Moak and W. R. Wisseman, *Phys. Semiann. Prog. Rep. Sept. 10, 1955*, ORNL-1975, p 13.

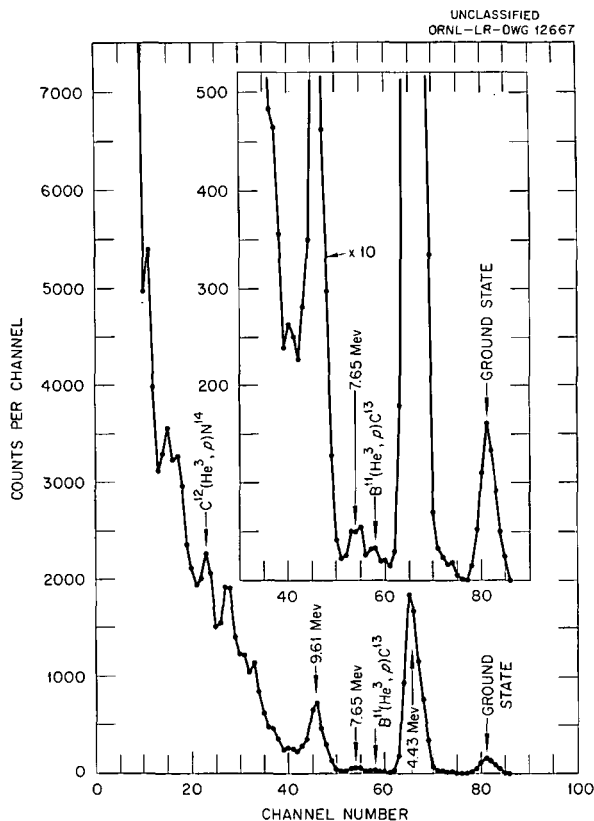


Fig. 1. Spectrum of Protons Observed in the Reaction  $B^{10}(He^3,p)C^{12}$ . The insert is drawn to 10 times the scale of the main figure.

### AN EMPIRICAL KINEMATICAL NUCLEAR MODEL

E. D. Klema

R. K. Osborn

An empirical parameter has been found which enables one to obtain nuclear shape factors from first-excited-state data of even-even nuclei in terms of the kinematical model used previously for the correlation of nuclear ground-state magnetic and quadrupole moments. From the shape factors so obtained, it is possible in seven cases to calculate the expected quadrupole moments of the neighboring odd-even nuclei and to compare these calculated values with the experimentally observed ones. Satisfactory agreement is found.

The parameter referred to provides an estimate of that fraction of the uniformly distributed mass

of a spheroidal rigid rotator which is presumed to participate in collective nuclear motion. This parameter, employed in conjunction with the explicit dependence of the spacing of rigid-rotator levels upon nuclear mass and shape, makes possible the determination of shape factors for even-even nuclei - that is, ratios of the semimajor to semiminor axes of the spheroids - from a knowledge of the energy of their spin 2 first excited states. This fractional mass parameter,  $k$ , is defined to be the ratio of the number of particles outside filled major shells (both protons and neutrons) or the number of holes, whichever is the

smaller, to the total number of particles in the nucleus.

This concept of fractional mass participating in nuclear rotations has a natural extension to, and provides a significant modification of, the interpretation of the data on electrodynamic transitions between nuclear ground states and rotational levels. This extension follows as a consequence of the assumption that the mass and charge densities of nuclear matter are uniform. Hence, if it is assumed that only a certain fraction of the uniformly distributed mass participates in collective motion, then for the sake of consistency it should be assumed that only the same fraction of the charge participates in the motion. This emphasizes the fact that the prescription proposed for the determination of the mass fraction in terms of the excess of particles or holes outside filled major shells must be interpreted as providing an estimate of only the magnitude of the fraction and not its character in the sense of a dependence upon the particular kind of particles outside the major

shells in a given case.

Since both rates for radiative transitions<sup>1</sup> from, and cross sections for coulomb excitation<sup>2</sup> of, nuclear rotational levels are proportional to the nuclear current, it is seen that the interpretation of the data relative to such processes will be explicitly dependent upon the charge fraction participating in the collective motion. Conversely, the static quadrupole moments depend upon the total nuclear charge. If both the spectroscopic and transition data on nuclear shapes are interpreted in the context of the present rigid-rotator model, satisfactory agreement is found among the shape factors as computed from quadrupole moments, the energies of first excited states of even-even nuclei, and cross sections for coulomb excitation of first excited states of even-even nuclei.

<sup>1</sup>J. M. Blatt and V. F. Weisskopf, *Theoretical Nuclear Physics*, Wiley and Sons, New York (1952).

<sup>2</sup>L. C. Biedenharn, J. L. McHale, and R. M. Thaler, *Phys. Rev.* 100, 376 (1955).

## GAMMA-RAY YIELDS FROM COULOMB EXCITATION

P. H. Stelson

F. K. McGowan

The complex gamma-ray spectrum resulting from the coulomb excitation of normal ruthenium (seven isotopes) has been resolved into the contributions of the different isotopes by the use of isotopically enriched targets. Metallic targets were prepared by sintering metallic powders into thin foils. A summary of the information obtained on the even-even isotopes of ruthenium is given in Table 1. The first column lists the nucleus to which the gamma ray given in column 2 is assigned. The observed yields of the gamma rays for different proton energies are given in columns 3 and 4. The transitions per microcoulomb (column 7) are deduced by the use of the isotopic enrichment (column 5) and the total internal conversion coefficient,  $\alpha_{total}$  (column 6). Column 8 gives the

evaluation of the integral

$$\int_0^E E \beta_2(\xi) \frac{dE}{d\rho x}$$

in units of  $\text{keV} \times \text{mg}/\text{cm}^2$ . The last column lists the values obtained for the reduced electric quadrupole transition probability,  $B(E2)_{ex}$ , in units of  $\text{cm}^4$ .

A summary of the information on the values for  $B(E2)_{ex}$  for the medium-weight even-even nuclei is given in Table 2.

Figure 1 is a plot of the ratio  $B(E2)_d/B(E2)_{sp}$  vs neutron number, [ $B(E2)_d = \frac{1}{5}B(E2)_{ex}$ ]. The  $B(E2)_{sp}$  is the Weisskopf single-particle estimate based on a radius given by  $1.2 \times 10^{-13} A^{1/3}$ .

PHYSICS PROGRESS REPORT

The positions of the excited states of even-even nuclei and the corresponding electric quadrupole transition probability show an interesting correlation. Figure 2 shows the observed  $B(E2)_{ex}$  (open circles) and also the quantity  $2.80/E$  (Mev) (solid circles). The value 2.80 was chosen to give the best over-all agreement.

TABLE 1. SUMMARY OF GAMMA-RAY YIELDS AND INFORMATION NEEDED TO OBTAIN THE REDUCED E2 TRANSITION PROBABILITIES FOR EXCITATION

Nucleus	$E_\gamma$ (keV)	$E_p$ (Mev)	$I$ (gammas per microcoulomb)	Isotopic Abundance (%)	$\alpha_{total}$	Transitions per Microcoulomb	$\int_0^E \frac{E_j g_2(\xi) dE}{dE/dpx}$	$B(E2)_{ex} \times 10^{48} \text{ cm}^4$
Ru <sup>104</sup>	358	3.0	$1.49 \times 10^6$	95.1	0.0188	$1.58 \times 10^6$	$2.60 \times 10^4$	0.840
		2.7	$8.80 \times 10^5$			$9.31 \times 10^5$	$1.56 \times 10^4$	0.825
		2.4	$4.39 \times 10^5$			$4.61 \times 10^5$	$8.17 \times 10^3$	0.780
		2.1	$1.94 \times 10^5$			$2.02 \times 10^5$	$3.52 \times 10^3$	0.793
		1.8	$6.11 \times 10^4$			$6.30 \times 10^4$	$1.09 \times 10^3$	0.796
		1.5	$1.01 \times 10^3$			$1.03 \times 10^4$	$1.88 \times 10^2$	0.759
Ru <sup>102</sup>	475	3.0	$6.85 \times 10^5$	94.24	0.0076	$7.19 \times 10^5$	$1.48 \times 10^4$	0.671
		2.7	$3.37 \times 10^5$			$3.52 \times 10^5$	$7.79 \times 10^3$	0.625
		2.4	$1.49 \times 10^5$			$1.54 \times 10^5$	$3.42 \times 10^3$	0.622
		2.1	$4.96 \times 10^4$			$5.09 \times 10^4$	$1.12 \times 10^3$	0.627
		1.8	$1.03 \times 10^4$			$1.04 \times 10^4$	$2.31 \times 10^2$	0.622
		1.5	$8.4 \times 10^2$			$8.35 \times 10^2$	$1.84 \times 10$	0.627
Ru <sup>100</sup>	540	3.0	$3.34 \times 10^5$	88.9	0.0052	$3.69 \times 10^5$	$1.06 \times 10^4$	0.483
		2.7	$1.73 \times 10^5$			$1.90 \times 10^5$	$5.15 \times 10^3$	0.510
		2.4	$7.05 \times 10^4$			$7.67 \times 10^4$	$2.02 \times 10^3$	0.525
		2.1	$1.84 \times 10^4$			$1.98 \times 10^4$	$5.64 \times 10^2$	0.485
Ru <sup>98</sup>	654	3.0	$1.04 \times 10^4$	65.1	0.0032	$1.55 \times 10^5$	$5.52 \times 10^3$	0.388
		2.7	$4.61 \times 10^4$			$6.83 \times 10^4$	$2.30 \times 10^3$	0.410
		2.4	$1.54 \times 10^4$			$2.26 \times 10^4$	$7.21 \times 10^2$	0.434
		2.1	$3.32 \times 10^3$			$4.81 \times 10^3$	$1.41 \times 10^2$	0.472
Ru <sup>96</sup>	840	3.0	$8.89 \times 10^4$	95.51	0.0017	$8.91 \times 10^4$	$1.75 \times 10^3$	0.703
		2.7	$3.33 \times 10^4$			$3.31 \times 10^4$	$5.54 \times 10^2$	0.826
		2.4	$4.56 \times 10^3$			$4.48 \times 10^3$	$1.04 \times 10^2$	0.595

TABLE 2. SUMMARY OF LEVEL POSITIONS AND REDUCED E2 TRANSITION PROBABILITIES FOR EXCITATION FOR MEDIUM-WEIGHT EVEN-EVEN NUCLEI

Nucleus	$E_\gamma$ (kev)	$B(E2)_{ex} \times 10^{48} \text{ cm}^4$	Nucleus	$E_\gamma$ (kev)	$B(E2)_{ex} \times 10^{48} \text{ cm}^4$
Mo <sup>94</sup>	874	0.242 ± 0.020	Pd <sup>108</sup>	433	0.625 ± 0.040
Mo <sup>96</sup>	775	0.259 ± 0.020	Pd <sup>110</sup>	374	0.739 ± 0.040
Mo <sup>98</sup>	780	0.237 ± 0.020	Cd <sup>106</sup>	630	0.425 ± 0.040
Mo <sup>100</sup>	530	0.530 ± 0.030	Cd <sup>108</sup>	630	0.47 ± 0.12
Ru <sup>96</sup>	840	(0.71 ± 0.12)*	Cd <sup>110</sup>	656	0.44 ± 0.02
Ru <sup>98</sup>	654	0.42 ± 0.03	Cd <sup>112</sup>	610	0.468 ± 0.020
Ru <sup>100</sup>	540	0.503 ± 0.020	Cd <sup>114</sup>	555	0.505 ± 0.025
Ru <sup>102</sup>	475	0.630 ± 0.025	Cd <sup>116</sup>	517	0.534 ± 0.020
Ru <sup>104</sup>	358	0.799 ± 0.030	Te <sup>126</sup>	673	0.46 ± 0.05
Pd <sup>104</sup>	555	0.466 ± 0.025	Te <sup>128</sup>	750	0.36 ± 0.04
Pd <sup>106</sup>	513	0.569 ± 0.020	Te <sup>130</sup>	850	0.31 ± 0.07

\*This value may be too large because of a possible contribution from a light-element impurity.

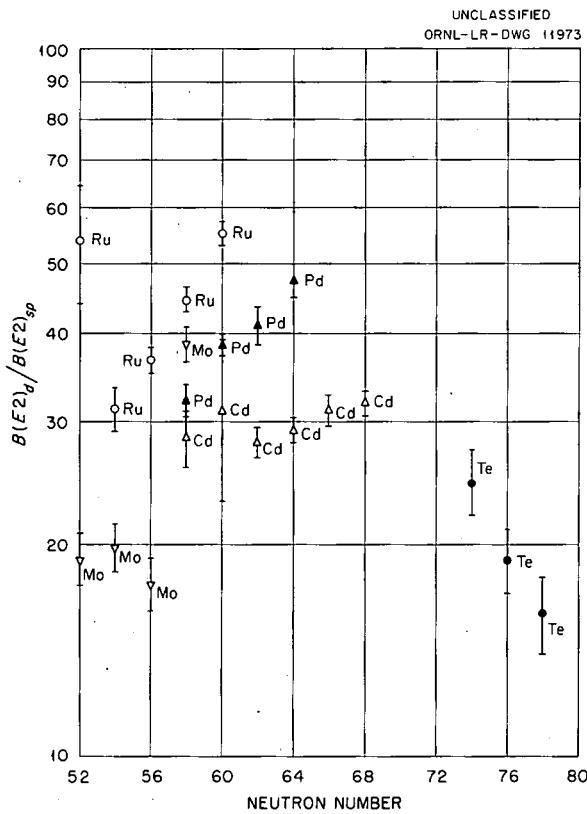


Fig. 1. Values for  $B(E2)_d / B(E2)_{sp}$  vs Neutron Number.

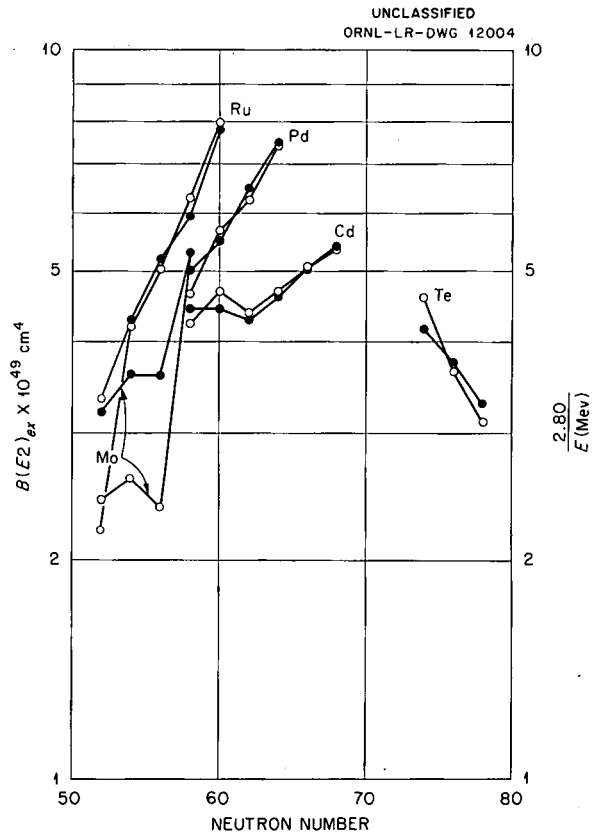


Fig. 2. Plots of  $B(E2)_{ex}$  (open circles, left-hand ordinate) and  $2.80/E$  (MeV) (solid circles, right-hand ordinate) vs Neutron Number.

POLARIZATION OF GAMMA RAYS FOLLOWING COULOMB EXCITATION

F. K. McGowan

P. H. Stelson

Coulomb excitation of levels in odd-A nuclei frequently results in the emission of mixed  $E2 + M1$  gamma rays. An angular-distribution measurement gives information on  $(E2/M1)^{1/2}$ , and this, combined with the cross section for excitation, yields the reduced transition probability for the magnetic dipole transition. However, several cases have been encountered in which the angular distribution was equally well fitted by two rather different values for  $(E2/M1)^{1/2}$ . Calculations of the polarization-direction correlation with polarization of the mixed radiation being measured showed that this correlation was quite different for the two values of  $(E2/M1)^{1/2}$ . A polarimeter based on the Compton scattering mechanism has been constructed, and its effectiveness has been determined by measurements of the known polarization of gamma rays from coulomb excitation of  $2^+$  levels in even-even nuclei. Polarization measurements of five transitions of the type  $\frac{3}{2}(E2 + M1)^{1/2}$  have resolved the ambiguity in the values of  $(E2/M1)^{1/2}$ .

Biedenharn and Rose<sup>1</sup> have expressed in a convenient form the polarization-direction correlation with polarization of the mixed radiation being measured. The correlation function has for a gamma-gamma cascade the form

$$w(\theta, \phi) = w_{\parallel} + \delta^2 w_{\perp} + 2\delta w_{\parallel\perp} ,$$

where  $\delta$  is  $(E2/M1)^{1/2}$ .  $w_{\parallel}$ ,  $w_{\perp}$ , and  $w_{\parallel\perp}$  are the polarization-direction correlation functions for pure  $2^{L_1}$  pole-pure  $2^{L_2}$  pole, pure  $2^{L_1}$  pole-pure  $2^{L_2+1}$  pole, and the interference term, respectively. For gamma rays following coulomb excitation, one replaces  $A_{\nu}$  appearing in the correlation functions above by  $A_{\nu} a_{\nu}$ , where  $a_{\nu}$  is the energy-dependent coefficient that enters in the coulomb excitation process, and takes  $L_1 = 2$  (electric quadrupole excitation).  $\phi$  is the angle between the direction of polarization and the normal to the plane defined by the proton beam and the gamma ray from coulomb excitation.

A cross section through the polarimeter in the plane defined by the proton beam and the gamma ray is shown in Fig. 1. The anthracene scatterer

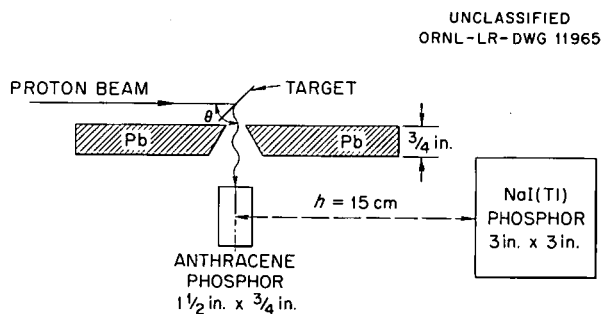


Fig. 1. Cross Section Through the Polarimeter in the Plane Defined by the Proton Beam and the Gamma Ray.

and the  $3 \times 3$  in. NaI crystal which are connected to photomultiplier tubes constitute the polarization-sensitive device. The NaI scintillation spectrometer detects the radiation scattered through a mean angle of 90 deg, and the anthracene scintillation spectrometer detects the Compton recoil electron. The detector of the scattered radiation rotates about an axis through the scatterer and the target. One measures  $N_{\parallel}/N_{\perp}$ , the ratio of the coincidence rate for the detector of the Compton scattered photon in the plane of the proton beam and the gamma ray to the coincidence rate for the perpendicular position. This ratio is connected to the ratio of the linear polarization intensities of the incident gamma ray through the relation

$$\frac{N_{\parallel}}{N_{\perp}} = \frac{P + R}{PR + 1} ,$$

where the quantity  $P$  is  $w(90^{\circ}, 90^{\circ})/w(90^{\circ}, 0^{\circ})$  in the notation of Biedenharn and Rose and  $R$  is the sensitivity of the polarimeter. For ideal geometry,  $R$  is simply the ratio of differential Compton cross section averaged over polarizations of the scattered photon; that is,

$$R = \frac{(d\sigma/d\Omega)_{\beta=\pi/2}}{(d\sigma/d\Omega)_{\beta=0}} ,$$

<sup>1</sup>L. C. Biedenharn and M. E. Rose, *Revs. Mod. Phys.* 25, 729 (1953).

and  $\beta$  is the angle between direction of polarization of the incident gamma ray and plane of scattering. The finite extent of the detectors reduces the value of the asymmetry ratio  $R$ . In practice one determines  $R$  by measurement of the known polarization of gamma rays having pure multipole character and for which the spins of the levels are known. In Table 1 the transitions that were used to calibrate the polarimeter are listed. The values for  $P$  are those for a thick target. The results for the asymmetry ratio  $R$  are also shown in Fig. 2

and may be compared with those for ideal geometry. The peculiar shape of  $R_{exp}$  as a function of  $E_\gamma$  is in part due to the choice of window widths used in the scintillation spectrometers.

For transitions of the type  $\frac{3}{2}(E2 + M1)\frac{1}{2}$  several cases have been encountered in which the angular distribution was equally well fitted by two rather different values for  $(E2/M1)^{1/2}$ . These cases are listed in Table 2, along with the calculated values of  $P$  and the experimental results. The coincidence counting rate ranged from 1 to 6 counts/sec for a beam current between 0.5 to 1.0  $\mu\text{a}$  on a thick target and the random coincidence rate was 0.1% of this rate, or less. For these five cases a measurement of the polarization-direction correlation clearly removes the ambiguity in the value of  $(E2/M1)^{1/2}$ .

Directional angular-distribution measurements complemented by polarization-direction measurements of gamma rays following coulomb excitation appear to be valuable for use in the nuclear spectroscopy of low-lying nuclear levels. In the past, polarization-direction correlation measurements of successive nuclear radiations were performed primarily to determine the relative parities of excited states involving the emission of pure multipole radiation. In this case, if the angular distribution is isotropic, the polarization-direction correlation is also isotropic; that is,  $P(\theta) = 1$ . For mixed transitions, if the angular distribution is isotropic, the polarization-direction correlation is not necessarily isotropic; that is,  $P(\theta) \neq 1$ . As an example, the directional correlation for the sequence  $\frac{1}{2}(E2)\frac{3}{2}(E2 + M1)\frac{1}{2}$  is isotropic for  $(E2/M1)^{1/2} = -3.65$ , but  $P(\theta = \pi/2)$  is 2.52 if the polarization direction of the mixed radiation

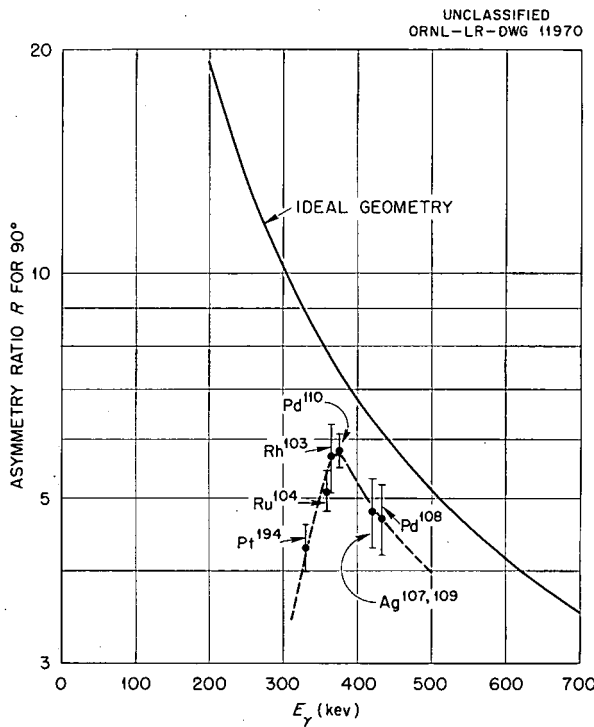


Fig. 2. Asymmetry Ratio  $R$  as a Function of  $E_\gamma$  for Both Ideal and Finite Geometry.

TABLE 1. SUMMARY OF TRANSITIONS USED TO CALIBRATE POLARIMETER

Nucleus	$E_\gamma$ (keV)	$E_p$ (MeV)	Transition	Character	$P(\theta = \pi/2)$	$(N_{  }/N_{\perp})_{exp}$	$R$
Pt <sup>194</sup>	330	4.0	2 → 0	E2	2.173	0.626 ± 0.009	4.3 ± 0.3
Ru <sup>104</sup>	358	2.7	2 → 0	E2	2.511	0.551 ± 0.007	5.1 ± 0.3
Pd <sup>110</sup>	374	2.7	2 → 0	E2	2.605	0.522 ± 0.006	5.8 ± 0.3
Pd <sup>108</sup>	433	3.0	2 → 0	E2	2.607	0.550 ± 0.016	4.7 ± 0.5
Ag <sup>107,109</sup>	420	2.7	$\frac{5}{2} \rightarrow \frac{1}{2}$	E2	2.210	0.604 ± 0.015	4.8 ± 0.5
Rh <sup>103</sup>	365	2.7	$\frac{5}{2} \rightarrow \frac{1}{2}$	E2	2.071	0.607 ± 0.012	5.7 ± 0.6

PHYSICS PROGRESS REPORT

is measured. Such a case has already been encountered in our measurements. The angular distribution of the 300-keV gamma ray following coulomb excitation in Cd<sup>113</sup> was nearly isotropic, and the polarization-direction correlation was quite large.

Listed in Table 3 are reduced transition probabilities for decay for some odd-A nuclei deduced

from the angular-distribution and cross-section measurements.  $B(E2)_{sp}$  is taken to be

$$\frac{1}{4\pi} \left| \frac{3}{5} R_0^2 \right|^2,$$

where  $R_0$  is equal to  $1.2 \times 10^{-13} A^{1/3}$  cm.

TABLE 2. SUMMARY OF TRANSITIONS FOR WHICH A POLARIZATION MEASUREMENT HAS RESOLVED THE AMBIGUITY IN THE VALUE OF  $(E2/M1)^{1/2}$

Nucleus	$E_\gamma$ (keV)	$E_p$ (MeV)	Transition	$(E2/M1)^{1/2}$	$P(\theta = \pi/2)$	R	$N_{  }/N_{\perp}$	$(N_{  }/N_{\perp})_{exp}$	$P_{exp}$
Ag <sup>107,109</sup>	315	2.7	$3/2 \rightarrow 1/2$	-0.18	0.708	3.6	1.214	$1.24 \pm 0.02$	$0.68 \pm 0.04$
				-1.2	1.422	3.6	0.821		
Ag <sup>107</sup>	320	2.7	$3/2 \rightarrow 1/2$	-0.18	0.706	3.8	1.224	$1.25 \pm 0.02$	$0.68 \pm 0.04$
				-1.2	1.426	3.8	0.814		
Rh <sup>103</sup>	305	2.7	$3/2 \rightarrow 1/2$	-0.18	0.717	3.2	1.189	$1.19 \pm 0.02$	$0.71 \pm 0.04$
				-1.2	1.403	3.2	0.838		
Cd <sup>113</sup>	300	2.7	$3/2 \rightarrow 1/2$	0.29	0.537	3.1	1.366	$1.33 \pm 0.04$	$0.57 \pm 0.05$
				-4.0	1.861	3.1	0.733		
Cd <sup>111</sup>	342	2.7	$3/2 \rightarrow 1/2$	0.385	0.509	4.7	1.535	$1.44 \pm 0.04$	$0.56 \pm 0.04$
				-6.6	1.967	4.7	0.651		

TABLE 3. SUMMARY OF REDUCED TRANSITION PROBABILITIES FOR SOME ODD-A NUCLEI

Nucleus	$E_\gamma$ (keV)	Transition	$(E2/M1)^{1/2}$	$B(E2)_d \times 10^{48}$	$B(M1)_d$	$B(E2)_d/B(E2)_{sp}$
<sup>48</sup> Cd <sup>113</sup>	582	$5/2 \rightarrow 1/2$	$\infty$	$0.092 \pm 0.013$		28.4
	300	$3/2 \rightarrow 1/2$	0.29	$0.050 \pm 0.007$	$3.76 \times 10^{-2}$	15.6
<sup>48</sup> Cd <sup>111</sup>	610	$5/2 \rightarrow 1/2$	$\infty$	$0.039 \pm 0.005$		12.3
	342	$3/2 \rightarrow 1/2$	0.385	$0.050 \pm 0.007$	$2.72 \times 10^{-2}$	15.7
<sup>47</sup> Ag <sup>107,109</sup>	420	$5/2 \rightarrow 1/2$	$\infty$	$0.122 \pm 0.018$		39.4
	315	$3/2 \rightarrow 1/2$	-0.18	$0.113 \pm 0.017$	$2.62 \times 10^{-1}$	37.3
<sup>45</sup> Rh <sup>103</sup>	365	$5/2 \rightarrow 1/2$	$\infty$	$0.120 \pm 0.018$		41.5
	305	$3/2 \rightarrow 1/2$	-0.18	$0.104 \pm 0.016$	$2.12 \times 10^{-1}$	35.2
<sup>42</sup> Mo <sup>95</sup>	203	$3/2 \rightarrow 5/2$	-0.8	$0.048 \pm 0.006$	$2.18 \times 10^{-3}$	18.7
		$5/2 \rightarrow 5/2$	0.4	$0.032 \pm 0.004$	$5.83 \times 10^{-3}$	12.5
		$5/2 \rightarrow 5/2$	0.8	$0.032 \pm 0.004$	$1.46 \times 10^{-3}$	12.5

POLARIZATION OF GAMMA RAYS IN Ta<sup>181</sup>

F. K. McGowan

P. H. Stelson

Excited states at 137, 480, and 612 keV in Ta<sup>181</sup> are observed following the β<sup>-</sup> decay of Hf<sup>181</sup>. Directional angular-correlation measurements of the 132-480-keV gamma-ray cascade have indicated two possible spin assignments for the 480- and 612-keV states.<sup>1,2</sup> The spin assignment  $\frac{5}{2}(E2)\frac{9}{2}(E2 + M1)\frac{7}{2}$  for the 132-480-keV cascade<sup>1</sup> hinged on the assumption that the angular distribution is strongly perturbed by a time-dependent interaction which could be present in a source in the liquid state. This assignment is also compatible with the measured K-shell internal conversion coefficient.<sup>3</sup> The main objection to this assignment is that one would expect the 612-keV transition to be M1 or E2 radiation. For E2 single-particle transitions one would expect the 612-keV transition to be 2000 times faster than the 132-keV transition, but instead it is observed to be about 65 times slower. The other assignment<sup>2</sup>  $\frac{1}{2}(E2)\frac{5}{2}(E2 + M1)\frac{7}{2}$  for the 132-480-keV cascade removes the objection concerning the 612-keV transition, since the transition would be M3 and would not compete favorably with the 132-keV transition. Furthermore, this assignment requires only a weak perturbation from the time-dependent interaction for the 480-keV state. The ratio of E2/M1 deduced from this assignment is not in agreement with the measured K-shell internal conversion coefficient for the 480-keV transition.

A calculation of the expected polarization-direction correlation with polarization measurement

of mixed radiation in the 480-keV transition showed that this correlation was quite different for the two spin assignments. The results are given in Table 1. The ratio P of polarization intensities is  $W(90^\circ, \phi = \pi/2)/W(90^\circ, \phi = 0)$  in the notation of Biedenharn and Rose,<sup>4</sup> and G<sub>2</sub> and G<sub>4</sub> are the attenuation coefficients which represent the effect of perturbing interaction in the intermediate state of the nucleus. Here φ is the angle between the direction of polarization and the normal to the plane of the two gamma rays.

A polarimeter based on the Compton scattering mechanism has been constructed, and its effectiveness has been determined by measurements of the known polarization of gamma rays following coulomb excitation of 2<sup>+</sup> levels in even-even nuclei (see the preceding section, "Polarization of Gamma Rays Following Coulomb Excitation"). A cross section through the polarimeter in the plane defined by the two gamma rays is shown in Fig. 1.

<sup>4</sup>L. C. Biedenharn and M. E. Rose, *Revs. Mod. Phys.* 25, 729 (1953).

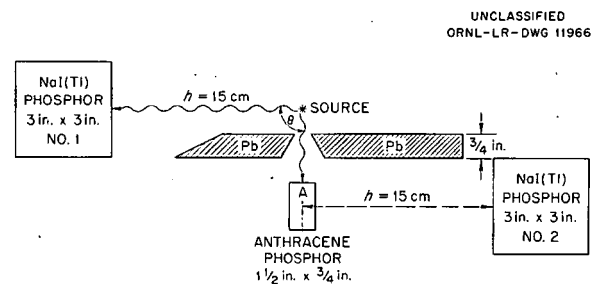


Fig. 1. Cross Section Through the Polarimeter in the Plane Defined by the Two Gamma Rays.

<sup>1</sup>F. K. McGowan, *Phys. Rev.* 93, 471 (1954).

<sup>2</sup>H. Paul and R. M. Steffen, *Phys. Rev.* 98, 231 (1955).

<sup>3</sup>F. K. McGowan, *Phys. Rev.* 93, 163 (1954).

TABLE 1. THE RATIO OF POLARIZATION INTENSITIES

Spin Sequence	(E2/M1) <sup>1/2</sup>	G <sub>2</sub>	G <sub>4</sub>	P*
$\frac{5}{2}(E2)\frac{9}{2}(E2 + M1)\frac{7}{2}$	-1.7	0.735	0.497	1.10
$\frac{1}{2}(E2)\frac{5}{2}(E2 + M1)\frac{7}{2}$	6.3	1.0	1.0	0.67
$\frac{1}{2}(E2)\frac{5}{2}(E2 + M1)\frac{7}{2}$	6.3	0.20	0.11	0.91

\*The calculations include also the effect of the finite extent of detector No. 1.

One measures  $N_{||}/N_{\perp}$ , the ratio of the triple-coincidence rate for the detector of the Compton scattered photons in the plane of the two gamma rays to the triple-coincidence rate for the perpendicular position. This ratio and  $P$  are connected through the relation

$$\frac{N_{||}}{N_{\perp}} = \frac{P + R}{PR + 1}$$

where  $R$  is the sensitivity of the polarimeter. For ideal geometry,  $R$  is simply the ratio of differential Compton cross section averaged over polarizations of the scattered photon; that is,

$$R = \frac{(d\sigma/d\Omega)_{\beta=\pi/2}}{(d\sigma/d\Omega)_{\beta=0}}$$

and  $\beta$  is the angle between direction of polarization of the incident photon and plane of scattering. For our polarimeter we chose a mean scattering angle of 90 deg. The finite extent of the detectors will reduce the value of the asymmetry ratio  $R$ , and at 480 keV the value of  $R$  is  $4.0 \pm 0.5$ . The triple-coincidence counting rate was of the order of 1.2 counts/min, and the random rate was 12% of this rate. In Table 2 the experimental results are summarized for two runs of each type of source. The purpose of the measurement with a dry polycrystalline source of  $\text{HfF}_4$  was to check on possible systematic errors. With this source the directional angular correlation of the 132-480-keV cascade is known to be attenuated<sup>1</sup> to the "hard core" value for static interactions in the intermediate state. As a result one expects an attenuated value for  $P$ , which is the last entry in Table 1. The agreement between the experimental and the expected

TABLE 2. SUMMARY OF DATA FOR POLARIZATION-DIRECTION CORRELATION OF THE 132- TO 480-keV GAMMA-RAY CASCADE

Form of Source	$N_{  }/N_{\perp}$	$P_{\text{exp}}$
$\text{HfF}_4$ in 50% HF	$1.24 \pm 0.03$	$0.71 \pm 0.05$
$\text{HfF}_4$ in 50% HF	$1.19 \pm 0.05$	
Polycrystalline $\text{HfF}_4$	$1.09 \pm 0.03$	$0.88 \pm 0.05$
Polycrystalline $\text{HfF}_4$	$1.07 \pm 0.03$	

values of  $P$  is quite good for the two types of sources, and we conclude that the correct spin assignment is  $\frac{1}{2}(E2)\frac{5}{2}(E2+M1)\frac{7}{2}$ .

The transition probabilities for electromagnetic radiation are known for all the transitions from the low-lying states in  $\text{Ta}^{181}$  either from direct lifetime measurements or from coulomb excitation. A decay scheme of  $\text{Ta}^{181}$ , with the spin assignments of the excited states and the character of the gamma rays, is shown in Fig. 2. Listed in Table 3 are reduced transition probabilities for decay, and these are compared with those expected for single-particle transitions. The values given for  $B(E2)$  and  $B(M1)$  are actually those for the quantities  $B(E2)/e^2$  and  $B(M1)/(e\hbar/2mc)^2$ .  $B(M1)_{sp}$  is approximately unity, and  $B(E2)_{sp}$  is taken to be

$$\frac{1}{4\pi} \left| \frac{3}{5} R_0^2 \right|^2$$

where  $R_0$  is equal to  $1.2 \times 10^{-13} A^{1/3}$  cm. The total internal conversion coefficients  $\alpha_t$  are taken from Rose *et al.*<sup>5</sup> The variation in the reduced transition probabilities is quite large. The 612-keV transition is probably M3, and the ratio  $B(M3)_d/B(M3)_{sp}$  is 0.26.

<sup>5</sup>M. E. Rose *et al.*, *Phys. Rev.* **83**, 79 (1951) and *Tables of Internal Conversion Coefficients* privately circulated by Dr. Rose.

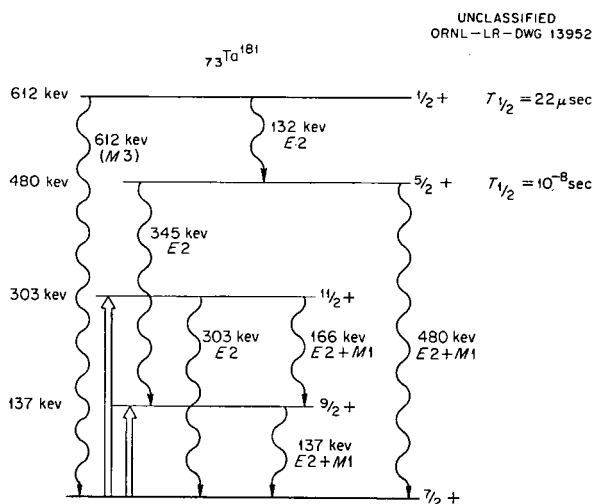


Fig. 2. Decay Scheme of  $\text{Ta}^{181}$  with the Spin Assignments of the Excited States and the Character of the Gamma Rays. The arrows pointing upward indicate excitation by coulomb excitation.

TABLE 3. SUMMARY OF REDUCED TRANSITION PROBABILITIES FOR  $T_{\alpha}^{181}$ 

$E_{\gamma}$ (keV)	$(E2/M1)^{1/2}$	$\alpha_t$	$B(E2)_d \times 10^{48} \text{ cm}^4$	$B(E2)_d/B(E2)_{sp}$	$B(M1)_d$
137	0.5	2.09	2.00	330	$1.05 \times 10^{-1}$
166	0.5	1.08	3.05	503	$2.66 \times 10^{-1}$
303	$\infty$	0.079	0.416	68.5	
132	$\infty$	1.34	$2.74 \times 10^{-5}$	$4.5 \times 10^{-3}$	
343	$\infty$	0.0574	$1.58 \times 10^{-4}$	$2.6 \times 10^{-2}$	
480	6.3	0.024	$1.82 \times 10^{-4}$	$3.0 \times 10^{-2}$	$7.4 \times 10^{-7}$

## DIRECTIONAL ANGULAR CORRELATIONS OF GAMMA RAYS IN CASCADE

E. D. Klema

## STRONTIUM-88

The directional angular correlation of the 909–1850-keV gamma-gamma cascade in  $\text{Sr}^{88}$  has been measured with a coincidence scintillation spectrometer using NaI detectors. Because the spins and parities of the initial and intermediate states of the cascade at 2760 and 1850 keV are known to be  $3^-$  and  $2^+$ , respectively, from other measurements,<sup>1</sup> the precise measurement of the angular correlation is a sensitive test of the purity of the first transition of the cascade.

In order to achieve the maximum precision obtainable at present in the measurement of the coefficients of the angular-distribution function, a statistical ratio test has been used to determine the proper number of terms with which to represent the data. In addition, the effect of errors in centering the source on the axis of rotation of the movable detector has been considered carefully in terms of the theory developed by Breitenberger.<sup>2</sup>

The observed correlation function obtained with a dilute  $\text{YCl}_3$  aqueous solution source, after correction for the finite angular resolution of the

detectors, is given by

$$W(\theta) = 1 - (0.0699 \pm 0.0025) P_2(\cos \theta) .$$

The theoretical correlation function for the sequence  $3(D) 2(Q) 0$  is

$$W(\theta) = 1 - 0.07143 P_2(\cos \theta) ;$$

hence, it is concluded that both the transitions of the cascade are pure multipoles.

## LUTETIUM-175

The angular correlation of the 89.3–342.9-keV gamma-gamma cascade in  $\text{Lu}^{175}$  has been measured and found to be given by

$$W(\theta) = 1 - (0.0006 \pm 0.0043) P_2(\cos \theta) + (0.0051 \pm 0.0074) P_4(\cos \theta) .$$

This cascade is of particular interest for several reasons. It is known that both the gamma rays of the cascade are mixtures from the  $K$  conversion coefficient measurement on the 342.9-keV gamma ray and from the  $L$ -subshell conversion coefficient measurements on the 89.3-keV gamma ray.<sup>3</sup> The

<sup>1</sup>G. R. Bishop and J. P. Perez y Jorba, *Phys. Rev.* 98, 89 (1955).

<sup>2</sup>E. Breitenberger, *Phil. Mag.* 45, 497 (1954).

<sup>3</sup>J. P. Mize, M. E. Bunker, and J. W. Starnes, *Phys. Rev.* 100, 1390 (1955).

fact that the observed correlation function is isotropic greatly simplifies the analysis of the results and makes an unambiguous interpretation possible. Finally, these nuclear levels have been discussed in terms of the Bohr-Mottelson strong-coupling unified model.<sup>4</sup>

The present correlation measurement may be in doubt, because it may represent an attenuation of the true correlation function due to external fields, since in this case the lifetime of the intermediate state of the cascade has not been measured and since the parent Hf<sup>175</sup> decays by electron capture. However, both liquid and solid sources have been used and have yielded the same results. It would seem highly unlikely that the observed isotropy is the result of perturbations, since interactions can in certain circumstances lead to isotropy in the case of liquid sources, while in the case of solid sources there are "hard-core" values of the coefficients of the correlation function which do not vanish.

Assuming that the observed correlation function is unperturbed, one can make unique spin assignments to the initial and intermediate states of the cascade. The expression for  $A_2$  in the function

$$W(\theta) = 1 + A_2 P_2(\cos \theta) + A_4 P_4(\cos \theta)$$

for the case of a mixed-mixed cascade can be written as the product of two factors, one involving only the first transition and the other involving only the second. The mixing ratio of the 342.9-keV gamma ray is known, and it can be shown that the factor involving this transition does not vanish. Thus the values of the mixing ratio of the 89.3-keV gamma ray for which  $A_2$  vanishes can easily be solved for, and the laborious calculation of the mixed-mixed correlation function needs to be done only for those spins which yield a value of the mixing ratio in agreement with that obtained from the *L*-subshell conversion coefficient measurements.

<sup>4</sup>D. M. Chase and L. Wilets, *Phys. Rev.* **101**, 1038 (1956).

All nine possible sequences of  $\frac{3}{2}, \frac{5}{2}, \frac{7}{2}, \frac{9}{2}, \frac{11}{2}(D+Q), \frac{5}{2}, \frac{7}{2}, \frac{9}{2}(D+Q), \frac{7}{2}$  with spin differences of one or two units between the states involved in a given transition have been considered. Only the sequence  $\frac{5}{2}(D+Q), \frac{5}{2}(D+Q), \frac{7}{2}$  gives a value for the mixing ratio of the 89.3-keV gamma ray which agrees with that obtained from the *L*-subshell conversion coefficient measurements. For this case the angular-correlation measurement yields a value of the square of the mixing ratio,  $\delta$ , of 0.15, to be compared with the *L*-subshell value of about 0.1. The corresponding coefficient of  $A_4$  is -0.002. The sequence  $\frac{7}{2}(D+Q), \frac{5}{2}(D+Q), \frac{7}{2}$ , for example, leads to values of  $\delta^2$  of 0.010 or 17.5.

#### HAFNIUM-177

The angular correlation of the 208.36–112.97-keV gamma-gamma cascade in Hf<sup>177</sup> has been measured and found to be given by

$$W(\theta) = 1 - (0.1614 \pm 0.0015) P_2(\cos \theta).$$

Again the levels involved in this cascade are of interest, since they have been discussed in terms of the unified model.<sup>4</sup> In addition, the spin of the ground state has recently been measured by F. A. Jenkins and O. R. Speck at Berkeley to be  $\frac{7}{2}$ , in disagreement with previous results. This has necessitated the re-examination of our early results on this cascade.<sup>5</sup>

This angular-correlation measurement should be free of perturbing effects, since an upper limit for the lifetime of the intermediate state has been measured to be  $4 \times 10^{-10}$  sec by F. K. McGowan and P. H. Stelson at this Laboratory and since the parent Lu<sup>177</sup> decays by beta emission.

The analysis of the data is complicated by the fact that a number of mixed-mixed correlation functions must be computed in detail. This work has not yet been completed.

<sup>5</sup>F. K. McGowan, E. D. Klema, and P. R. Bell, *Phys. Rev.* **85**, 152 (1952).

DECAY OF  $\text{Sb}^{125}$ 

N. H. Lazar

The gamma rays following the decay of  $\text{Sb}^{125}$  have been studied by means of scintillation spectrometry, and a decay scheme consistent with all the known facts has been deduced. The source was separated from the parent activity,  $\text{Sn}^{125}$ , in the spring of 1953, for a different investigation, and spectral measurements were carried out during 1954 and 1955. The scintillation spectrometers, coincidence arrangements, and associated electronic equipment used for these measurements have been described elsewhere.<sup>1</sup>

The pulse-height spectrum obtained with a source placed on the axis of a  $3 \times 3$  in. NaI(Tl) cylinder, 9.3 cm from the face of the crystal, is shown in Fig. 1. The results of an analysis of the spectrum into the individual gamma-ray components are also shown. For this analysis, use was made of the spectra of the 0.479- and 0.661-Mev gamma rays from  $\text{Be}^7$  and  $\text{Cs}^{137}$ , which were obtained under similar geometrical conditions, as a guide for the shapes of the individual gamma rays in  $\text{Sb}^{125}$ . The relative intensities of the gamma rays were then determined from the areas in the peaks

by using the empirical peak efficiencies previously determined.<sup>2</sup> Some assumptions involving the decay scheme were required in order to properly include the contribution from the summing of the 0.427- and 0.595-Mev gamma rays with x rays following conversion of the 0.035-Mev transition. However, the first two excited stages (Fig. 4) are well established from a study of the 58-day isomer of  $\text{Te}^{125}$ , and there should be little controversy over these assumptions. The results of these computations are indicated in the third column of Table 1. The existence of the weak gamma rays of 0.377 and 0.113 Mev was confirmed, as will be discussed below, by means of coincidence spectrometry.

The half life for  $\text{Sb}^{125}$  was determined by measuring the areas under the 595–637-Mev peaks observed with  $3 \times 3$  in. NaI(Tl) crystals with the source in the same geometry, in November of 1954 and 1955. The half life was found to be  $2.0 \pm 0.2$  years.

<sup>1</sup>N. H. Lazar and E. D. Klema, *Phys. Rev.* 98, 710 (1955).

<sup>2</sup>P. R. Bell, R. C. Davis, and N. H. Lazar, *Phys. Semiann. Prog. Rep. Sept. 10, 1955*, ORNL-1975, p 72.

TABLE 1. ENERGIES AND RELATIVE INTENSITIES OF GAMMA RAYS FROM  $\text{Sb}^{125}$ 

	Measured Energy (Mev)	Relative Intensity of Gamma Rays From Single-Crystal Data	Relative Intensity of Gamma Rays From Coincidence Data
$\gamma_1$	0.637	$0.23 \pm 0.02$	
$\gamma_2$	0.595	$0.88 \pm 0.09$	
$\gamma_3$	0.463	$0.31 \pm 0.03$	
$\gamma_4$	0.427	1.0	
$\gamma_5$	0.377	$0.038 \pm 0.008$	
$\gamma_6$	0.320		$0.0088 \pm 0.0020$
$\gamma_7$	0.214		$0.006 \pm 0.003$
$\gamma_8$	0.205		$0.008 \pm 0.002$
$\gamma_9$	0.175	$0.19 \pm 0.02$	
$\gamma_{10}$	0.175		$0.006 \pm 0.003$
$\gamma_{11}$	0.113	$0.014 \pm 0.007$	

PHYSICS PROGRESS REPORT

Coincidence spectra were obtained with all the main gamma rays. Figure 2 shows the results obtained in coincidence with a window placed over the region of 0.425 Mev. The intensity of the 0.175-Mev gamma ray is much too weak for it to be  $\gamma_9$  (see Table 1), and thus a second gamma ray with the same energy must be postulated.  $\gamma_{10}$  and the 0.210-Mev transition,  $\gamma_7$ , were found with the same relative intensity when the window was moved to either side of the peaks at 0.425 and 0.460 Mev. Coincidences with the window set at 0.115 Mev showed a peak at 0.37 Mev. The coincidences at

0.115 Mev, shown in Fig. 2, arose from the tail of the 0.37-Mev gamma ray falling into the window.

The window was moved to the 0.175-Mev region, and Fig. 3 shows the resultant coincident spectrum. The peak at 0.320 Mev must be caused by a previously unidentified gamma ray. The peak at 0.210 Mev cannot be in coincidence with  $\gamma_{10}$ , since there is insufficient energy in the decay, nor can it be the previously identified  $\gamma_7$  in coincidence with  $\gamma_9$  (see Fig. 4). Thus a second gamma ray of 0.21 Mev must be assumed.

The results of these measurements are contained in the decay scheme shown in Fig. 4. The spins of the first two states are those given by Hill

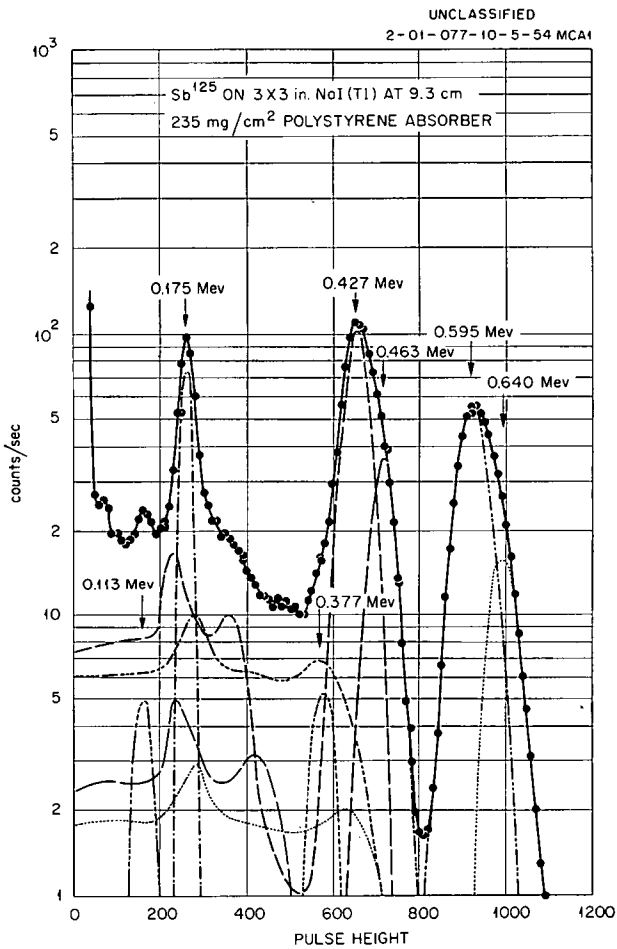


Fig. 1. Pulse-Height Spectrum from Gamma Rays of  $Sb^{125}$  Obtained with  $3 \times 3$  in. NaI(Tl) Crystal. The analysis of the spectrum into the individual gamma-ray components was performed by successive subtractions of the pulse-height distributions from the highest energy gamma ray.

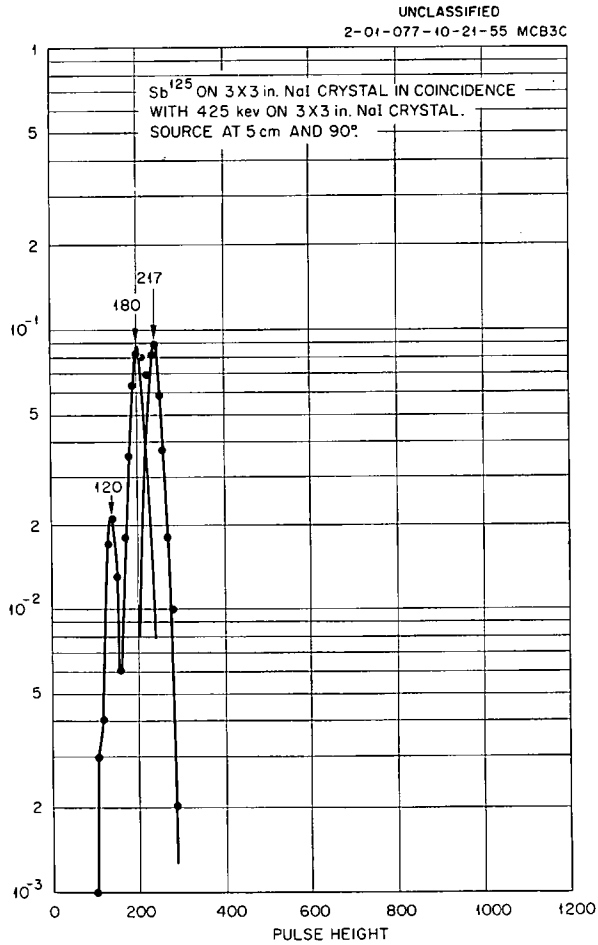


Fig. 2. Pulse-Height Spectrum in Coincidence with Pulses in the Region of 0.425 Mev.

et al.,<sup>3</sup> Siegbahn and Forsling,<sup>4</sup> and Bove and Axel<sup>5</sup> from the analysis of the Te<sup>125</sup> isomer. The remaining states probably have even parity. This conclusion is based on the comparative half lives

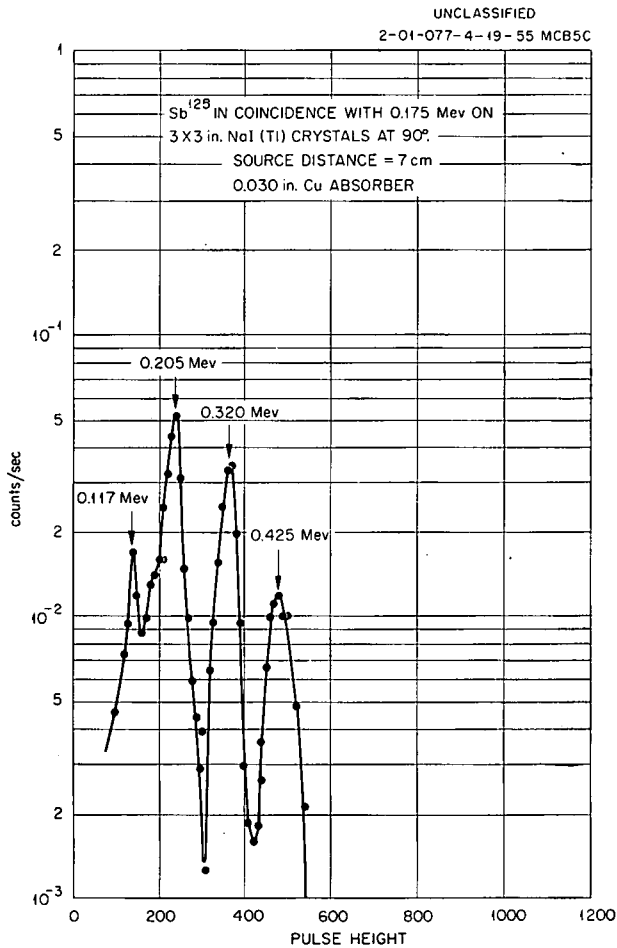


Fig. 3. Pulse-Height Spectrum in Coincidence with Pulses in the Region of 0.175 Mev.

(determined from the gamma-ray intensities) for the beta transitions which must feed the observed levels, and on the probable parity of the ground state of Sb<sup>125</sup>. However, the spins of the excited levels cannot be predicted from the gamma-ray intensities, since the transition probabilities are very likely greatly affected by configuration mixing and therefore cannot be simply calculated.

- <sup>3</sup>R. D. Hill et al., *Phys. Rev.* **75**, 324 (1949).
- <sup>4</sup>K. Siegbahn and W. Forsling, *Arkiv Fysik* **1**, 505 (1950).
- <sup>5</sup>J. C. Bove and P. Axel, *Phys. Rev.* **85**, 858 (1952).

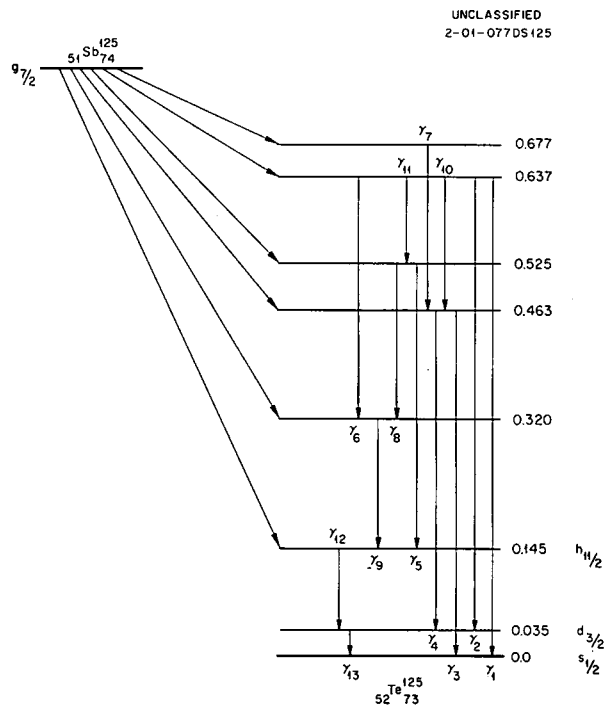


Fig. 4. Decay Scheme of Sb<sup>125</sup>.

THE 2.07-Mev RESONANCE IN THE  $C^{12}(n,n)C^{12}$  REACTION

J. E. Wills, Jr.

Some uncertainty has existed concerning the parameters describing the 2.07-Mev level in the  $C^{12}(n,n)C^{12}$  reaction.<sup>1</sup> Previous measurements had indicated that the level probably had a spin of  $J = 3/2$  and an even parity, but the resolution of measurements was insufficient to make possible a final decision.

Total cross-section measurements employing standard techniques were made in the vicinity of the resonance. A target of metallic lithium having a thickness of 1.7 kev served as a neutron source in the  $Li^7(p,n)Be^7$  reaction. Protons resolved in energy were supplied by the ORNL 5.5-Mv Van de Graaff generator. The carbon sample consisted of high-purity graphite having  $2.10 \times 10^{23}$  nuclei/cm<sup>2</sup>. Both Hornyak buttons and propane recoil counters biased against gamma radiation were used to detect

the neutrons. Results, shown in Fig. 1, indicate a spin of  $3/2$  and a width of 11 kev for the resonance.

Phase shifts used in calculating the cross sections were obtained from an analysis of angular distribution of neutrons scattered from carbon at 0.66, 1.05, 1.45, and 2.15 Mev. The first three distributions were analyzed as being due to potential scattering only, while the distribution at 2.15 Mev showed some interference due to the presence of a  $D_{3/2}$  resonance at 2.07 Mev. The distributions are shown in Figs. 2 through 5.

A measurement of the asymmetries of the angular distribution of scattered neutrons in the vicinity of the resonance showed the resonance to be due to  $d$  waves. The differential cross sections were measured at 51 and 121 deg in the laboratory, which corresponded to the angles in the barycentric system where  $\cos \theta$  was +0.58 and -0.58. The ratio of these measurements is shown in Fig. 6. The results are entirely consistent with the assumption of a resonance due to  $d$  waves.

<sup>1</sup>F. Ajzenberg and T. Lauritsen, *Revs. Mod. Phys.* 27, 77 (1955).

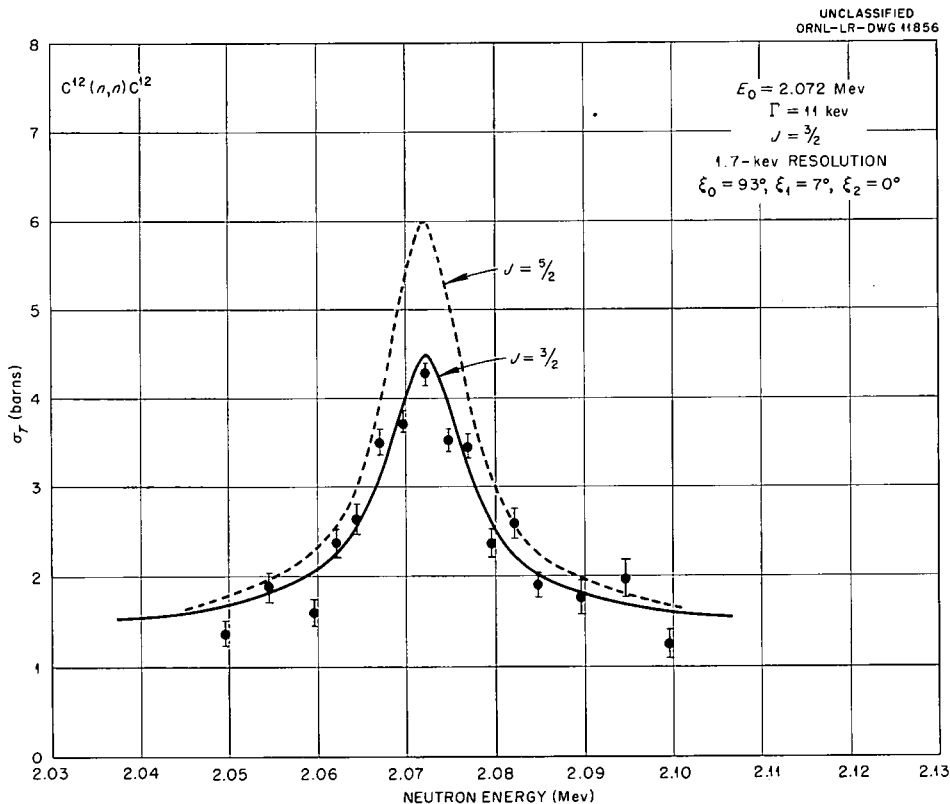


Fig. 1. Neutron Total Cross Section of Carbon.

UNCLASSIFIED  
ORNL-LR-DWG 11852

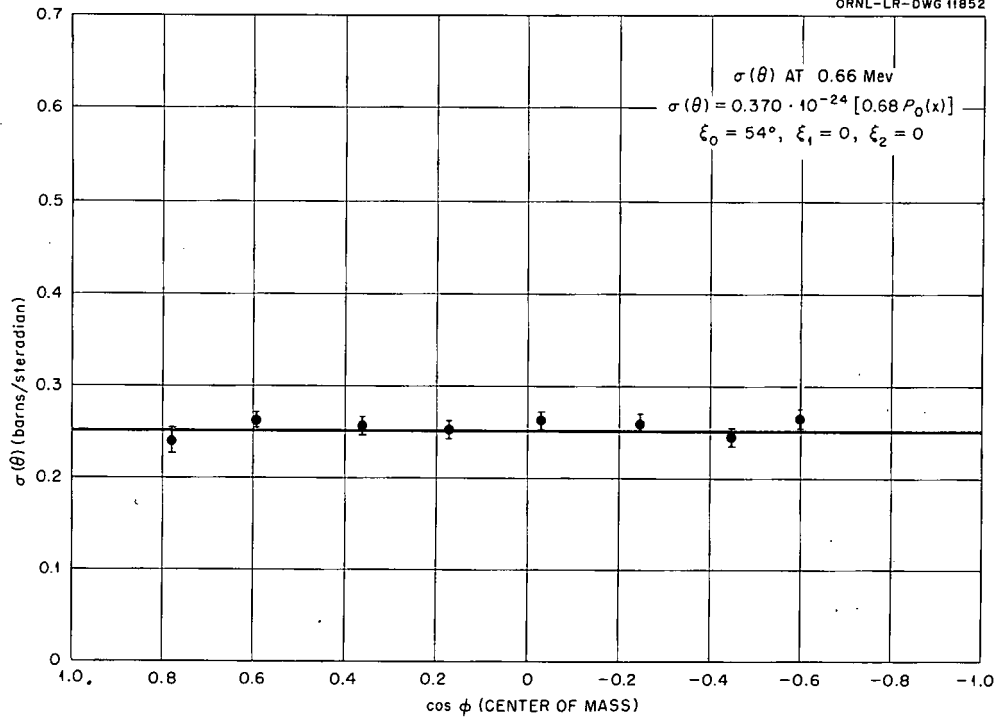


Fig. 2. Angular Distribution of Neutrons Scattered from Carbon at 0.66 Mev.

UNCLASSIFIED  
ORNL-LR-DWG 11853

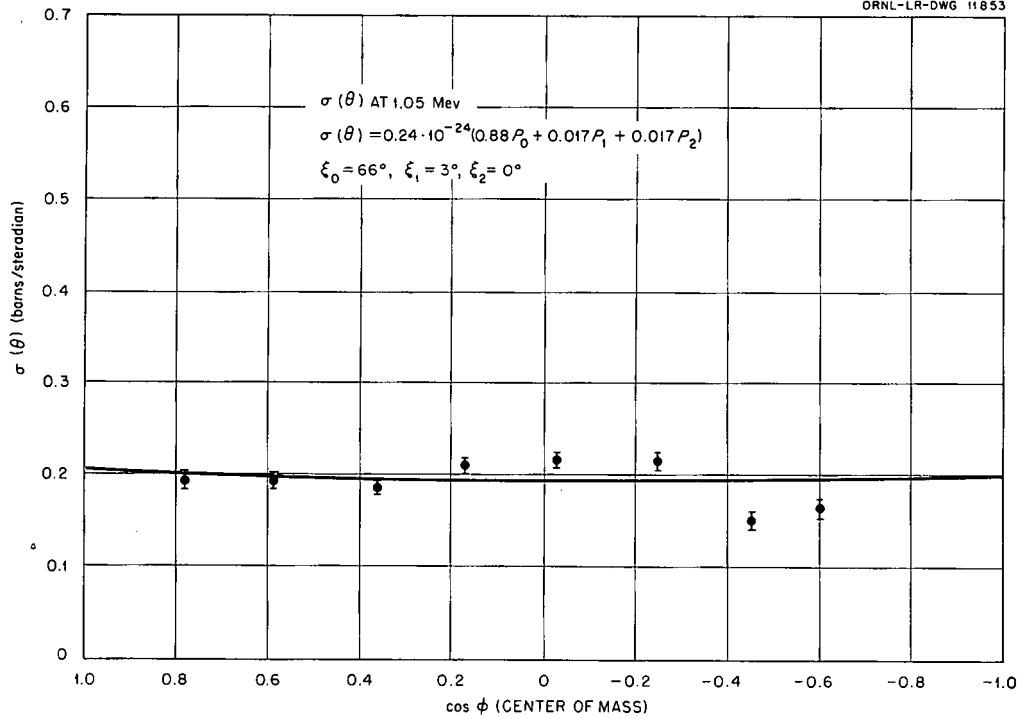


Fig. 3. Angular Distribution of Neutrons Scattered from Carbon at 1.05 Mev.

UNCLASSIFIED  
ORNL-LR-DWG 11854

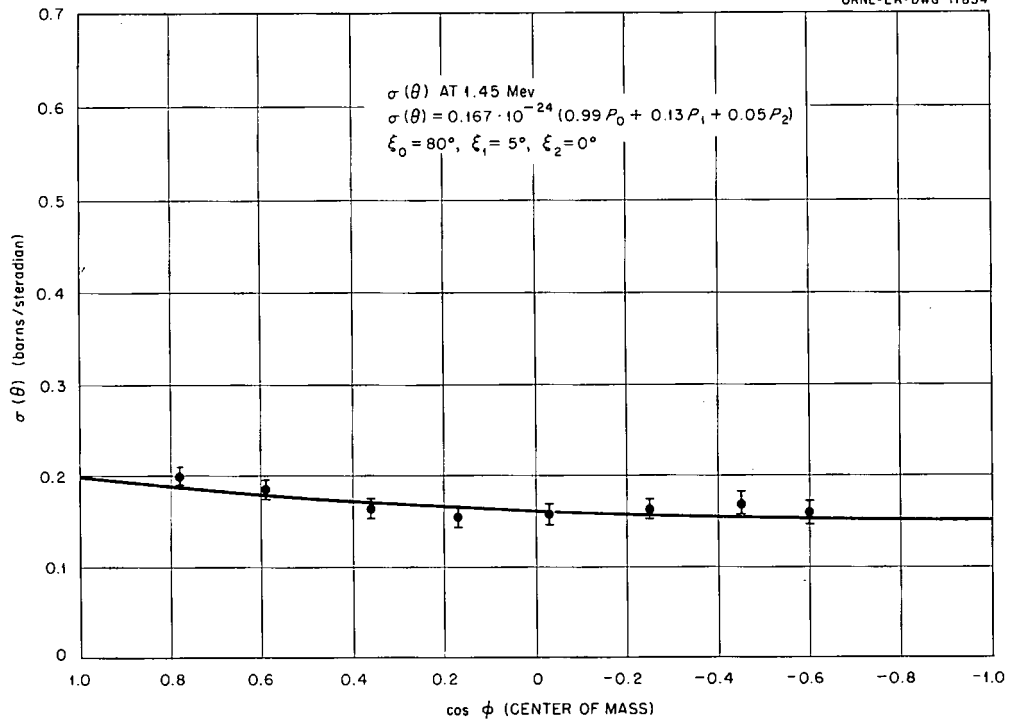


Fig. 4. Angular Distribution of Neutrons Scattered from Carbon at 1.45 Mev.

UNCLASSIFIED  
ORNL-LR-DWG 11855

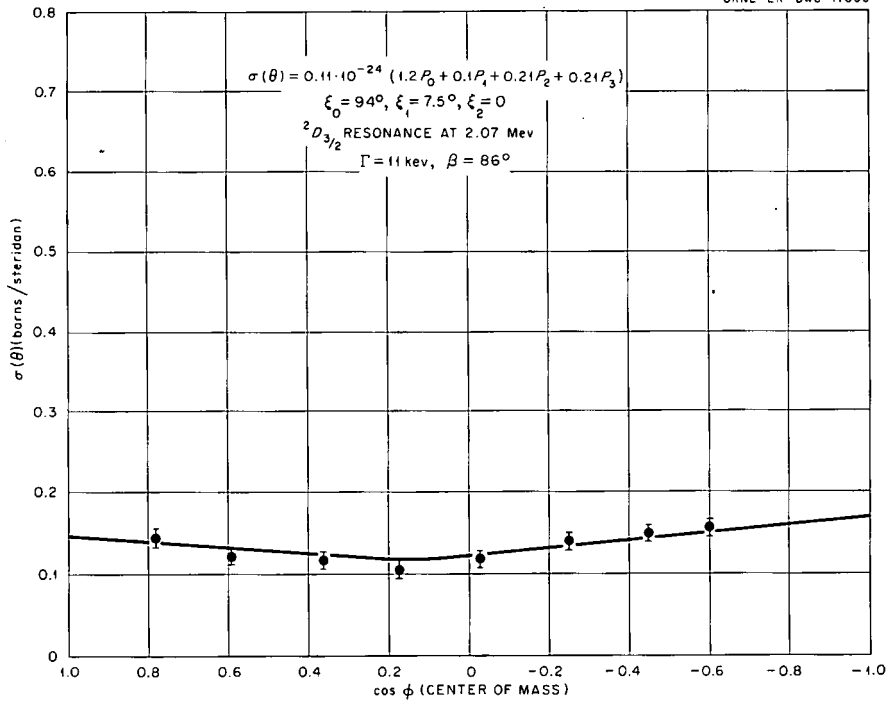


Fig. 5. Angular Distribution of Neutrons Scattered from Carbon at 2.15 Mev.

UNCLASSIFIED  
ORNL-LR-DWG 11857

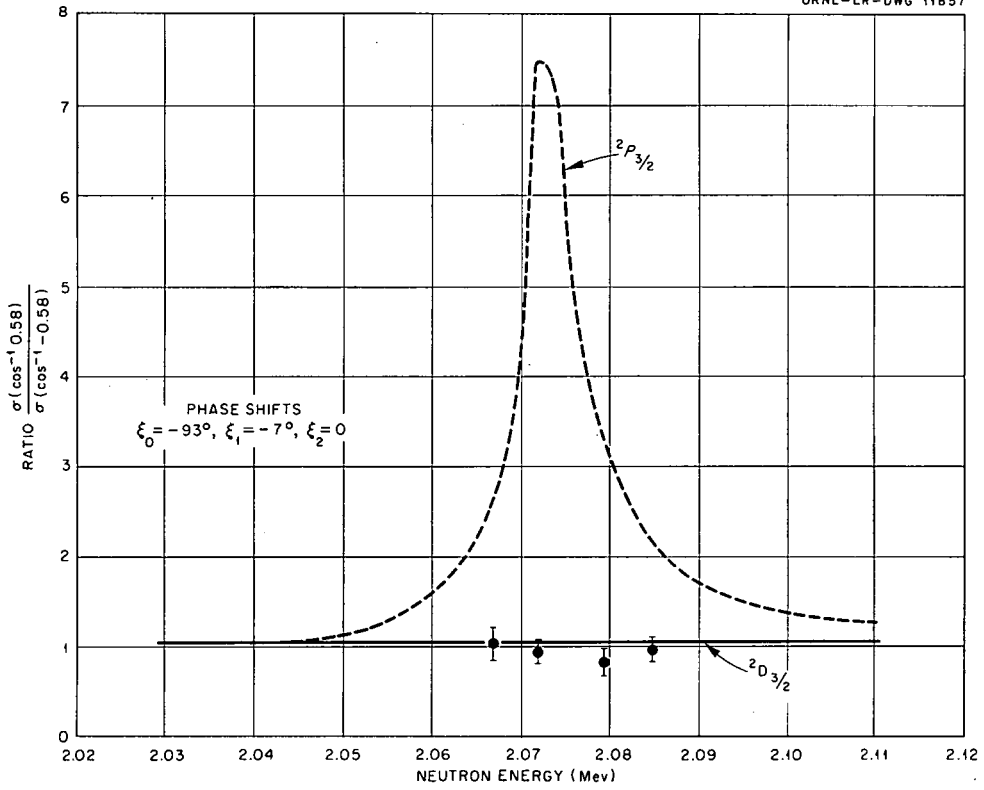


Fig. 6. Ratio of the Differential Cross Sections of Neutrons  $\frac{\sigma(\cos^{-1} 0.58)}{\sigma(\cos^{-1} -0.58)}$  Scattered from Carbon.

DIFFERENTIAL ELASTIC SCATTERING AT 1.62- AND 1.68-Mev NEUTRON RESONANCE IN NEON

J. L. Fowler

H. O. Cohn

The method<sup>1</sup> of determining differential elastic scattering by measuring coincidences between nuclear recoils in a gas-filled proportional counter and scattered neutrons detected with an anthracene crystal has been used to investigate two resonance levels of neon. Figure 1 shows the experimental setup. The LiF-impregnated paraffin shield has a

proton beam. For a gas cell this effect appeared to be small. With the reduced neutron yield of a Zr-T target, however, there is probably an appreciable effect due to these gamma rays. This would constitute a relatively constant background, which would not effect the change in the angular distribution to be observed at the resonances. A comparison of off-resonance data taken with both the Zr-T target and the gas cell indicates that the background due to source gamma rays in the former case amounted to approximately 30%.

In Figs. 2 and 3 the relative differential measurements at  $\cos \theta = \pm 0.58, 0,$  and  $-0.78$  ( $\theta =$  C.M. neutron scattering angle) are presented. While the

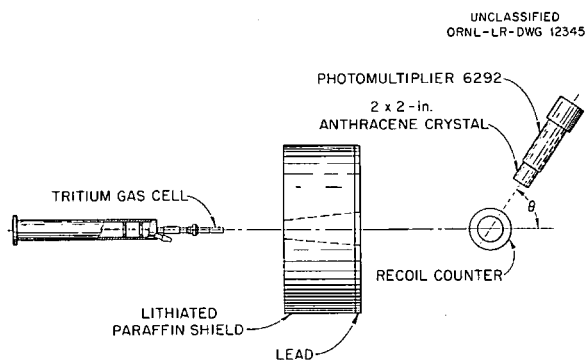


Fig. 1. Experimental Arrangement for Determining Differential Elastic Scattering.

rectangular slot to allow the source neutrons to be incident upon the 2-in.-dia, 5-in.-long counting volume of the proportional counter. The response for the 2 x 2 in. anthracene crystal for neutrons in the energy region of interest has been already described.<sup>1</sup> Since the 1.68-Mev level<sup>2</sup> is narrower than the energy spread of neutrons obtainable with a gas target,<sup>3</sup> a Zr-T target has been used as a target for producing the  $T(p,n)$  neutrons needed for the present investigation. The target thickness was 7 kev at the energies at which it was used. Gamma-ray background due to source neutrons captured in the shielding was evaluated by removing the source neutrons from the counter with an LiF plug in the shielding. This procedure does not allow an evaluation of the background effect of gamma rays produced at the Zr-T target by the

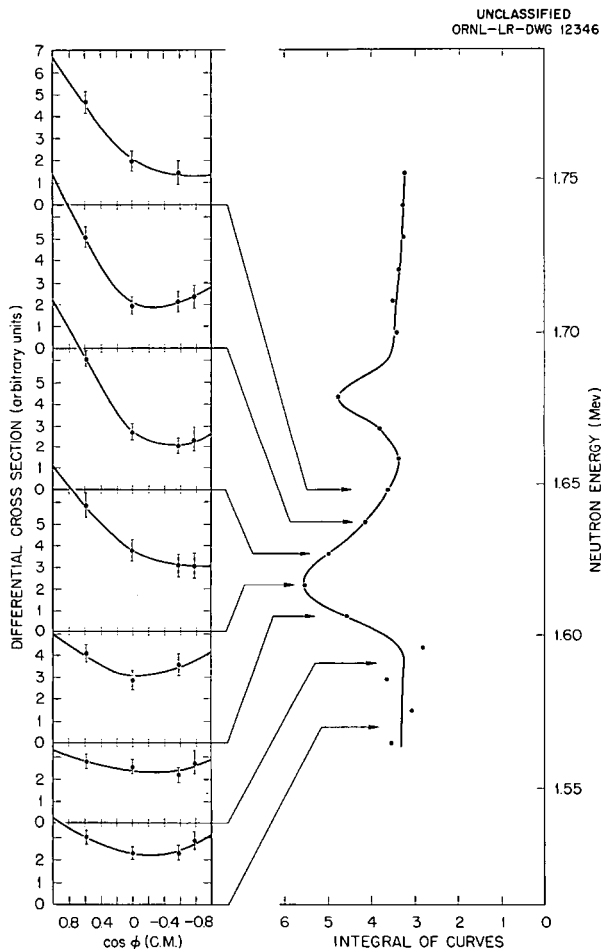


Fig. 2. Angular-Distribution Curves Around the 1.62-Mev Resonance.

<sup>1</sup>H. O. Cohn and J. L. Fowler, *Phys. Semiann. Prog. Rep. Sept. 10, 1955*, ORNL-1975, p 28.

<sup>2</sup>H. O. Cohn and J. L. Fowler, *Phys. Semiann. Prog. Rep. March 20, 1955*, ORNL-1879, p 6-7.

<sup>3</sup>J. L. Fowler and C. H. Johnson, *Phys. Rev.* 98, 728 (1955).

ordinate scale on the left-hand side should be considered arbitrary, one unit is approximately 0.1 barn/steradian. As mentioned above, the zero of the scale should be shifted to account for background due to source gamma rays. The plot on the right-hand sides of Figs. 2 and 3 shows the areas of the curves on the left plotted as a function of neutron energy and shows clearly the positions of the resonances. This serves to identify the energy position at which the measurements are made. The energy corresponding to the resonance peaks agrees well with the values published earlier.<sup>4</sup> It is clearly seen that the differential scattering at  $\cos \theta = \pm 0.58$  is symmetrical about  $\cos \theta = 0$  for the 1.68-Mev level, whereas for the 1.62-Mev level the cross section is peaked toward forward neutron scattering. If the potential scattering is predominantly *s*-wave, and off-resonance scattering suggests this to be the case, then the results indicate that the 1.62-Mev level has odd parity and the 1.68-Mev level has even parity.<sup>3,5</sup>

<sup>4</sup>H. O. Cohn and J. L. Fowler, *Phys. Rev.* **99**, 1625 (1955).

<sup>5</sup>H. B. Willard, J. K. Bair, and J. D. Kington, *Phys. Rev.* **98**, 669 (1955).

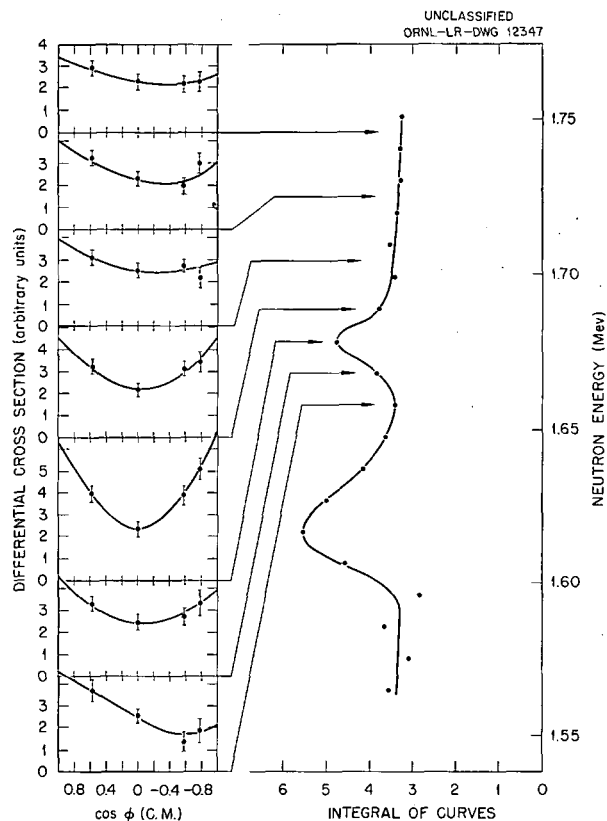


Fig. 3. Angular-Distribution Curves Around the 1.68-Mev Resonance.

## NEUTRON ACTIVATION OF IODINE NEAR 25 kev

R. L. Macklin

Reliable reaction cross-section data in the kilovolt neutron range have been rare. Long counter extrapolations form the basis for many of the reported results.<sup>1</sup> Hummel and Hamermesh<sup>2</sup> and Kimball and Hamermesh<sup>3</sup> have measured many activation cross sections with an antimony-beryllium source by comparison with thermal cross sections. Their 2.2-barn result for iodine (25-min beta activation) seems unexpectedly high. It seemed worth

<sup>1</sup>For references see D. J. Hughes and J. A. Harvey, *Neutron Cross Sections*, BNL-325 (July 1, 1955).

<sup>2</sup>V. Hummel and B. Hamermesh, *Phys. Rev.* **82**, 67 (1951).

<sup>3</sup>C. Kimball and B. Hamermesh, *Phys. Rev.* **89**, 1306 (1953).

while to remeasure this cross section by absolute beta counting in an NaI(Tl) crystal as done at higher energies by Martin and Taschek.<sup>4</sup>

A standard ORNL Sb-Be source (a  $\frac{3}{4}$ -in.-dia by  $\frac{3}{4}$ -in.-long antimony cylinder in a hollow  $1\frac{3}{16}$ -in.-dia by  $1\frac{3}{16}$ -in.-long beryllium cylinder) calibrated at the National Bureau of Standards was used. The source strength per unit solid angle was measured by rotating the source in front of a BF<sub>3</sub> counter. For the axial directions (used in the iodine irradiations) the flux was  $0.915 \pm 0.03$  times the average. The equatorial flux, incidentally, was very near the average and constant with longitude as expected.

<sup>4</sup>H. C. Martin and R. F. Taschek, *Phys. Rev.* **89**, 1302 (1953).

PHYSICS PROGRESS REPORT

Several  $1\frac{1}{2} \times 1\frac{1}{2}$  in. NaI(Tl) crystals canned in aluminum foil with a thin glass window at one end were used in the experiment. Each was irradiated in an attic 25 ft above the concrete floor at 19 to 41 cm from the neutron source. The separation was carefully measured with a vertical cathetometer from a safe distance. After irradiation, the crystal was mounted on an RCA-5819 photomultiplier tube, and the energy scale was checked against the 661-keV Cs<sup>137</sup> photopeak. The iodine beta activity was counted with an integral bias of about 140 keV. Room background at 1.8 counts/sec ranged from 8 to 33% of the beta counts. Extrapolation of the integral-bias curve below 50 keV showed that the beta counting efficiency under these conditions was  $0.93 \pm 0.015$ . The I<sup>128</sup> decay has been studied recently at Columbia University,<sup>5</sup> and a 6.9% electron-capture branch has been reported. About 95% of the electron-capture decay is to the ground state and would not have been observed in the present experiment. The reproducibility of the activations corrected to saturated activity (and multiplied by the square of the separation) was not significantly different from the reproducibility calculated from the counting statistics and the cathetometer accuracy. The average of eight runs is considered reproducible to 0.7% (standard deviation).

A few small effects were considered in calculating the cross section. Air scattering gave a computed 1.1% increase in neutron flux at the crystal. Effective center displacement for source and crystal led to corrections ranging from 0.2 to 1.0% at the extreme distances. The effect of multiple scattering in the crystal, calculated from the measured total cross sections of sodium<sup>6</sup> and iodine,<sup>1</sup> was +3.1%. The corrected  $I^{127}(n,\gamma)I^{128}$  cross section is  $0.82 \pm 0.06$  barn.

The primary energy of the neutrons is not well known.<sup>7</sup> The energy loss by collisions with beryllium has been estimated by use of a homogeneous cylinder model with the primary source uniform throughout the outer beryllium shell region of the actual source. A spherical beryllium shell model,

with the antimony ignored, gives comparable results. The following tabulation shows the calculated percentage of emitted neutrons above fractions of the primary energy corresponding to maximum loss in 0, 1, 2, and 3 collisions with beryllium:

E	N (%)
0.998	67.6
0.640	93.6
0.410	98.6
0.262	99.2

Weighting the detailed energy distribution by  $(E_0)^{-1/2}$  corresponding to the expected  $1/v$  iodine cross-section dependence in the neighborhood of 20 keV (but with an upper limit of 3 for this factor), the area under the curve becomes 1.074. Thus neutron energy loss in the source increases the observed cross section about 7.4%. Stated another way, the effective source energy is 87% of the primary energy. An effective neutron energy of about 25 keV as given by Kimball and Hamermesh<sup>3</sup> seems reasonable.

The early work of Linenberger and Miskel<sup>1</sup> at several energies gives an interpolated value of about 1 barn at 25 keV, with an uncertainty of perhaps 0.2 or 0.3 barn for the absolute value. The Hummel and Hamermesh value of  $2.2 \pm 0.4$  barns obtained with an Sb-Be neutron source is certainly at variance with the present result. A few points of technique in favor of the present work, such as less ambiguity in incident-flux measurement, high-efficiency beta counting, and no reliance on a thermal-cross-section comparison, can hardly account for the difference.

One question that deserves a little thought in the present experiment is the possibility of self-absorption. Since the average probability of neutron absorption in the crystal was only 0.03 (i.e., 97% of the incident neutrons escape from the crystal), this at first glance seems negligible. If the absorption were due to a few, narrow, isolated resonances, it might still be expected that self-absorption would be important. Several of the iodine resonances below 100 eV have been examined.<sup>1</sup> Taking the gamma width (0.1 eV) and the extreme values of the reduced neutron widths ( $3 \times 10^{-4}$  and  $7 \times 10^{-3}$  eV) found there as typical at 24 keV, it can be shown that the scattering cross section remains about ten times as large as

<sup>5</sup>N. Benczer *et al.*, *Phys. Rev.* 101, 1027 (1956).

<sup>6</sup>H. Newson, private communication.

<sup>7</sup>Recent data on the beryllium  $(\gamma, n)$  threshold and the unpublished value of Tomlinson (1.692 MeV) for the antimony gamma energy give 27 keV for the primary energy.

the absorption cross section at the (Doppler broadened) peaks. The maximum peak absorption calculated is only about twice the average value found in the experiment. Since the average energy

loss on scattering is about 400 ev and scattering is ten times as probable as absorption, the self-shielding at a single resonance must be completely negligible.

### MILLIMICROSECOND TIME-OF-FLIGHT NEUTRON SPECTROMETRY

H. E. Banta

J. H. Gibbons

W. M. Good

J. H. Neiler

The terminal pulser described by King and Parker<sup>1</sup> has been installed in the 2.5-Mv Van de Graaff. The average pulsed current now obtained is approximately  $0.5 \mu\text{a}$  for burst widths of 10 to 12  $\mu\text{sec}$ . This is about twice as good as was possible when the pulsing was performed by deflecting the accelerated beam. The present current apparently is limited by the ion-source output, since the tube loading of the machine is determined by the average current rather than the peak values in the pulse. Measurements in both the kev and Mev neutron-energy ranges have been made by use of the terminal pulsing. However, further work is necessary to improve the reliability of operation. The performance of the pulser is critically dependent on the beam-focusing conditions at the ion source, in the Einzel lens which constitutes the "wiggler," and at the strong lens which forms the entrance to the machine. So far, the useful life of an ion source for pulser operation has been only a few days.

The background<sup>2</sup> in the kev-neutron transmission measurements has been greatly improved by reducing the lithium target thickness and thus the crystal activation by the high-energy group from the  $\text{Li}^7(p,n)$  reactions. Terminal pulsing has virtually eliminated the "machine-on" background, and the doubled pulsed current has halved the counting time. Tests with several sample sizes have shown that measurements are possible with sample sizes of the order of a few centimeters diameter, so that measurements with separated isotopes may be feasible. Cross sections have

been measured for manganese, titanium, and selenium. The neutron-energy scale for the manganese total cross section, Fig. 1, is probably in error because of a poor time calibration for this particular run. The two peaks represent a significant splitting of the single peak shown in BNL-325<sup>3</sup> and are probably identical with those reported by Marshak and Newson.<sup>4</sup> This doublet has been of some value in resolution comparisons between choppers and accelerators. A relatively thick ( $5.66 \times 10^{22}$  atoms/cm<sup>2</sup>) sample was used for this measurement.

<sup>3</sup>D. J. Hughes and J. A. Harvey, *Neutron Cross Sections*, BNL-325 (July 1, 1955).

<sup>4</sup>H. Marshak and H. W. Newson, *Phys. Rev.* 98, 1162 (1955).

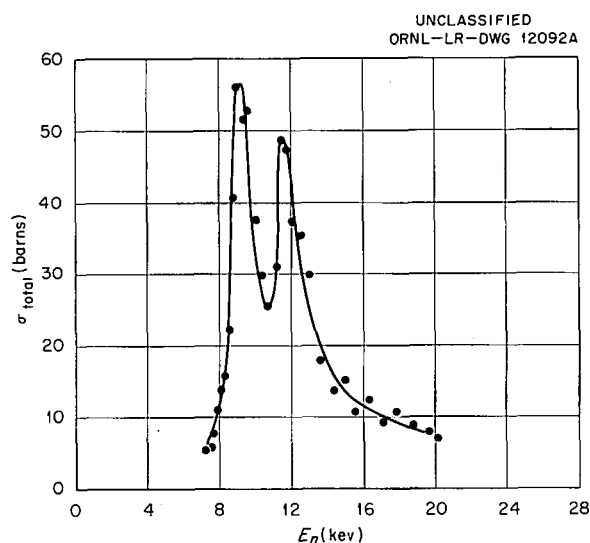


Fig. 1. Total Cross Section of Manganese vs Energy (ORNL Time-of-Flight Measurements, 0.50-m Flight Path).

<sup>1</sup>R. F. King and V. E. Parker, *Phys. Semiann. Prog. Rep. Sept. 10, 1955*, ORNL-1975, p 65.

<sup>2</sup>J. H. Neiler et al., *Phys. Semiann. Prog. Rep. Sept. 10, 1955*, ORNL-1975, p 32.

The peak cross sections would be considerably enhanced if a thinner sample were used. The previously reported<sup>3</sup> resonances at 4 and 17 kev have been observed with a metallic sample of titanium. Another level has been found at 8.0 kev, as well as some evidence that the unusually wide 17-kev level may be more than a single level. Because of the isotopic complexity further measurements are being deferred until separated isotopes are obtained. The results of several determinations of the total cross section of selenium are shown in Fig. 2. Previous measurements in this region had indicated only a single broad maximum. This element is also isotopically complex, so that separated isotopes should be obtained.

The background in the measurements of fast-neutron spectra from (*d,n*) reactions has been im-

proved an order magnitude by the terminal pulsing. Figure 3 is an example of a spectrum obtained with the best resolution. The conversion from pulse height to flight time is essentially linear. The numbers in parentheses over the peaks are the neutron energies which should be expected from the known *Q*'s for this reaction. The other numbers are obtained from a pulse-height flight-time calibration in which the 1.33-Mev peak was used as a reference point. The relative intensities of the peaks have not been corrected for detector efficiency. The relative intensities of the missing neutron groups are not known for this bombarding energy, but recent measurements with 1-Mev deuterons have shown that the group corresponding to the 0.903-Mev neutrons is about 10% as intense as the other member of the doublet. Figure 4 is the spectrum of neutrons from  $F^{19}(d,n)Ne^{20}$ . The relatively low yield is evident by comparison with Fig. 2. This spectrum also gives some indication of the difficulties which may be expected when working with targets having high gamma yields. Beam leakage between bursts is thought to account for an appreciable part of the large background underlying the neutron peaks. Note also the large yield from  $C^{12}$  contamination of the target, which was not evident in the beryllium run.

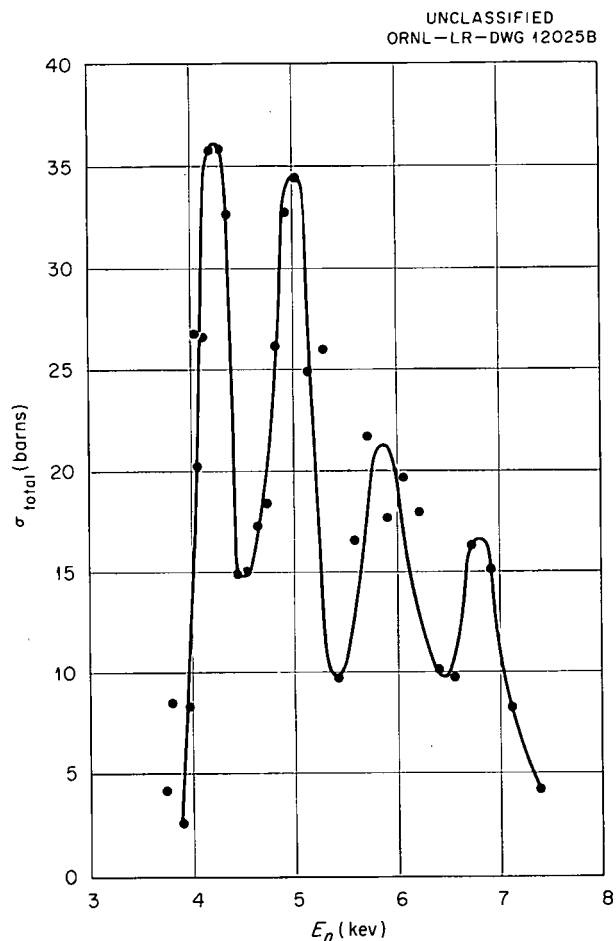


Fig. 2. Total Cross Section of Selenium vs Energy (ORNL Time-of-Flight Measurements, 0.45-m Flight Path).

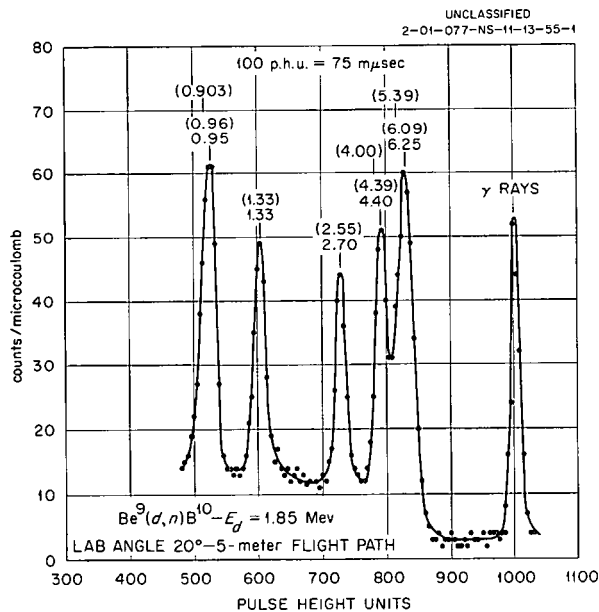


Fig. 3. Neutron Spectrum from  $Be^9(d,n)B^{10}$ .

UNCLASSIFIED  
ORNL-LR-DWG 11670A

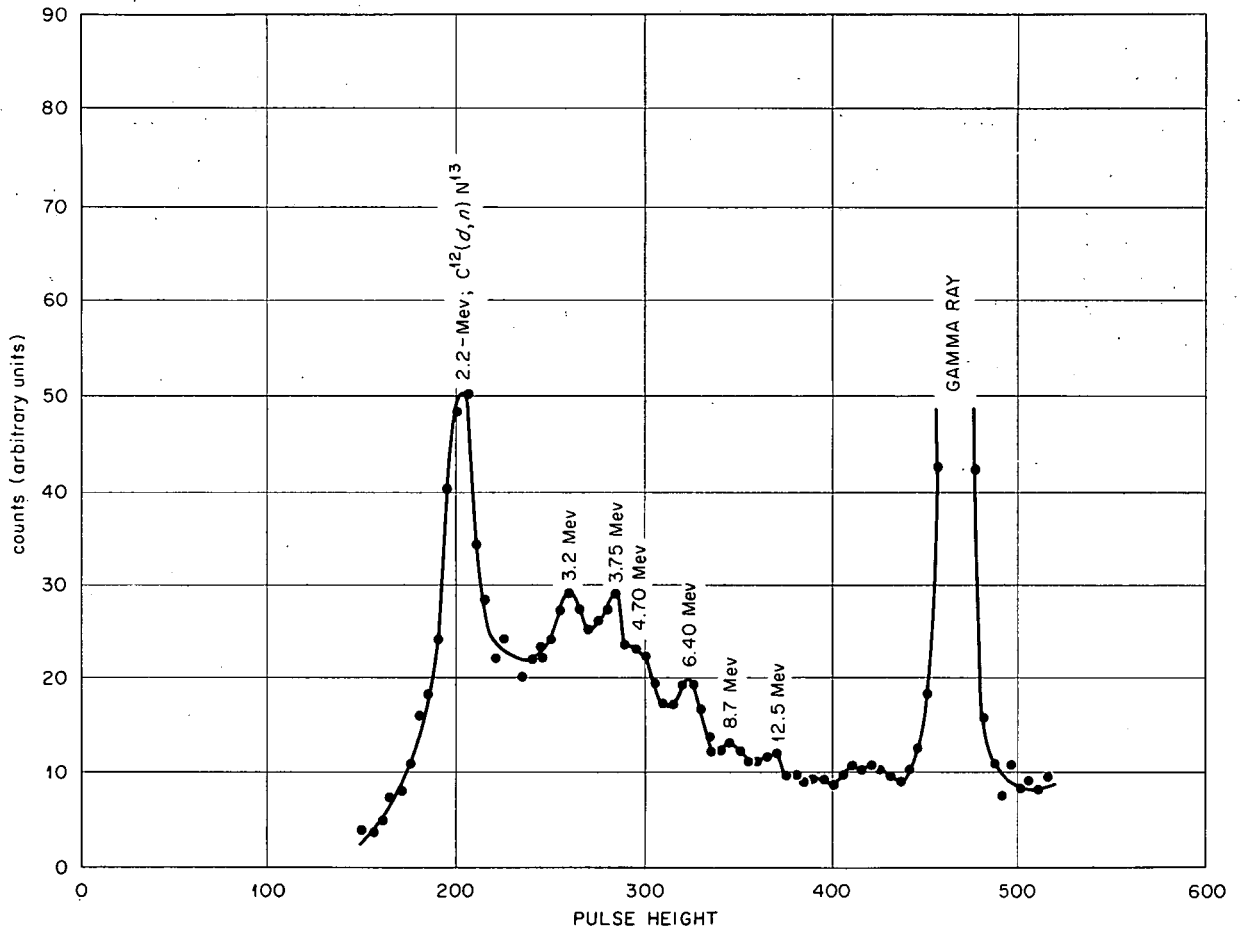


Fig. 4. Neutron Spectrum from  $F^{19}(d,n)Ne^{20}$  ( $\theta = 10$  deg,  $E_d = 2.5$  Mev).

EXPERIMENTS WITH PULSED-NEUTRON SOURCE

E. C. Campbell

P. H. Stelson

Measurements of delayed nuclear effects resulting from fast-neutron bombardment of a target have been made with the ORNL 5.5-Mv accelerator being used as a square-wave-modulated neutron source of variable frequency and with a synchronized multichannel time analyzer. By variation of the frequency of the master control oscillator, half-life measurements in the whole range from seconds to microseconds can be made.

APPARATUS

A block diagram of the apparatus used is shown in Fig. 1. The apparatus shown below the dashed line is located in the control room, while that

shown above the dashed line is located next to the accelerator. The scale-of-10 consists of a single Burroughs beam-switching tube. This is driven by a master oscillator which opens up in sequence the ten time channels. In addition, the signal which closes channel 10 operates both the pulse gate and the beam gate, which are so phased that pulses from the detector can be passed through only during the interval during which the proton beam is deflected from the target by a 10-kv potential applied to a deflector plate. Use is made of ten scales-of-16 and of registers of the standard ORNL 20-channel analyzer for recording the pulses. For convenience there is also a

UNCLASSIFIED  
ORNL-LR-DWG 11472

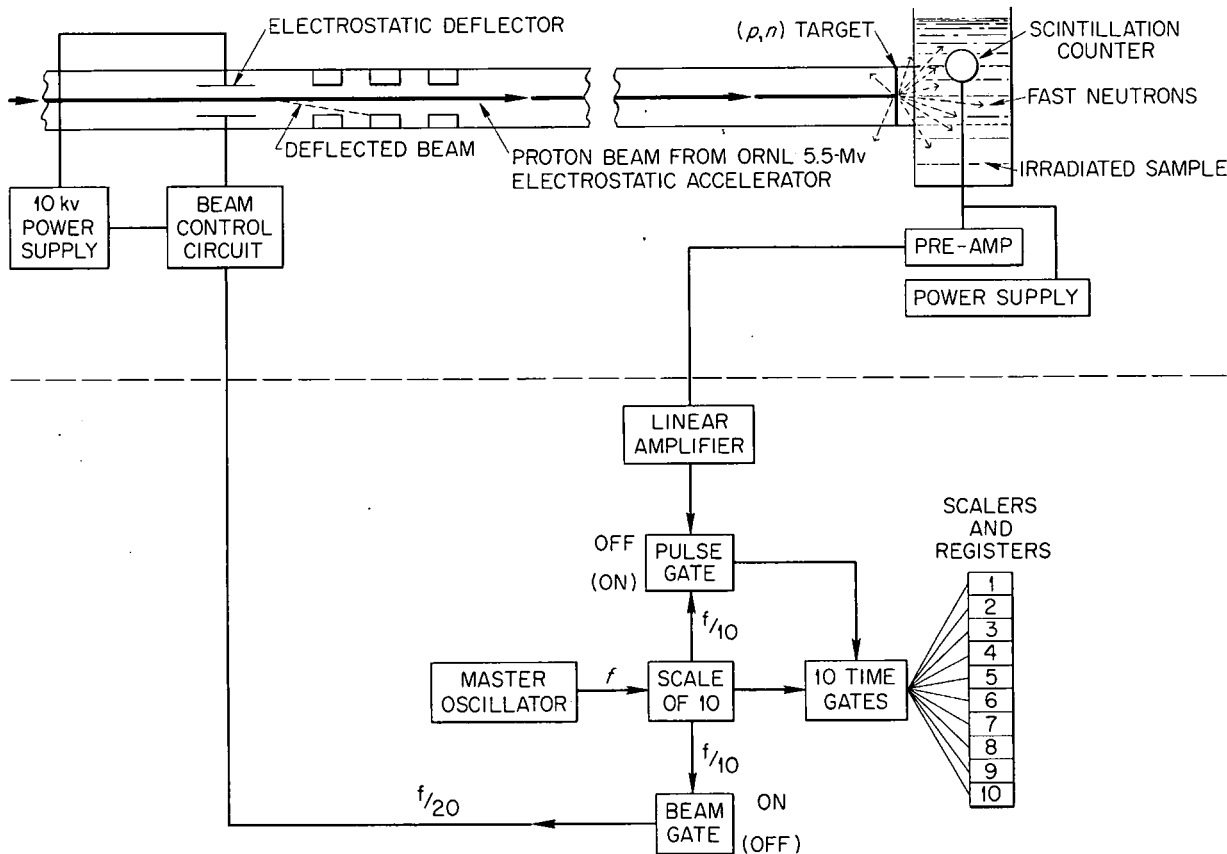


Fig. 1. Schematic Diagram of Apparatus for Fast-Decay Measurements Showing Means of Producing Square-Wave Neutron Pulses, Together with Multichannel Time Analyzer.

total-count channel (not shown) which feeds the scale-of-256. In some experiments the scale-of-10 is bypassed so that the total number of pulses received during the beam-off period may be studied as a function of the oscillator frequency. The oscilloscope photograph (Fig. 2) was taken with the sweep synchronized with the beam gate and shows the rather sharp cutoff obtained with square-wave beam pulses 1000  $\mu$ sec in length. Each

UNCLASSIFIED  
ORNL-LR-DWG 42692

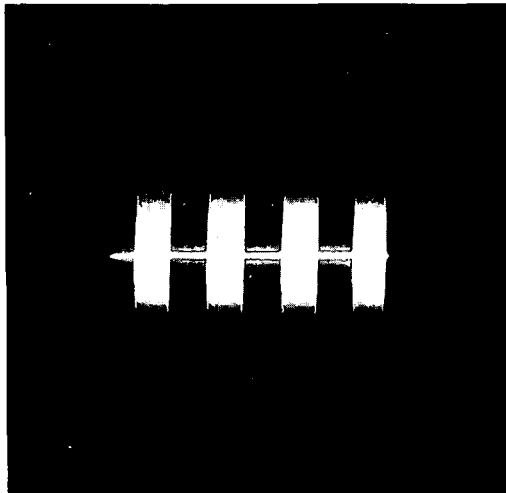


Fig. 2. Oscilloscope Photograph Showing Square-Wave Neutron Pulses as Detected with an Anthracene Scintillation Counter. Each neutron pulse is made up of thousands of short detector pulses superposed. The length of the neutron pulse is 1000  $\mu$ sec.

beam pulse is made up of thousands of short (1- $\mu$ sec) unresolved pulses from an anthracene scintillation detector which detects fast neutrons and gammas from the target. Use was made of a fast Fairstein double-delay-line amplifier so that rapid recovery would be made between the high counting rate associated with the beam-on period and the low counting rate of the beam-off period. The pulse output of this amplifier gives a positive as well as a negative signal for each pulse, as can be seen in the symmetrical disposition of pulses in Fig. 2. Particular care was taken to make the rise and fall times of the beam pulse as short as possible. As measured on an oscilloscope, these times are 5 and 1  $\mu$ sec, respectively.

### SHORT-PERIOD ISOMERS

It was shown earlier<sup>1</sup> that the average counting rate of a sample activated by a square-wave pulsed-neutron source of frequency  $f$  and counted only during the beam-off period was given by

$$A = \frac{A_s}{4} \frac{f}{f_0} \tanh \frac{f_0}{f},$$

where  $A_s$  is the saturated counting rate for infinite bombardment time in a continuous neutron flux of the same intensity as that of the pulsed source and  $f_0$  is simply related to the decay constant  $\lambda$  and the half life  $\tau_{1/2}$  by  $f_0 = \lambda/4 = 0.173/\tau_{1/2}$ .

The theoretical curve consists of two parts: for  $f \ll f_0$  one obtains a linear function of  $f$ , while for  $f \gg f_0$  the curve is constant. The extrapolation of the linear part of the curve intersects the flat portion of the curve at  $f = f_0$ . The first experimental verification of the expected behavior was obtained with  $\text{He}^6$  produced in the reaction  $\text{Be}^9(n,\alpha)\text{He}^6$ , as shown in Fig. 3. The experimental value of  $f_0$  was 0.212  $\text{sec}^{-1}$ , leading to a value for the half life of 0.817 sec, which is in good agreement with previous results. The various runs have been normalized to a constant number of incident neutrons.

The same method was used to search for a short-lived isomer  $\text{As}^{75m}$  recently reported by Schardt,<sup>2</sup> who used a delayed-coincidence method to identify it in the decay of  $\text{Se}^{75}$ . He obtained a half life of  $18.0 \pm 1.5$  msec. The same isomer was found in 22-Mev betatron bremsstrahlung bombardment of arsenic by Vegors and Axel,<sup>3</sup> who report a half life of  $12 \pm 3$  msec. Figure 4 shows the results obtained by bombardment of a large sample of arsenic metal with 1.35-Mev neutrons. A good fit is obtained with the theoretical curve if  $f_0$  is taken to be 8.2  $\text{sec}^{-1}$ . This leads to a half life of  $21 \pm 2$  msec. The reaction leading to the formation of the metastable level is  $\text{As}^{75}(n,n')\text{As}^{75m}$ .

<sup>1</sup>E. C. Campbell, *Phys. Semiann. Prog. Rep.* March 20, 1955, ORNL-1879, p 19.

<sup>2</sup>A. W. Schardt, *Bull. Am. Phys. Soc.* 1, Series II, No. 2 (1956), Abstract D1.

<sup>3</sup>S. H. Vegors, Jr., and P. Axel, *Phys. Rev.* 101, 1067 (1956).

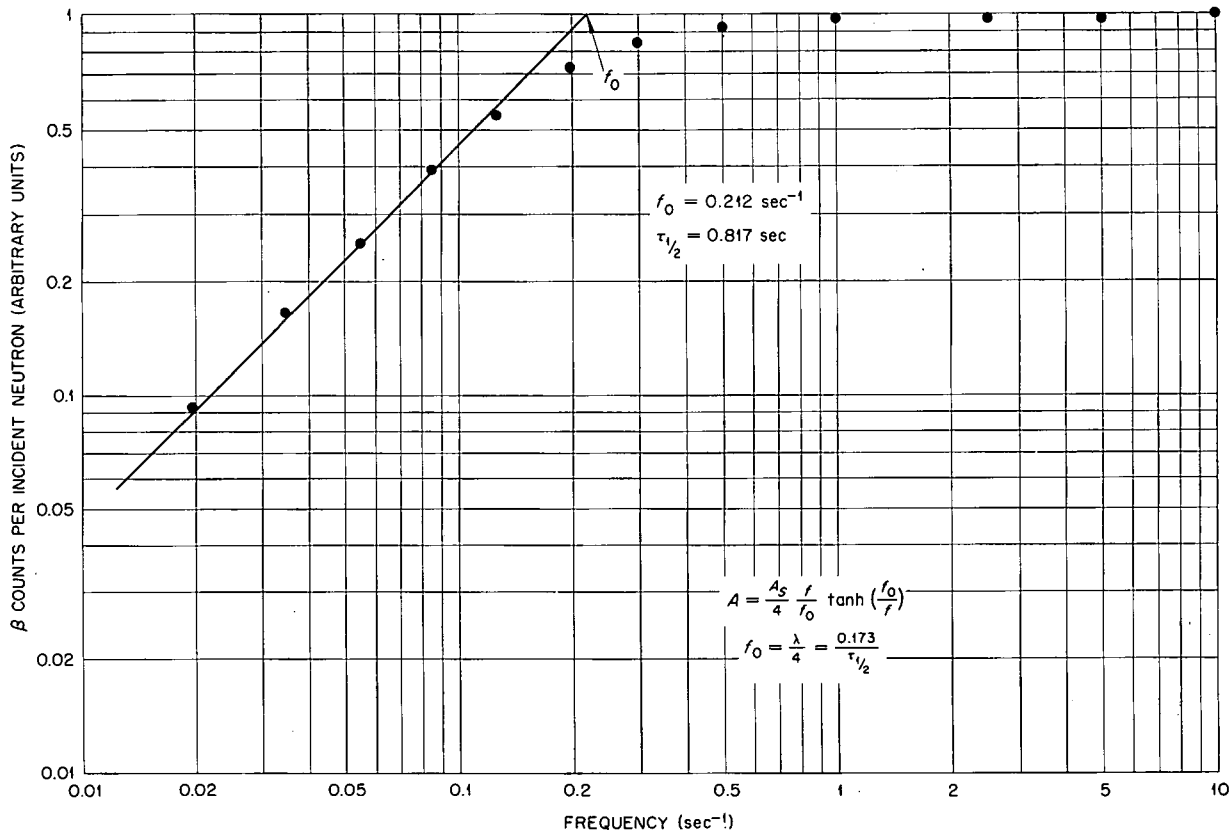


Fig. 3. Measurement of Half Life of  $\text{He}^6$  Produced by  $\text{Be}^9(n,\alpha)\text{He}^6$  from Frequency Dependence of Activation with Square-Wave Modulated Neutron Source.

Fast-neutron bombardment of tantalum results in the production of the well-known isomer  $\text{Ta}^{181m}$  by the reaction  $\text{Ta}^{181}(n,n')\text{Ta}^{181m}$ . For this measurement use was made of the multichannel time analyzer described above. The data, as shown in Fig. 5, lead to a half life of  $18 \pm 3 \mu\text{sec}$ , in fair agreement with other published measurements:<sup>3</sup>  $18.5 \pm 2.5$ ,  $18.8 \pm 0.8$ ,  $16 \pm 3$ ,  $20.1 \pm 0.7$ , and  $22 \mu\text{sec}$ .

Fast-neutron bombardment of natural lead gave evidence for the well-known 0.8-sec  $\text{Pb}^{207m}$ , as well as for another isomer of about  $150 \mu\text{sec}$  half life presumed to be  $\text{Pb}^{206m}$ . Unfortunately, in this case the background of the  $\text{Pb}^{207m}$  was too high to permit an accurate half-life measurement to be made.

For the above measurements the gamma detector was a  $1\frac{1}{2} \times 1$  in. anthracene crystal mounted on a Du Mont 6292 photomultiplier tube. The bias setting of the amplifier was in each case adjusted

to permit detection of the gamma rays associated with the decay. The energy of neutrons produced by a  $\text{T}(p,n)$  reaction was chosen to be well above threshold for the  $(n,n')$  reaction.

Two difficulties of the present method were encountered in this work. The first is associated with the background produced by activation of the  $\text{H}^3$  gas target cell by the incident protons. This difficulty could perhaps be remedied by constructing the  $\text{H}^3$  cell out of a material with a high  $Z$  which does not give delayed gammas from the  $(n,n')$  reaction. For very short bombardment times a time-dependent background with a half life of about  $10 \mu\text{sec}$  was found. This effect is associated with the production, by slowing down, of thermal neutrons in the anthracene crystal; these neutrons leak out or are absorbed by the hydrogen in the crystal. It was found that the effect is enhanced considerably by covering the crystal with a cadmium foil, since thermal neutrons that would

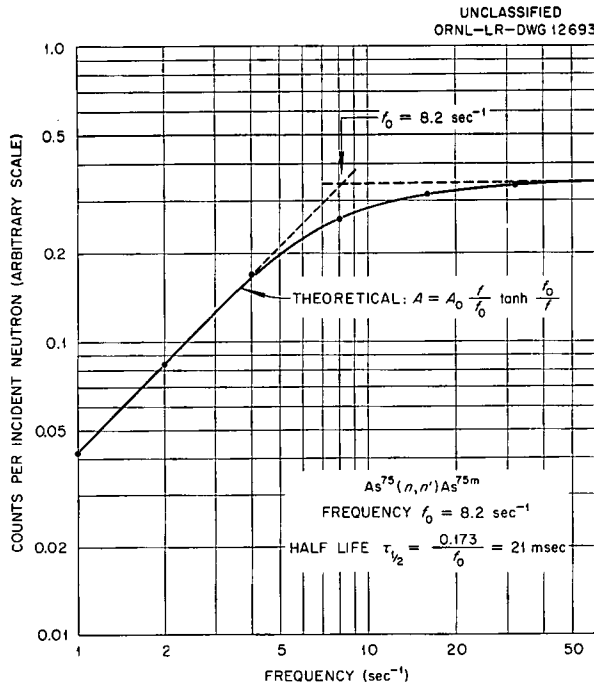


Fig. 4. Frequency Dependence of Fast-Neutron Activation of Arsenic to Produce  $As^{75m}$  ( $21 \pm 2$  msec).

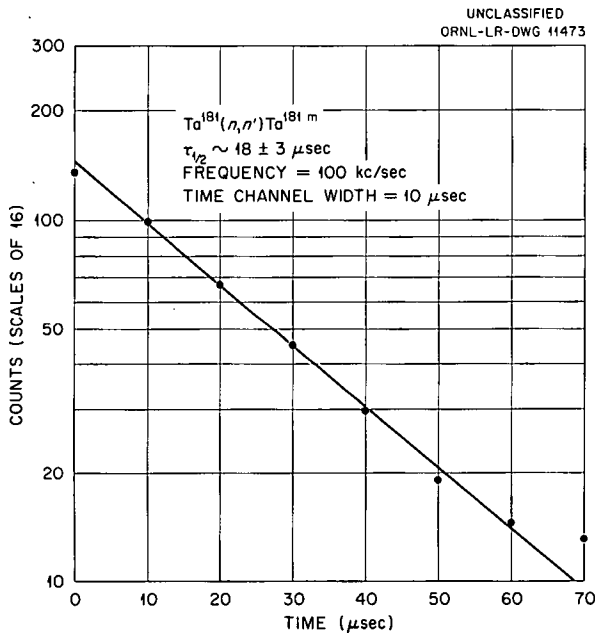


Fig. 5. Decay Curve of  $Ta^{181m}$  ( $18 \pm 3$   $\mu$ sec) Obtained with Square-Wave Modulated Neutron Source and Multichannel Time Analyzer.

otherwise leak out of the crystal would now be absorbed by the cadmium, giving rise to easily detected cadmium capture-gamma rays. It appeared useful to conduct a systematic study of this effect with extended moderators, since the present apparatus appeared to offer certain advantages for this type measurement. These experiments are described in the next section.

#### THERMAL-NEUTRON DIFFUSION MEASUREMENTS IN $H_2O$ AND BERYLLIUM

The rate of decay of the thermal-neutron intensity arising from a burst of fast neutrons in a finite moderator has been the subject of investigation by several groups<sup>4-7</sup> who have studied  $H_2O$  (refs. 4-7), Be (ref. 6), BeO (ref. 7), and graphite (ref. 6). The method consists in measuring the decay rate of the intensity of thermal neutrons resulting from slowing down in the moderator following a burst of fast neutrons from an external source. According to diffusion theory, the decay constant of the fundamental mode is given by

$$(1) \quad \lambda = v \Sigma_a + DB^2,$$

where  $v$  is the thermal-neutron velocity,  $\Sigma_a$  is the macroscopic thermal-neutron absorption cross section of the moderator,  $B^2$  is the fundamental buckling, and  $D$  is the diffusion constant of thermal neutrons in the moderator.  $D$  is related to the transport mean free path  $\lambda_t$  by the expression  $D = \lambda_t v/3$ .

Thermal neutrons leaking from the moderator were detected with a small  $Li^{61}(Eu)$  scintillation counter or with a 1-in. cadmium disk on an anthracene scintillation counter. A representative decay curve of thermal neutrons leaking from an  $H_2O$  cylinder 5 in. in diameter and 5 in. in height is shown in Fig. 6.

<sup>4</sup>G. von Dardel and N. G. Siöstrand, *Phys. Rev.* **96**, 1245 (1954).

<sup>5</sup>F. R. Scott, D. B. Thomson, and W. Wright, *Phys. Rev.* **95**, 582 (1954).

<sup>6</sup>A. V. Antonov et al., *A Study of Neutron Diffusion in Beryllium, Graphite and Water by the Impulse Method*, Paper 661, International Conference on the Peaceful Uses of Atomic Energy, Geneva, Switzerland.

<sup>7</sup>R. Ramanna et al., *On the Determination of Diffusion and Slowing Down Constants of Ordinary Water and Beryllium Oxide Using a Pulsed Neutron Source*, Paper 872, International Conference on the Peaceful Uses of Atomic Energy, Geneva, Switzerland.

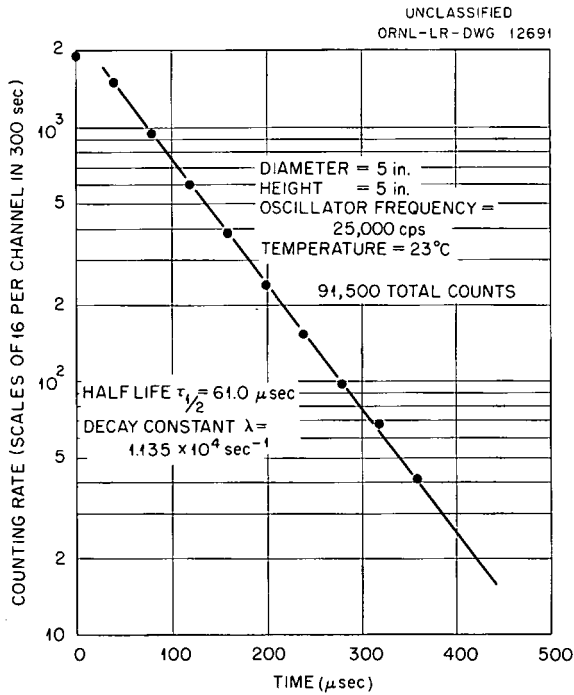


Fig. 6. Decay Curve of Thermal Neutrons Diffusing out of H<sub>2</sub>O Cylinder as Detected with Li<sup>6</sup>I(Eu) Scintillation Counter.

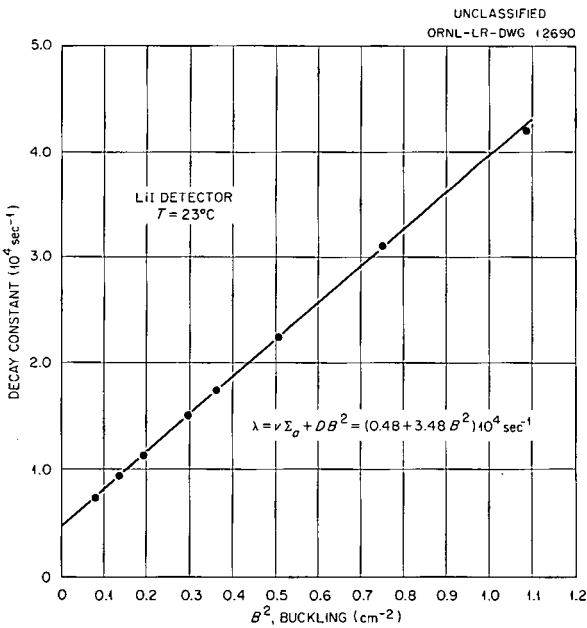


Fig. 7. Dependence of Decay Constant of Thermal Neutron Diffusing out of H<sub>2</sub>O Cylinders on the Size of the Cylinder as Given by the Geometrical Buckling B<sup>2</sup>.

In Figs. 7 and 8 are shown the experimental results of the dependence of decay constant on buckling (Eq. 1) for H<sub>2</sub>O and beryllium, respectively. No evidence was found for the curvature reported by other groups<sup>4,6</sup> and attributed to diffusion cooling.

The time and spatial dependence of the neutrons diffusing out of a long block of beryllium is shown in Fig. 9. Fourier analysis of these curves permits one to separate out the higher diffusion modes, which decay somewhat more rapidly than the fundamental mode. The curves are drawn to show the spatial dependence of the burst at successive 100-μsec intervals. The decay curves taken at different positions of the cadmium detector have been normalized to each other for constant number of incident neutrons. For this series of runs the neutrons were produced by the Be<sup>9</sup>(p,n) reaction. The charge collected at the target was 320 μcoulombs for each decay curve.

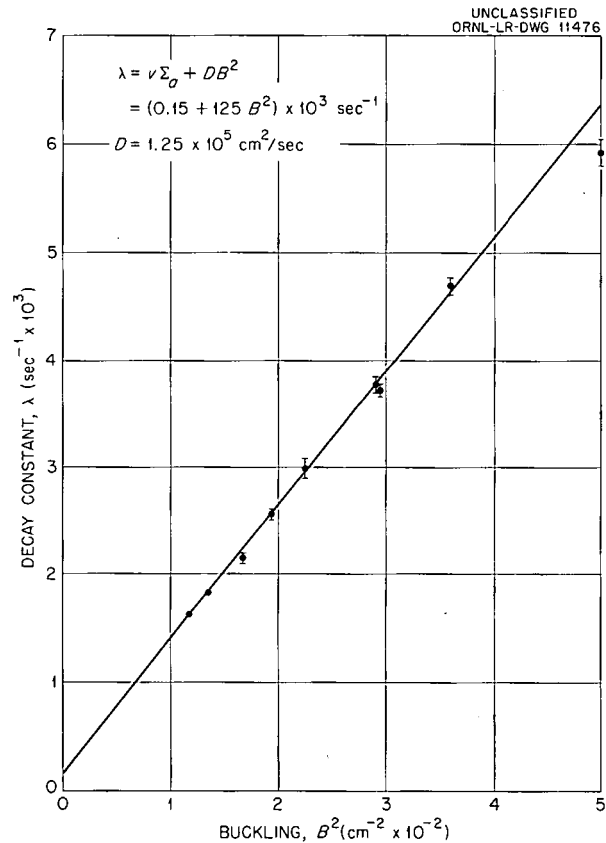
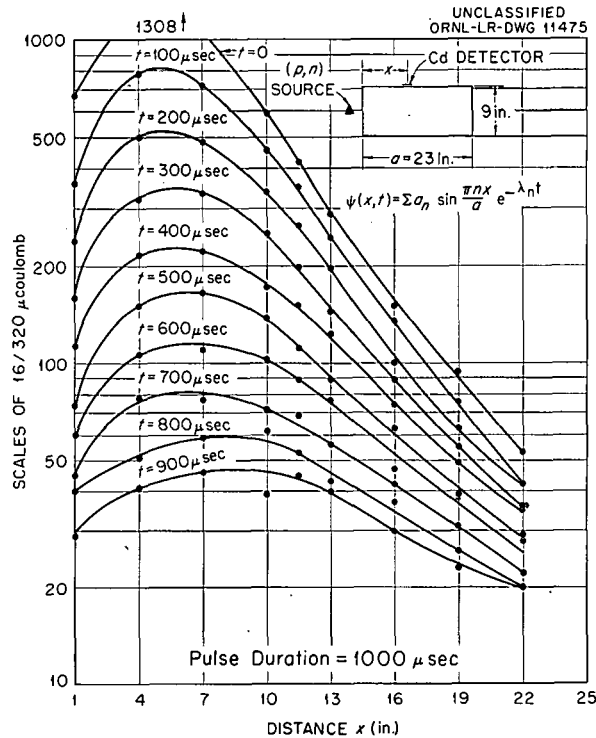


Fig. 8. Dependence of Decay Constant of Thermal Neutrons Diffusing out of Rectangular Prisms of Beryllium on the Geometrical Buckling B<sup>2</sup>.



**Fig. 9. Time-Space Distribution of Thermal Neutrons Diffusing out of a Beryllium Block ( $9 \times 11\frac{1}{4} \times 23$  in.) Following 1000- $\mu$ sec Bursts of Fast Neutrons. The curves show the shapes of the distribution at successive 100- $\mu$ sec time intervals. The presence of higher diffusion modes (harmonics), which decay more rapidly than the fundamental mode, can be seen from the gradual shift to the symmetrical fundamental mode.**

### REACTOR PARAMETERS OF A SMALL ENRICHED SUBCRITICAL REACTOR BY PULSED-NEUTRON TECHNIQUES

E. C. Campbell      P. H. Stelson

The time constant for the decay of the fundamental mode of an enriched subcritical  $U^{235}$ - $H_2O$  reactor has been measured by the use of a square-wave pulsed-neutron source and a multichannel time analyzer. The method is analogous to that used in the investigation of electronic amplifiers, whereby the response to a square-wave signal fed to the input provides an accurate picture of the characteristics of the amplifier. One may consider that a reactor is in fact a neutron amplifier in which multiplication of neutrons via the fission process plays the role of positive feedback in the

system. By measuring for different reactor sizes the time constant for the decay of neutron flux in the reactor following a short burst of incident neutrons from an external source, one may deduce with the aid of elementary reactor theory numerical values of the parameters needed to describe the reactor.

For the present experiment there was available 8 liters of uranyl fluoride solution in ordinary water containing 53.0 g of  $U^{235}$  per liter. Four 12-in.-high aluminum cylindrical vessels of nominal diameters 4, 5, 6, and 8 in. were used to

contain the solution. These were suspended about 2 in. from a beryllium target in which neutrons were produced by the proton beam of the ORNL 5.5-Mv electrostatic accelerator. The height of the vessel was adjusted so that the target lay in the median plane of the cylinder of liquid. Neutrons leaking from the cylinder during the off-periods of the beam, which was modulated by an electrostatic deflector, were detected by a small ( $2 \times 10 \times 10$  mm)  $\text{Li}^{61}(\text{Eu})$  scintillation counter. This was placed on the cylinder at an azimuthal position of 90 deg to the direction of the beam and at a vertical position of  $\frac{1}{3} H$ , where  $H$  is the extrapolated height of the liquid cylinder.

On the basis of elementary diffusion theory one can derive the following expression for the decay constant of the fundamental mode of a subcritical thermal reactor:

$$(1) \quad \lambda = \nu \Sigma_a + DB^2 + \nu \Sigma_F [1 - \eta \bar{P}(B^2)] .$$

Here  $\Sigma_a$  denotes the macroscopic thermal absorption cross section of the moderator;  $\nu$ , the neutron speed;  $D$ , the diffusion constant of the moderator;  $B^2$ , the geometrical buckling of the fundamental mode, equal to the lowest eigenvalue of the equation  $\nabla^2 \chi + B^2 \chi = 0$  subject to the condition that  $\chi = 0$  on the extrapolated boundary of the reactor. The first term represents the probability per second for absorption in the moderator, while the second gives the probability per second for leakage of neutrons from the reactor. Since these two processes are mutually exclusive, the sum of the first two terms represents the decay rate of neutrons in the pure moderator. The third term involves the properties of fissile material, which is assumed to be distributed homogeneously throughout the moderator. Here  $\Sigma_F$  is the macroscopic thermal absorption cross section of the fissile material,  $\eta$  is the number of prompt fast neutrons produced per thermal neutron absorbed in the fissile material, and  $\bar{P}(B^2)$  denotes the probability that a fast neutron produced in fission will be slowed down to thermal energies inside the reactor having buckling  $B^2$ . In reactor theory  $\bar{P}(B^2)$  is called the Fourier transform of the slowing-down kernel. The meaning of the third term is evident when one considers that the effect of the fissile material is twofold: namely, extra neutron absorption which is partially compensated by the neutron multiplication. It is assumed that the characteristic time for the slowing-down process is sufficiently small compared with the

time constant of the reactor and that the effect of multiplication in the fissile material can be regarded as merely reducing its absorption cross section, an effect which depends on the size of the reactor through the quantity  $B^2$ , the geometrical buckling of the fundamental mode.

We see then that as  $B^2$  is decreased by increasing the size of the reactor the third term will change sign from positive to negative. The value of  $B^2$ , which is a solution of  $1 - \eta \bar{P}(B^2) = 0$ , is called "neutral buckling." At this buckling the reactor decay constant is independent of the concentration of fissile material and is equal to that of the pure moderator. In other words the absorption and multiplication effects of the fissile material exactly balance. The critical buckling must be smaller than the neutral buckling.

The decay constant deduced from the decay curves for various-size cylindrical samples of the  $\text{U}^{235}\text{-H}_2\text{O}$  solution is plotted in Fig. 1 as a

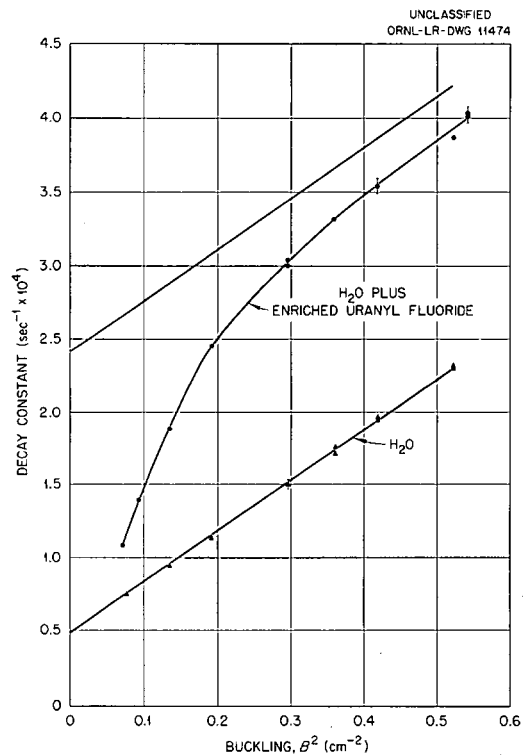


Fig. 1. Decay Constant of Thermal Neutrons Diffusing out of Cylinders of  $\text{U}^{235}\text{-H}_2\text{O}$  Solution as a Function of Geometrical Buckling. Over the range of buckling from  $0.072$  to  $0.54 \text{ cm}^{-2}$ , the measured half life varied from  $64.2$  to  $17.9 \mu\text{sec}$ .

function of the geometrical buckling calculated from the extrapolated dimensions of the cylinders. The corresponding points for  $H_2O$  are also given. The unlabeled line with an intercept at  $2.41 \times 10^4 \text{ sec}^{-1}$  represents the expected behavior of the curve for the case of a nonfissioning absorber with the same macroscopic thermal cross section as that

of the  $U^{235}$  in the solution. The difference is ascribed to the "effective negative absorption" associated with the last term in Eq. 1. A reasonably good fit to the experimental points is obtained with the assumption that  $\bar{P}(B^2)$  has the form of the Fourier transform of a diffusion kernel, namely  $(1 + \tau B^2)^{-1}$  with  $\tau$  equal to  $25 \text{ cm}^2$ .

## RECOIL SPECTROMETRY

A. H. Snell

F. Pleasonton

### IONIZATION FOLLOWING RADIOACTIVE DECAY OF $Xe^{131m}$ AND $Kr^{85}$

There are several mechanisms that can lead to internal ionization in atoms following radioactive decay. Those of main importance can be divided into three basic types:

1. The development of cascades in the Auger effect. — These are initiated by the appearance of a vacancy in one of the inner electron shells and will follow internal conversion (itself an ionizing process) and electron capture (not an ionizing event). If the vacancy is in the  $K$  shell, it can be filled for example in an Auger transition from the  $L$  shell with the ejection of another  $L$  electron, after which the two  $L$  vacancies can themselves be filled by Auger transitions so that four vacancies are produced, and so on — the vacancies multiply as they proceed outward through the electronic structure.

2. An electrostatic "shakeoff" produced by a change in nuclear charge. — This will follow beta emission. It has been extensively treated theoretically and has been observed experimentally by  $K$  x-ray measurements in the case of some of the rather light elements. It seems to be rather well understood as far as the inner electron shells are concerned.

3. A nonnuclear "shakeoff" produced by a change in electric field following the sudden loss of an electron. — This may also follow internal conversion and electron capture. Lacking any theoretical estimate of its importance, one might guess it to be comparable to the other "shakeoff" process.

The spectrometer has been used to study ionization following electron capture ( $A^{37} \rightarrow Cl^{37}$ ), internal conversion ( $Xe^{131m} \rightarrow Xe^{131}$ ), and beta-minus emission ( $Kr^{85} \rightarrow Rb^{85}$ ). The results of the work on  $A^{37}$  were given in the preceding progress report<sup>1</sup> and appear in complete detail elsewhere.<sup>2</sup>

The apparatus used for the measurement of the charge spectrum of  $Xe^{131}$  is a modification of that employed in the previous neutrino recoil experimentation using  $A^{37}$ . It is shown diagrammatically in Fig. 1. The radioactive gas is contained in a source volume at low pressure (about  $4 \times 10^{-6}$  mm total), and a beam of the ions that result from radioactive decay therein is taken from an aperture  $\frac{1}{2}$  in. in diameter, subjected to analysis by deflection through  $96.5$  deg in a two-directional focusing magnetic spectrometer, and finally accelerated through about  $5000$  v for counting by means of an electron multiplier. Differential pumping reduces the background that would otherwise inevitably be present because of direct flow of the radioactive gas to the region of the detector. In the xenon measurements we are no longer interested in the recoil energies of the ions, and a great gain in efficiency over the field-free  $A^{37}$  source-volume arrangement can be realized by supplying an electric collecting field that impels the ions toward the spectrometer. For this purpose a set of stainless steel field rings is assembled

<sup>1</sup>A. H. Snell and F. Pleasonton, *Phys. Semiann. Prog. Rep. Sept. 10, 1955*, ORNL-1975, p 51.

<sup>2</sup>A. H. Snell and F. Pleasonton, *Phys. Rev.* 100, 1396 (1955).

UNCLASSIFIED  
ORNL-LR-DWG 11287

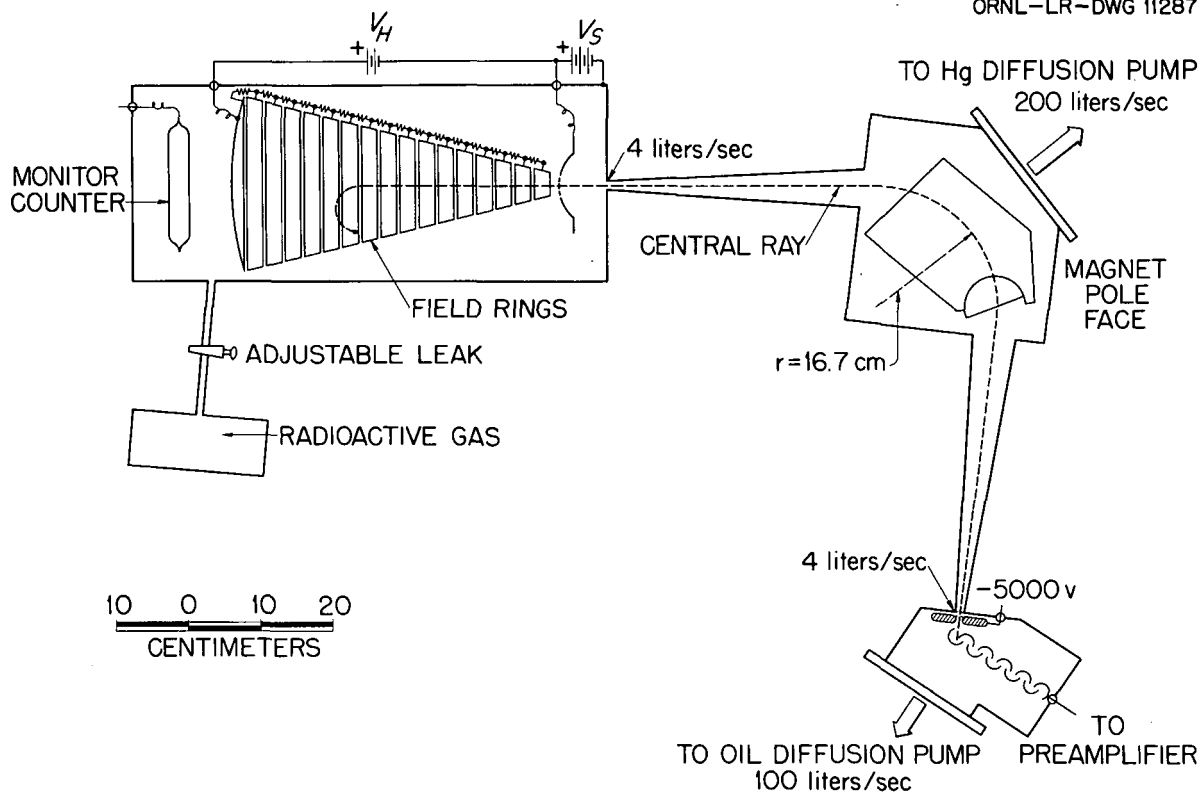


Fig. 1. Diagram of the Major Components of the Charge Spectrometer.

inside the source volume, so as to constitute a conical arrangement, and a potential drop  $V_H$  is divided among them in such a way as to establish a radial electric field similar to one that would surround a conducting sphere 2 in. in radius. Thus the electric lines of force inside the conical "howitzer" are straight, and they are arranged so as to converge toward a center near the object position for the spectrometer. Ions emerging from the howitzer into this region are accelerated further by a voltage  $V_S$  before entering the analyzer. The voltage  $V_S$  is made 40 times as large as  $V_H$  in order that the total energy spread arising from the point-of-origin effect in the source volume will be small compared with the transmission width of the spectrometer. The latter width is 2.8% in energy, full width at half maximum, so that at a single setting the spectrometer will

easily transmit the full intensity of the ions having a given  $e/m$  value. It is of course essential that the collecting and focusing be equally efficient from charge to charge. This is ensured by making  $V_H$  and  $V_S$  inversely proportional to the charge of the ion under investigation. A beta-gamma counter inside the source volume serves to monitor the source strength.

Since Auger cascades are probably of main importance in creating the highly charged states following both electron capture and internal conversion, it is not surprising that the shapes of the resulting charge spectra were found to be quite similar for  $A^{37}$  and  $Xe^{131m}$ . The latter peaks sharply at charge 8, dropping off rather rapidly thereafter, but persisting out to charge 29, and yields an average charge of 8.04. The observed distribution is given in Table 1 and is shown in a

**TABLE 1. THE CHARGE SPECTRUM OF  $Xe^{131m}$   
FOLLOWING INTERNAL CONVERSION**

Charge	Intensity (%)	Charge	Intensity (%)
1	$0.62 \pm 0.12$	16	$0.242 \pm 0.004$
2	$0.97 \pm 0.03$	17	$0.098 \pm 0.002$
3	$1.62 \pm 0.06$	18	$0.036 \pm 0.001$
4	$4.26 \pm 0.06$	19	$0.023 \pm 0.001$
5	$5.36 \pm 0.10$	20	$0.014 \pm 0.001$
6	$10.42 \pm 0.13$	21	$0.012 \pm 0.001$
7	$15.69 \pm 0.25$	22	$0.013 \pm 0.001$
8	$20.88 \pm 0.19$	23	$0.006 \pm 0.001$
9	$15.74 \pm 0.24$	24	$0.010 \pm 0.001$
10	$11.32 \pm 0.19$	25	$0.004 \pm 0.002$
11	$6.22 \pm 0.10$	26	$0.004 \pm 0.001$
12	$3.01 \pm 0.04$	27	$0.002 \pm 0.001$
13	$1.78 \pm 0.03$	28	$0.007 \pm 0.001$
14	$1.09 \pm 0.01$	29	$0.006 \pm 0.002$
15	$0.55 \pm 0.01$	30	$0.001 \pm 0.001$

semilogarithmic histogram in Fig. 2. The intensity for charge 1 indicates that in only 0.62% of the cases is the inner shell vacancy filled by purely radiative processes.

One objective test of the cascade hypothesis is to see if a cascade, every step of which is energetically possible, can be constructed which will throw off as many as 28 electrons. We have succeeded in constructing such a cascade, using the table of x-ray absorption edges given by Hill, Church, and Mihelich<sup>3</sup> as a guide to the energetic possibility of each step. The cascade is reproduced in Fig. 3, and it will require a paragraph of description.

An initial  $K$  vacancy is followed by a  $K-L_1L_1$  transition that gives rise to two main branches which can be almost identical, as shown at left and right. One reads the diagram under the supposition that the circles represent electron sites in the shell structure and that a wave of vacancies proceeds from the bottom upward. The arrows represent sites from which an electron is ejected. Both of the  $L_1$  vacancies in the second row from the bottom are filled with  $L_1-L_{11}N_1$  transitions, and the two resulting  $N_1$  vacancies

<sup>3</sup>R. D. Hill, E. L. Church, and J. W. Mihelich, *Rev. Sci. Instr.* 23, 523 (1952).

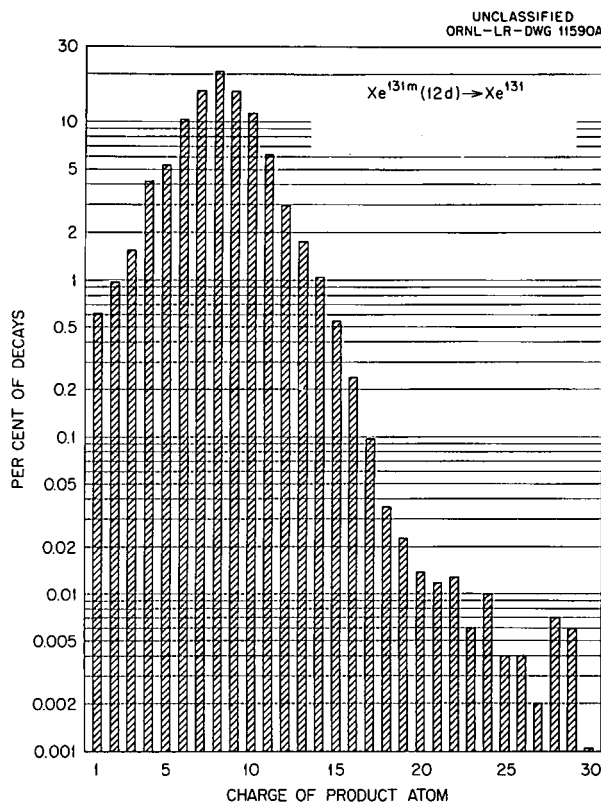


Fig. 2. Histogram of the Charge Spectrum Following Internal Conversion in  $Xe^{131m}$ .

are filled by  $N_1-N_{11}O_1$  processes. We are now through event No. 3, as numbered in the right-hand branch, but we will have to remember that the  $N_1$  positions are left occupied, for these electrons will be needed in the final step. Event No. 4 is an  $L_{11}-L_{111}N_{11}$  transition, and following it we come to a special situation in the  $M_1$  and  $M_{11}$  subshells. In general, it must be supposed that the two main branches will not develop simultaneously in time, and since we are proceeding on the assumption of well-defined states between Auger transitions, it seems to be no real strain to imagine that the two available  $M_1$  sites are simultaneously emptied in an  $L_{111}-M_1M_1$  transition in one branch (event No. 5) and that they are refilled from the  $M_{11}$  subshell (event No. 6) in time to permit a repetition of the  $L_{111}-M_1M_1$  transition in the other branch. The dotted lines are injected to call attention to this double use of the  $M_1$  positions. In the case of the two available  $M_{11}$  locations, there is no electron ejection, but the locations have to be used by two electrons that

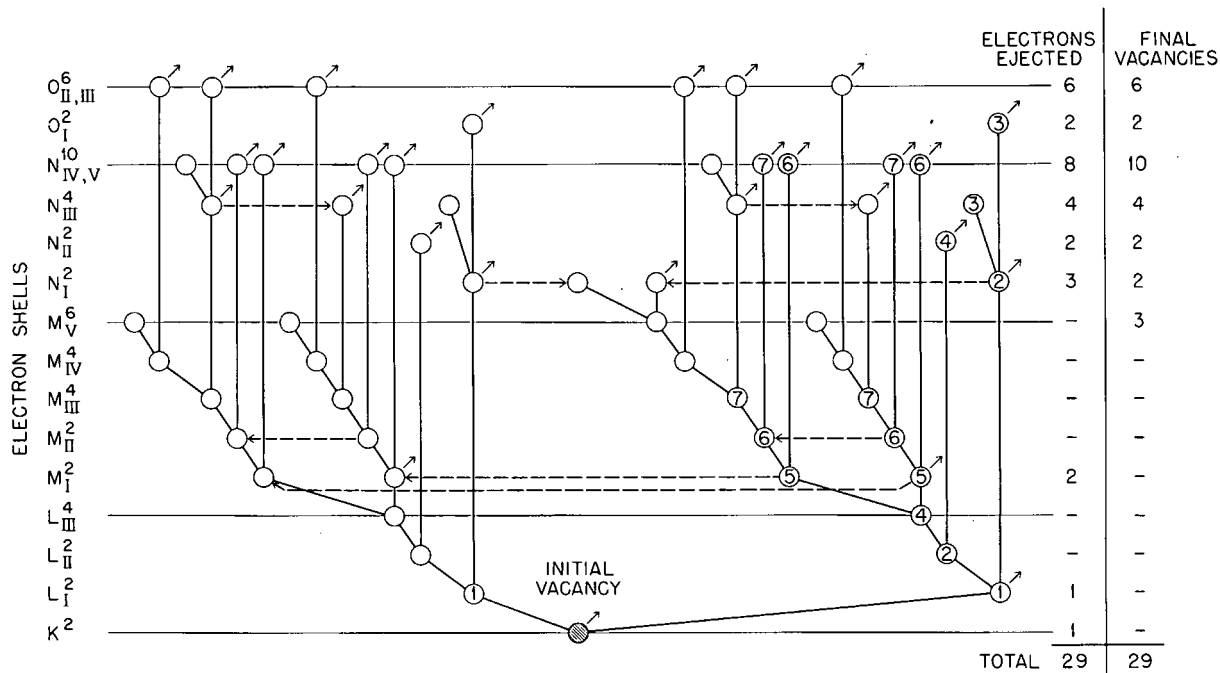


Fig. 3. A Conceptual Vacancy Cascade in Xenon, Showing How an Atom Initially Ionized in the K Shell Can Within the Limits of Energetic Possibility Throw Off 28 Additional Electrons. The circles represent electron positions in the various shells, and the vacancies are imagined to move upward, the electron positions filling in behind the vacancies. In the usual notation of the Auger effect, the first transition is  $K - L_I L_I$ , where the letters refer to vacancies. Event No. 2 is  $L_I - L_{II} N_I$ , and so on. The two  $L_I$  vacancies give rise to two main branches, left and right, which can be almost identical. The dotted lines direct attention to electron positions that are used twice, in time sequence. The arrows designate sites from which electrons are ejected into the continuum, and a count of the arrows indicates that the cascade results in 29-fold ionization.

filter through to fill  $M_I$  vacancies (event No. 6) before they are filled permanently in the event labeled 7,  $M_{II} - M_{III} N_{IV} v$ . Thereafter, the course of events may be clear from the diagram, transitions between the M subshells throwing off N and O electrons and two of the  $N_{III}$  positions being twice used. At the penultimate stage we have four vacancies in the  $M_V$  shell and the two occupied  $N_I$  positions left from early in the cascade. This prepares the situation for the ultimate step pictured in the center of the diagram, in which one of the  $N_I$  electrons falls into one of the  $M_V$  vacancies, thereby ejecting the other  $N_I$  electrons. The result of the total cascade is the ejection of

28 electrons, in addition to the initial internal conversion electron.

In contrast to the distributions found in the above studies is the one for the  $Rb^{85}$  following the beta decay of  $Kr^{85}$ . The work to date is summarized in the following abstract quoted from the *Bulletin of the American Physical Society*, Southeastern Section Meeting, 1956:

Magnetic analysis has been used to measure the charge spectrum of the rubidium atoms produced in the radioactive decay of  $Kr^{85}$ . This 9.4-year activity is almost a pure beta emitter. The results, which are still provisional in that pressure effects in the apparatus

have not yet been investigated, are as follows:

Charge	Per cent of Decays
1	75.60
2	12.57
3	4.50
4	3.56
5	2.09
6	0.77
7	0.51
8	0.25
9	0.11
10	0.04
11	Sought, not found

The charge 1 ions represent the clean emission of the negative beta particle; charge 2 and higher represent the cases in which beta emission is accompanied by some kind of an atomic ionization event. The totality of ions of charge 2 and higher indicates that ionization takes place in 25 per cent of the decays. This is considerably more than would be suggested by present theory, which admittedly does not hold for the outer electron shells. The shape of the charge spectrum indicates that most of the electrons are removed from the outer shells; this is qualitatively in agreement with theory when screening is taken into account, for the probability of ionization is expected to go as  $1/Z_{\text{eff}}^2$ .

From the experimental point of view the success of the "charge spectrometer" opens intriguing possibilities. By selecting other representatives in the family of radioactive rare gases, one can

throw more light on the matters of mechanism described in the first paragraph of this paper. There may also be ion-source possibilities, for clearly one way to produce multiply charged ions is simply to knock out an inner electron — the Auger cascades will do the rest. Molecular effects may be of great interest from a chemical point of view; an inner-shell ionization event in a constituent atom may have indirect ionizing consequences throughout the rest of the molecule. There may be a deepening and broadening of the whole field of hot-atom chemistry in this aspect, for no longer is one limited to following the fate of a radioactive atom alone, but one can see presumably what happens to the rest of the molecule after the radioactive decay of one of its atoms; the limitations in principle are only that the compound be available in the vapor phase and that the abundance of neutral molecular fragments will have to be a matter of inference. Perhaps the initiation of Auger cascades can be followed by using nonradioactive gas under electron bombardment, increasing the energy of the incident electrons through the ionization potentials of successively deeper electron shells, and adding detail to older work in which only the x rays were observed. Finally, the practically untouched field of the measurement of atomic and molecular collision and electron-capture cross sections for very highly ionized atoms seems to be within the reach of experimentation.

ANTIFERROMAGNETIC STRUCTURES OF ANHYDROUS  $\text{CoCl}_2$  AND  $\text{FeCl}_2$ 

M. K. Wilkinson

J. W. Cable

Anhydrous  $\text{CoCl}_2$  and  $\text{FeCl}_2$  both crystallize in the pseudohexagonal structure characteristic of  $\text{CdCl}_2$ . This structure is a hexagonal layer-type structure in which the layers of metal ions are separated by two layers of halogens similar to the arrangement in the  $\text{CdI}_2$  type of structure. However, in contrast to the  $\text{CdI}_2$  structure, where the metal ions in adjacent layers are directly above each other, the metal ions in adjacent layers of the  $\text{CdCl}_2$  structure are shifted slightly within the layers so that repetition occurs every third layer. Stacking faults are frequent in all types of hexagonal layer-type structures, and the metal ions become disordered with respect to the particular sets of interstices which they occupy between the halogen positions. In general, the crystal structure within a layer is normal, and the stacking faults merely shift the layers with respect to their proper crystallographic position. For this reason these structures are somewhat "two-dimensional" and have many interesting properties.

The temperature variation of the magnetic susceptibility<sup>1</sup> and the specific heat<sup>2,3</sup> of anhydrous  $\text{CoCl}_2$  and  $\text{FeCl}_2$  have shown anomalous behavior at low temperatures suggestive of antiferromagnetic transitions. The specific Néel temperatures indicated by these measurements are 25°K for  $\text{CoCl}_2$  and 24°K for  $\text{FeCl}_2$ . Hence, a neutron-diffraction investigation has been initiated to determine the existence of any long-range magnetic order in these compounds at low temperatures. Such experiments should give information concerning the type of magnetic coupling which is predominant in layer-type structures.

Because of the prevalence of stacking faults, extreme care must be taken in the preparation of these compounds to obtain crystallographically pure samples. Many methods of preparation were

attempted,<sup>4</sup> and most of the samples showed Bragg reflections which appeared to be due to stacking faults in the structures. The best samples were prepared by sublimation of anhydrous compounds which were obtained from the hydrates by dehydration in HCl at about 300°C. Enough material was prepared to obtain sufficient quantities of 100-mesh powder without the necessity of grinding the larger particles.

Two samples of  $\text{CoCl}_2$  have been studied in detail by neutron diffraction. One of these samples was prepared by sublimation and had reflections characteristic only of the  $\text{CdCl}_2$  structure, while the other had additional lines indicative of stacking faults in the layers. Both samples were studied at a series of temperatures down to 4.2°K, and both diffraction patterns at 4.2°K showed superstructure lines caused by antiferromagnetic ordering of the atomic magnetic moments. Figure 1 represents the difference between diffraction patterns taken at 4.2 and 43°K for the sublimed material, and the diffraction peaks are thereby characteristic only of the magnetic coherent scattering present at 4.2°K which was not present at 43°K. The diffraction patterns were taken with Soller slits limiting the horizontal divergence of the scattered radiation which reached the detector. However, the slit geometry allowed considerable vertical divergence of the scattered neutrons, and the asymmetry of the (003) magnetic reflection was probably the result of this divergence. The negative background in the difference pattern represents the paramagnetic diffuse scattering which occurred at 43°K. The data obtained for the other sample were quite comparable and suggest that the magnetic structure was not affected appreciably by stacking faults in the second sample. The antiferromagnetic intensity maxima can be indexed on the basis of a hexagonal magnetic unit cell in which the  $c$  axis is twice the  $c$  axis of the chemical cell and the  $a$  axis is identical to that of the chemical cell. This

<sup>1</sup>C. Starr, F. Bitter, and A. R. Kaufmann, *Phys. Rev.* 58, 977 (1940).

<sup>2</sup>O. N. Trapeznikowa and L. W. Schubnikow, *Physik. Z. Sowjetunion* 7, 66 (1935).

<sup>3</sup>O. Trapeznikowa, L. Schubnikow, and G. Miljutin, *Physik. Z. Sowjetunion* 9, 237 (1936).

<sup>4</sup>We are very much indebted to D. E. LaValle of the Analytical Chemistry Division for preparing these samples and to H. Yakel and R. M. Steele of the Metallurgy Division for help in determining crystallographic impurities by x-ray diffraction.

UNCLASSIFIED  
ORNL-LR-DWG 12665

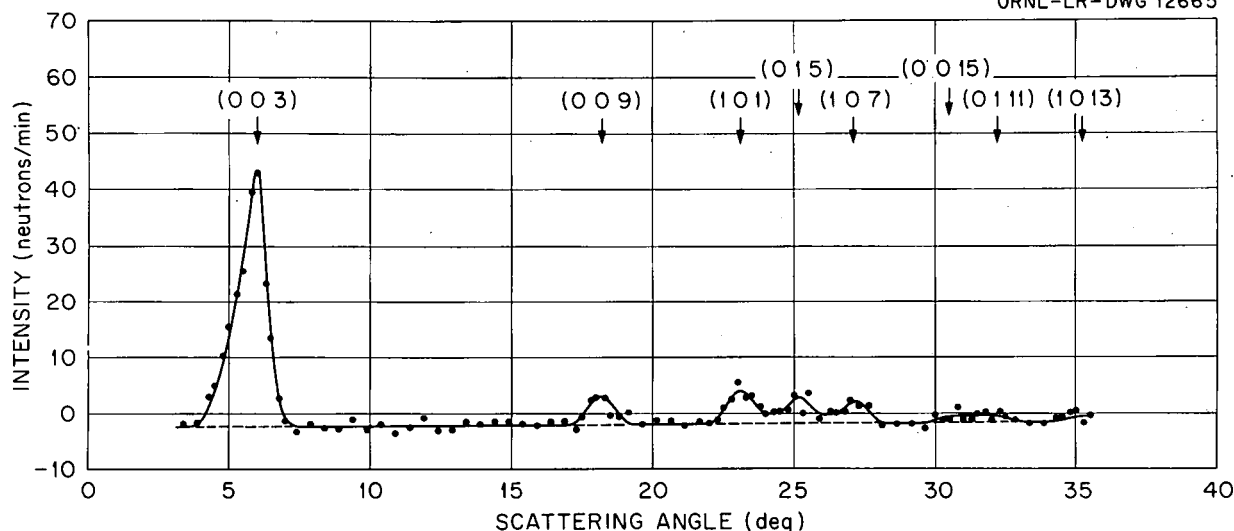


Fig. 1. Pattern of the Difference Between Diffraction Data from Anhydrous  $\text{CoCl}_2$  at 4.2 and 43°K. The data at 43°K were subtracted from those at 4.2°K.

suggested magnetic cell, therefore, represents an antiferromagnetic structure in which the cobalt moments are aligned parallel within each hexagonal layer and the moments of adjacent cobalt layers are aligned antiparallel. Furthermore, the direction of the moments is normal or nearly normal to the hexagonal axis. The intensity of the (003) magnetic reflection was studied as a function of temperature and the results are shown in Fig. 2. The temperatures were measured by a calibrated copper-constantan thermocouple and are probably accurate to about 1 degree. It is seen that the scattered magnetic intensity follows a Brillouin-type curve and suggests a Néel temperature of about 25°K, in good agreement with the specific-heat and magnetic-susceptibility anomalies obtained previously. Similar data for the sample which was crystallographically impure indicated the same value for the Néel transition. Therefore, within experimental accuracy, the stacking faults in one of the samples appeared to have no effect on the temperature at which antiferromagnetic ordering occurred.

Diffraction patterns have been obtained for anhydrous  $\text{FeCl}_2$  at a series of temperatures to 4.2°K. These data show antiferromagnetic reflections at 4.2°K which disappear at about 24°K, the Néel temperature predicted from specific-heat and magnetic-susceptibility measurements.

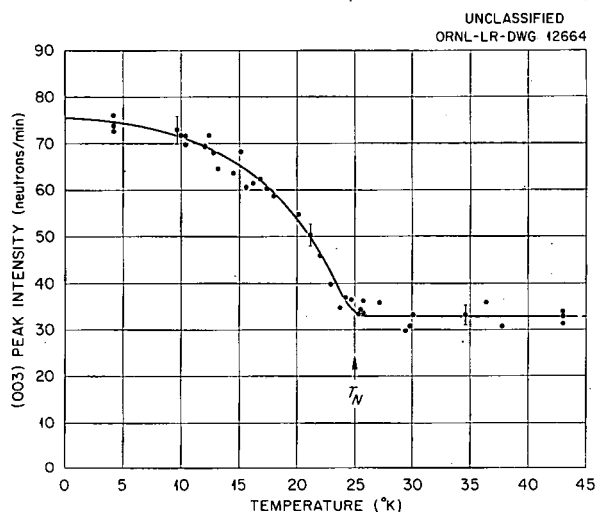


Fig. 2. Temperature Variation of the Peak Intensity of the (003) Magnetic Reflector from  $\text{CoCl}_2$ .

Furthermore, the magnetic reflections can be indexed on the basis of a similar antiferromagnetic structure in which the magnetic moments of the iron atoms within each hexagonal layer are aligned parallel, with antiparallel alignment between adjacent layers. However, in contrast to the suggested  $\text{CoCl}_2$  magnetic structure, where the moments are aligned normal or nearly normal to

the hexagonal axis, the moments in  $\text{FeCl}_2$  are parallel to that axis.

While the reason for the direction of moments within these structures is not understood, it is interesting that two materials with almost identical crystal structures and magnetic-ordering temperatures should have magnetic structures in which the direction of alignment of the atomic moments is quite different. This difference in the direction

of the atomic magnetic moments is quite similar to conditions that have been found for  $\text{MnBr}_2$  and  $\text{FeBr}_2$  by Koehler and Wollan.<sup>5</sup> However, in the case of the bromides, while the crystal structures are almost identical (both compounds have the hexagonal  $\text{CdI}_2$  structure), the magnetic-ordering temperatures are different.

<sup>5</sup>W. C. Koehler and E. O. Wollan, *Phys. Semiann. Prog. Rep. Sept. 10, 1955*, ORNL-1975, p 55.

### INVESTIGATIONS OF CRITICAL MAGNETIC SCATTERING

M. K. Wilkinson

C. G. Shull<sup>1</sup>

In a previous investigation<sup>2</sup> of the magnetic scattering properties of polycrystalline iron at high temperatures, pronounced small-angle scattering was found to occur in the vicinity of the Curie temperature of 770°C. This small-angle scattering has been interpreted<sup>3</sup> according to a theoretical treatment developed by Van Hove,<sup>4</sup> which predicts excessive small-angle scattering near  $T_c$  resulting from large spontaneous fluctuations in the magnetization. This situation is entirely analogous to the abnormally large scattering from a gas near the critical point and has been termed "critical magnetic scattering." It was of interest to investigate experimentally certain conditions which might influence the intensity of the observed critical magnetic scattering.

The small-angle scattering from a single crystal of pure iron (grown by the strain-anneal technique) was studied for comparison with that produced by a polycrystalline sample. In this experiment the scattered intensity of 1.218-Å neutrons was measured at a fixed scattering angle of 1 deg as the temperature of the iron was varied. The results for the two samples shown in Fig. 1 exhibit the

pronounced critical scattering which was observed near  $T_c$ . For convenient comparison purposes, the two samples were of exactly the same dimensions, and identical observational conditions were used in the two experiments. Therefore the intensity scales are directly comparable, and it

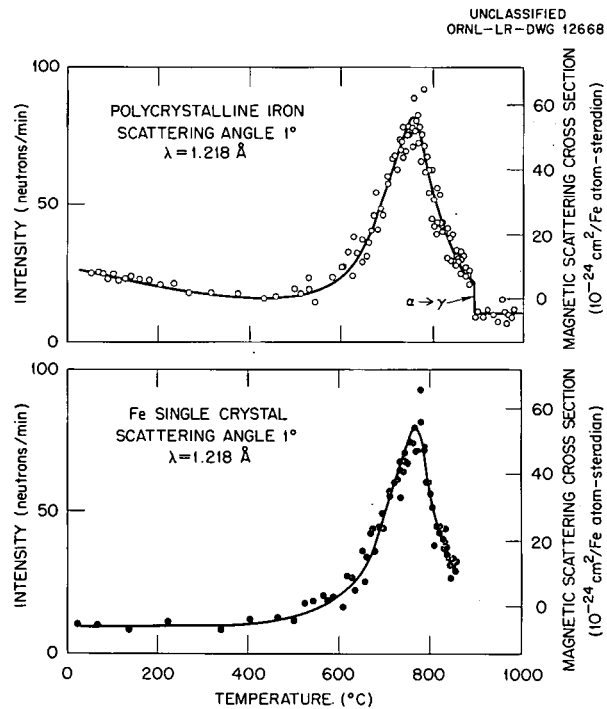


Fig. 1. Temperature Variation of the Scattered Intensities from Polycrystalline Iron and a Single Crystal of Iron.

<sup>1</sup>Now at Massachusetts Institute of Technology, assigned to Brookhaven National Laboratory.

<sup>2</sup>M. K. Wilkinson and C. G. Shull, *Phys. Semiann. Prog. Rep. March 10, 1954*, ORNL-1705, p 31.

<sup>3</sup>H. A. Gersch, C. G. Shull, and M. K. Wilkinson, *Phys. Semiann. Prog. Rep. Sept. 10, 1955*, ORNL-1975, p 53.

<sup>4</sup>L. Van Hove, *Phys. Rev.* 95, 1374 (1954).

is seen that the single-crystal results are the same as the polycrystalline results with respect to the development of scattering near the Curie temperature. Hence, critical magnetic scattering is independent of the size and orientation of the crystalline grains in the solid specimens. To indicate the very large intensities occurring in this type of scattering, an absolute differential-scattering cross-section scale is given for the data. As a comparison, the expected paramagnetic diffuse scattering in the forward direction from iron at temperatures above  $T_c$  is only 0.43 barn/steradian per iron atom. Also of interest in the results for the polycrystalline sample is the sharp decrease in intensity at the  $\alpha$ - $\gamma$  phase transformation when the structure changed from body-centered-cubic to face-centered-cubic. This discontinuity in the scattering intensity at an angle of 1 deg has been studied a number of times with different polycrystalline samples, and it exhibits the usual temperature hysteresis found for this phase transformation. The variation in the background scattering at low temperatures for the polycrystalline sample is believed to be due to changes with temperature of the domain structures in the sample. Such changes would cause the refractive-index type of magnetic scattering found by Hughes, Burgy, Heller, and Wallace<sup>5</sup> to have a temperature dependence, and the scattered radiation passing through the detector-Soller-slit system would be altered.

The intensity of ferromagnetic coherent scattering is usually sensitive to the application of an external magnetic field to the scattering specimen. This change in the scattered intensity results because a magnetic field of sufficient intensity will align the direction of magnetization of the magnetic domains along the field direction, and the magnetic scattering of neutrons depends on the relative orientation of the atomic magnetic moments with respect to the scattering vector. If the critical magnetic scattering were the result of a disruption in size of the static-domain regions, then it would be sensitive to the application of an external field. To perform this investigation, a special furnace was constructed between the pole pieces of an electromagnet so that sample temperatures up to 800°C could be obtained simultaneously with the application of an external field of

about 8000 oersteds. It was found that there was no effect of this external field on the small-angle scattering and consequently that critical scattering is the same irrespective of whether the specimen is in a single-domain state or is of random poly-domain nature.

A sample of electrolytically pure nickel was investigated at temperatures through its Curie transition (360°C) in a search for small-angle scattering, and Fig. 2 shows the results which were obtained. The lower curve indicates the scattered intensity as a function of temperature for a fixed detector angle of 1 deg, while the top curve shows the angular variation of the small-angle magnetic scattering for a temperature close to  $T_c$ . The latter curve represents the difference in the scattered intensity at 366°C relative to that at room temperature. An absolute cross-section scale is shown on the lower figure, and the critical scattering is seen to be very much smaller for nickel than that which was observed from iron. This difference would be expected, since the values for the atomic magnetic moments present in nickel are considerably smaller than those in iron. Specifically, the ferromagnetic atomic moment of nickel is  $0.61 \mu_B$  compared with  $2.22 \mu_B$  for iron.

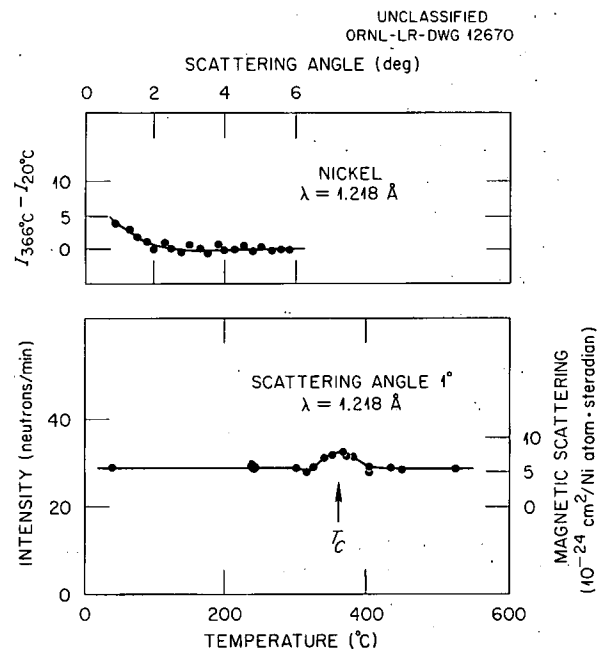


Fig. 2. Small-Angle Scattering Obtained from Nickel.

<sup>5</sup>D. J. Hughes *et al.*, *Phys. Rev.* **75**, 565 (1949).

Magnetite ( $\text{Fe}_3\text{O}_4$ ) is a *ferrimagnetic* type of material in which the three iron atoms per molecule exhibit magnetic moments of +5, +4, and  $-5 \mu_B$ . Although the individual atomic moments are large, the net ferromagnetic moment is much smaller ( $\frac{4}{3} \mu_B$  per iron atom) because of the antiparallel orientation of the moments. Small-angle scattering near the Curie temperature is shown in Fig. 3, and the absolute cross sections associated with this scattering are seen to be quite small. This indicates that the net ferromagnetic moment determines the strength of the critical scattering rather than the values of the individual moments and suggests that the molecular group retains the internal orientation of its atomic moments in passing through the Curie temperature.

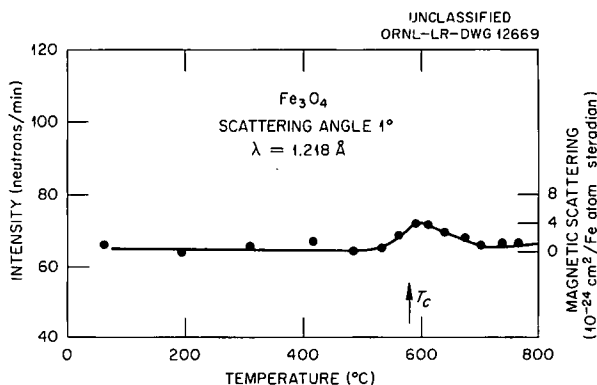


Fig. 3. Small-Angle Scattering Obtained from Magnetite.

## NEUTRON-DIFFRACTION OBSERVATIONS ON HOLMIUM OXIDE

W. C. Koehler  
E. O. Wollan

M. K. Wilkinson  
J. W. Cable

A neutron-diffraction study has been made of holmium oxide to measure the coherent nuclear scattering cross section of holmium and to investigate the magnetic properties of trivalent holmium ions in holmium oxide. The nuclear scattering data are reported here, together with preliminary results concerning the paramagnetic scattering at room temperature and the detection of long-range magnetic ordering of holmium ion moments at low temperatures. In spite of the fact that holmium is one of the least abundant of the rare earths, the extensive development of ion-exchange separation methods has accelerated the isolation of pure rare earths to the extent that the gram quantities necessary for neutron-diffraction study are now available.<sup>1</sup>

### NUCLEAR SCATTERING

The sesquioxides of the heavy rare earths, including  $\text{Ho}_2\text{O}_3$ , have the cubic  $\text{Tl}_2\text{O}_3$  structure, which contains 16 oxide molecules. The 32 metal

atoms occupy two sets of nonequivalent special positions of the space group  $T_b^7 \equiv Ia\bar{3}$ , and the 48 oxygens are in the general positions. In addition to the three oxygen parameters there is one metal parameter. Although these parameters have not been directly determined for the rare-earth sesquioxides, they have been measured by Pauling and Shappell<sup>2</sup> for the isomorphous mineral bixbyite,  $(\text{Fe},\text{Mn})_2\text{O}_3$ , and Zachariasen's<sup>3</sup> investigation of a series of isomorphous sesquioxides indicates that the parameters of the rare-earth oxides are not very much different from those of bixbyite. Neutron-diffraction data obtained from  $\text{Sc}_2\text{O}_3$  (ref. 4) and  $\text{Er}_2\text{O}_3$  (ref. 5) are also in accord with the bixbyite parameters.

In the interpretation of the room-temperature neutron-diffraction pattern of  $\text{Ho}_2\text{O}_3$ , the bixbyite

<sup>2</sup>L. Pauling and M. D. Shappell, *Z. Krist.* **75**, 128 (1930).

<sup>3</sup>W. H. Zachariasen, *Z. Krist.* **67**, 455 (1928).

<sup>4</sup>W. O. Milligan *et al.*, *J. Phys. Chem.* **57**, 535 (1953).

<sup>5</sup>W. C. Koehler and E. O. Wollan, *Phys. Rev.* **91**, 597 (1953).

<sup>1</sup>We wish to express our appreciation to F. H. Spedding, Iowa State College at Ames, for the loan of the  $\text{Ho}_2\text{O}_3$  sample.

parameters were assumed, and the holmium amplitude was determined primarily from the intensity of the (222) reflection, which has practically no oxygen contribution and is fairly insensitive to the metal parameter. Thus, even though the parameters of  $\text{Ho}_2\text{O}_3$  may be slightly different from those of bixbyite, a reliable scattering amplitude for holmium may be obtained. The scattering amplitude for holmium was found to be  $0.85 \times 10^{-12}$  cm, of positive phase, and the corresponding coherent nuclear scattering cross section is  $9.1 \pm 0.5$  barns. A comparison of observed and calculated  $|F|^2$  values based on the above cross section and the bixbyite parameters is given in Table 1.

The transmission of  $\text{Ho}_2\text{O}_3$  has been measured as a function of energy in the thermal region by Bernstein *et al.*,<sup>6</sup> from which data the total cross section of holmium as a function of energy was

<sup>6</sup>S. Bernstein *et al.*, *Phys. Rev.* 87, 487 (1952).

derived, and Pomerance<sup>7</sup> has reported a value of 64 barns for the capture cross section at a neutron energy of 0.025 ev. Transmission measurements made in the course of this investigation at 0.055 and 0.071 ev are in good agreement with the earlier measurements at the same neutron energies. Bernstein *et al.*, assuming that the capture cross section varied inversely as the neutron velocity, observed that the scattering cross section  $\sigma_s = \sigma_{tr} - \sigma_c$  decreased from 31 barns at 0.025 ev to 14 barns at 0.5 ev and suggested that the variation with energy of the scattering cross section be attributed to paramagnetic scattering from holmium ions. This interpretation is supported by recent experimental<sup>8</sup> and theoretical<sup>9</sup> investigations of

<sup>7</sup>H. Pomerance, *Phys. Rev.* 83, 641 (1951).

<sup>8</sup>W. C. Koehler and E. O. Wollan, *Phys. Rev.* 92, 1380 (1953).

<sup>9</sup>G. T. Trammell, *Phys. Rev.* 92, 1387 (1953).

TABLE 1. COMPARISON OF OBSERVED AND CALCULATED  $|F|^2$  VALUES FOR  $\text{Ho}_2\text{O}_3$

Index	$ F ^2_{\text{obs}}^* \left( \frac{10^{-24} \text{ cm}^2}{\text{molecule}} \right)$	$ F ^2_{\text{calc}}^{**} \left( \frac{10^{-24} \text{ cm}^2}{\text{molecule}} \right)$
110	0	0
200	0	0.0042
211	0.0934	0.106
220	0	0.0005
310	0	0
222	2.56	2.59
321	0.058	0.0543
400	0	0.0037
411	0	0.0303
420	0	0.0144
332	0.61	0.533
422	0	0.0188
431	0.10	0.146
521	Not measured	0.0388
440	6.95	6.76

\*The averages of three separate experiments.

\*\*Based on the bixbyite parameters and scattering amplitudes of  $0.85 \times 10^{-12}$  cm and  $0.58 \times 10^{-12}$  cm for holmium and oxygen, respectively.

the paramagnetic scattering of neutrons by rare-earth ions and by the present investigation.

The diffuse scattering in the room-temperature neutron-diffraction pattern of  $\text{Ho}_2\text{O}_3$  has been analyzed, with the result that the incoherent nuclear scattering cross section, which for holmium must be due to spin incoherence, is approximately 3.0 barns. This result is uncertain because of the difficulty of accurately evaluating multiple scattering in the pattern, but in any case an upper limit of 5.5 barns can be set. The total nuclear scattering cross section  $\sigma_{\text{coh}} + \sigma_{\text{inc}}$  at 0.055 eV is thus about 12 barns, which is well within experimental error of the 14 barns measured at 0.5 eV by Bernstein *et al.*,<sup>6</sup> at which energy paramagnetic scattering may be expected to be small. Further, since the coherent nuclear scattering cross section measured at 0.071 eV is, within experimental error, equal to that measured at 0.055 eV, the existence of a nuclear resonance at an energy lower than, but not distant from, 0.025 eV seems improbable. Finally, the magnitude and energy dependence of the total paramagnetic scattering cross section calculated from the present observations on the paramagnetic differential scattering cross section (to be described below) are in satisfactory agreement with the transmission data if it is assumed that the total nuclear scattering cross section is approximately constant over the energy range studied. The variation of the total paramagnetic cross section with energy for screening constants within the range of experimental uncertainty is shown in Fig. 1.

#### PARAMAGNETIC SCATTERING AT ROOM TEMPERATURE

The neutron-diffraction pattern of  $\text{Ho}_2\text{O}_3$  obtained at a neutron wave length of 1.218 Å is shown in Fig. 2. The coherent reflections are due to nuclear scattering, and the pronounced diffuse scattering is composed of contributions from (1) paramagnetic scattering, (2) thermal diffuse scattering, (3) spin incoherent nuclear scattering, and (4) multiple scattering. The separation of these contributions has been effected as described below.

It has been shown theoretically<sup>9</sup> for the rare-earth ions (except samarium and europium, which are special cases) and experimentally<sup>8</sup> for  $\text{Er}^{3+}$  and  $\text{Nd}^{3+}$  that the differential scattering cross

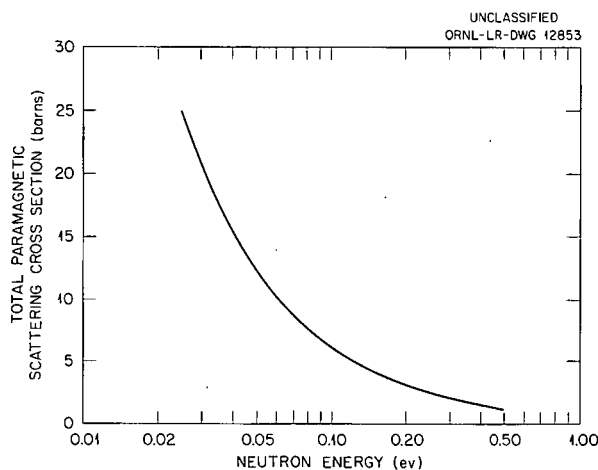


Fig. 1. Total Paramagnetic Scattering Cross Section of  $\text{Ho}^{3+}$  as a Function of Neutron Energy. The curve is based on screened hydrogenic wave functions for which  $Z - S = 20$ .

section for paramagnetic scattering in the forward direction is equal to

$$\frac{2}{3} \left( \frac{e^2 \gamma}{2mc^2} \right)^2 g^2 J(J + 1) ,$$

in which  $e$ ,  $m$ , and  $c$  have their usual significance,  $\gamma$  is the neutron magnetic moment in nuclear Bohr magnetons,  $g$  is the Landé splitting factor, and  $J$  is the total angular-momentum quantum number. For holmium this quantity, equal to 5.45 barns/steradian per ion, has been subtracted from the zero-angle extrapolation of the observed differential scattering cross section, and this gives a value of 0.95 barn/steradian per molecule for the scattering due to spin incoherent and multiple scattering.

This level is then taken as the isotropic base line from which to evaluate the paramagnetic and thermal diffuse scattering at scattering angles different from zero. It is not strictly true that the multiple scattering is isotropic, but, because of the relatively high capture cross section of holmium, its magnitude is small and the assumption of isotropy is a good approximation. The thermal diffuse scattering has been taken equal to that of  $\text{Er}_2\text{O}_3$  in view of the close similarity of the two compounds.

The angular variation of the paramagnetic differential-scattering cross section was obtained, and this is shown in Fig. 3. As in the case<sup>8</sup> of  $\text{Er}^{3+}$

UNCLASSIFIED  
ORNL-LR-DWG 12854

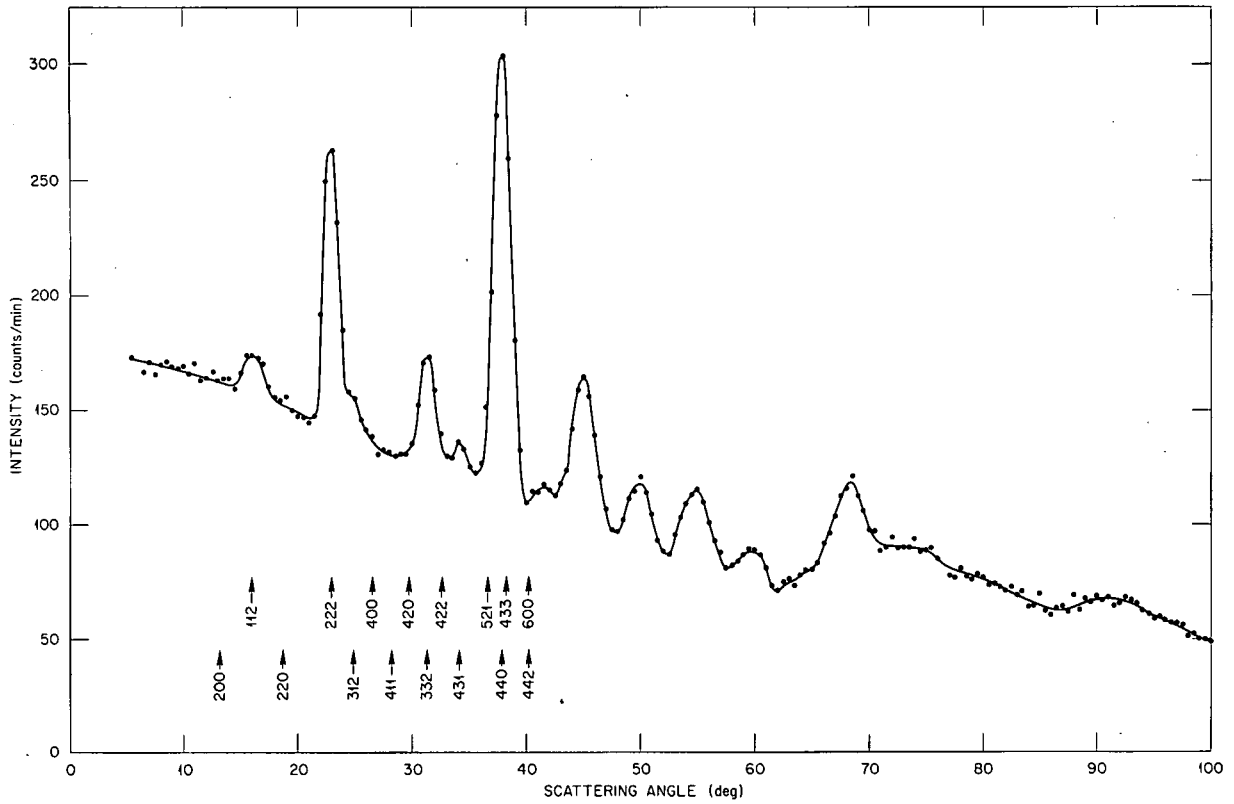


Fig. 2. Neutron-Diffraction Pattern of  $\text{Ho}_2\text{O}_3$ . Room temperature;  $\lambda = 1.218 \text{ \AA}$ .

UNCLASSIFIED  
ORNL-LR-DWG 12855

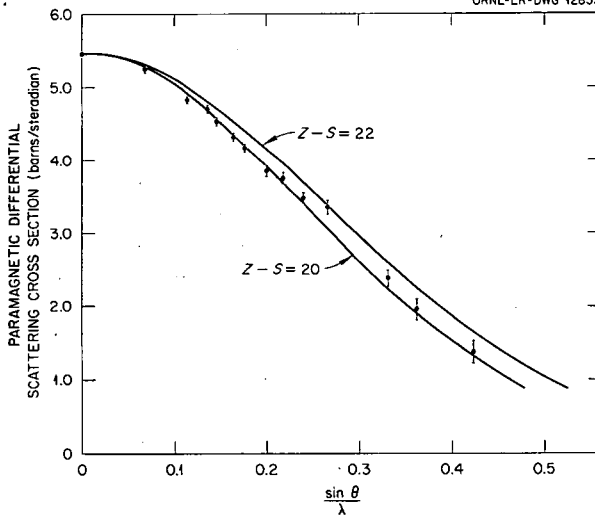


Fig. 3. Paramagnetic Differential-Scattering Cross Section of  $\text{Ho}^{3+}$ . The solid curves are calculated for screened hydrogenic wave functions with  $Z - S = 20$  and 22.

the form factor is strongly influenced by the orbital contribution to the moment. An approximate theoretical calculation of the angular dependence of the cross section has been made by following the general treatment of Trammell.<sup>9</sup> For scattering angles up to those for which moderate experimental accuracy can be obtained, the cross section can be represented to about 4% by the expression

$$\frac{d\sigma}{d\omega} = \frac{2}{3} \left( \frac{e^2\gamma}{2mc^2} \right)^2 [L_J f_0(k) + 2S_J g_0(k)]^2,$$

where

$$L_J = \frac{L \cdot J}{\sqrt{J(J+1)}},$$

$$S_J = \frac{S \cdot J}{\sqrt{J(J+1)}},$$

and  $f_0(k)$  and  $g_0(k)$  are explicitly evaluated by Trammell in terms of screened hydrogenic radial

wave functions. The parameter  $k$  is equal to

$$4\pi \left( \frac{\sin \theta}{\lambda} \frac{2a_0}{Z-S} \right),$$

where  $\theta$  is half the scattering angle and  $a_0$  is the Bohr radius. The calculated curves for  $Z-S=20$  and 22 are shown in Fig. 3 also.

The cross section obtained by integrating this calculated cross section over all scattering angles is the one plotted in Fig. 1.

#### DETECTION OF LONG-RANGE MAGNETIC ORDER IN $\text{Ho}_2\text{O}_3$

Observations made on  $\text{Ho}_2\text{O}_3$  at liquid-helium temperatures indicate the development of magnetic

ordering at these temperatures. At 4.2°K there is observed a pronounced broad maximum, which may possibly be due to antiferromagnetic short-range order. As the temperature is further reduced sharp coherent reflections appear at angular positions, suggestive of antiferromagnetic or ferrimagnetic ordering.

Although a definite structure has not yet been worked out, it may be noted that the magnetic structure of  $\text{Ho}_2\text{O}_3$  is unlike that of any so far observed for face-centered cubic structures even though the distribution of holmium atoms is approximately (neglecting the parameter) that of a face-centered cubic arrangement.

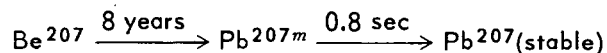
---

#### RAPID SEPARATION BY ION-EXCHANGE. YIELD FOR ANION-EXCHANGE SEPARATION OF $\text{Pb}^{207m}$ FROM $\text{Bi}^{207}$

E. C. Campbell

F. Nelson<sup>1</sup>

For establishing genetic relationships in nuclear decay schemes, the techniques of chemical separation have for many years been an invaluable tool of nuclear chemistry. The object of the present study was to investigate in some detail an ion-exchange technique for rapid separation. The study was carried out with the decay series



and makes use of the earlier observation<sup>2,3</sup> that  $\text{Pb}^{207m}$  could rapidly be separated from a shallow bed of anion-exchange resin on which the long-lived parent  $\text{Bi}^{207}$ , as  $\text{Bi}(\text{III})$ , was adsorbed.

Dry-screened quaternary amine resin beads (Dowex 1, 230 to 270 mesh, 10% divinyl benzene) in the chloride form were used. The average "wet" radius, based on photomicrographs of the beads, was  $3.5 \times 10^{-3}$  cm. About 15 mg of resin was equilibrated for a day with  $\text{Bi}^{207}$  in about

5 ml of 0.5 M hydrochloric acid to transfer most of the  $\text{Bi}^{207}$  as a  $\text{Bi}(\text{III})$  chloride complex to the resin phase. The beads were placed in a small column ( $0.12 \text{ cm}^2 \times 0.1 \text{ cm}$ ) and then eluted rapidly with 0.5 M hydrochloric acid. The decrease in the counting rate of the small resin bed under conditions of rapid flow was followed with an NaI crystal counter biased at 380 kev. Typical results are shown in Fig. 1, in which it may be seen that the counting rate of the resin decreases about 17% during the period of rapid flow (16.7 cm/sec) and then increases to a new equilibrium value when the flow is stopped. Most of the observed decrease is associated with the removal of  $\text{Pb}^{207m}$  from the resin into the flowing liquid during the short interval between production and decay. The new equilibrium value of the counting rate observed on stopping the flow is 5% less than the original, indicating that 5% of the  $\text{Bi}^{207}$  had diffused out during the run and that  $\text{Bi}(\text{III})$  diffuses relatively more slowly than the  $\text{Pb}^{207m}$  species.

From the decay scheme it can be estimated that approximately 93% of the gamma counting rate of  $\text{Bi}^{207}$  in an NaI crystal biased at 380 kev is associated with the isomeric state, while the remaining 7% is associated with the prompt

<sup>1</sup>Chemistry Division.

<sup>2</sup>E. C. Campbell and F. Nelson, *Phys. Quar. Prog. Rep. Dec. 20, 1952*, ORNL-1496, p 8, and *Phys. Rev.* 91, 499 (1953).

<sup>3</sup>E. C. Campbell, *Phys. Semiann. Prog. Rep. Sept. 10, 1953*, ORNL-1620, p 14.

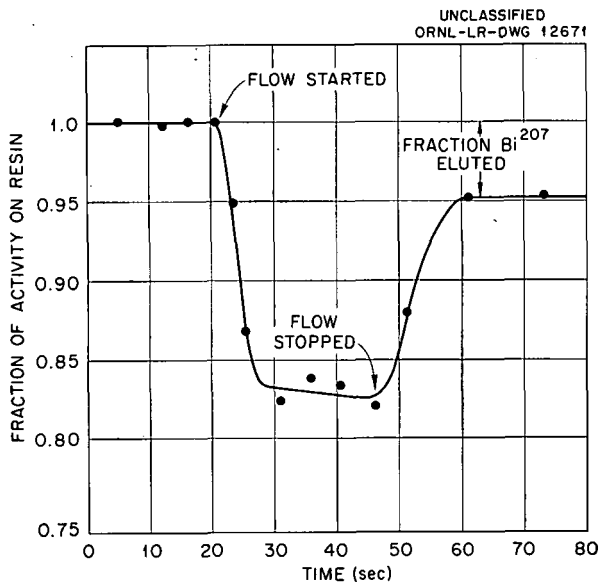


Fig. 1. Counting Rate of Anion-Exchange Resin Containing Bi<sup>207</sup> Under Conditions of Fast Liquid Flow and of No Flow. The drop in counting rate is associated with diffusion from the resin beads of the 0.8-sec Pb<sup>207m</sup> formed in the decay of Bi<sup>207</sup>. The Pb<sup>207m</sup> is transported downstream by the liquid flow.

transition to the stable ground state of Pb<sup>207</sup>. The actual yield, defined as the fraction of the Pb<sup>207m</sup> produced which decays outside the resin, is therefore somewhat larger than the percentage decrease in the counting rate by the ratio 1/0.93. This gives a yield of 18.3%.

It is evident that the yield of the process depends on the relative magnitudes of the rate of diffusion of the Pb<sup>207m</sup> from the resin and of its rate of decay. The yield can be calculated on the basis of a simple diffusion model. It is assumed that the Pb<sup>207m</sup> is produced uniformly at a rate  $Q$  per unit volume throughout a resin sphere of radius  $R$ . The flow rate of the liquid is assumed to be rapid enough that all Pb<sup>207m</sup> which diffuses out of the resin sphere is very quickly washed downstream. The boundary condition on the concentration of diffusing species  $\Phi(r)$  is  $\Phi(R) = 0$ . The diffusion equation may be written

$$D \nabla^2 \Phi(r) + \lambda \Phi = Q, \quad r \leq R,$$

where  $D$  is the diffusion coefficient of Pb<sup>207m</sup> inside the resin sphere and  $\lambda$  is the radioactive decay constant of the Pb<sup>207m</sup>. A solution satisfying the boundary condition is

$$\Phi(r) = \frac{Q}{\lambda} \left[ 1 - \frac{R \sinh \sqrt{(\lambda/D)} r}{r \sinh \sqrt{(\lambda/D)} R} \right].$$

The yield  $Y$  as previously defined is given by

$$Y(u) = \frac{4\pi R^2 [-D(d\Phi/dr)]_{r=R}}{(4/3)\pi R^3 Q} = \frac{3}{u^2} (u \coth u - 1),$$

where  $u = \sqrt{(\lambda/D)} R$ . The function  $Y(u)$  is plotted in Fig. 2. For  $u \gg 1$  (small yield)  $Y(u) = 3/u$ .

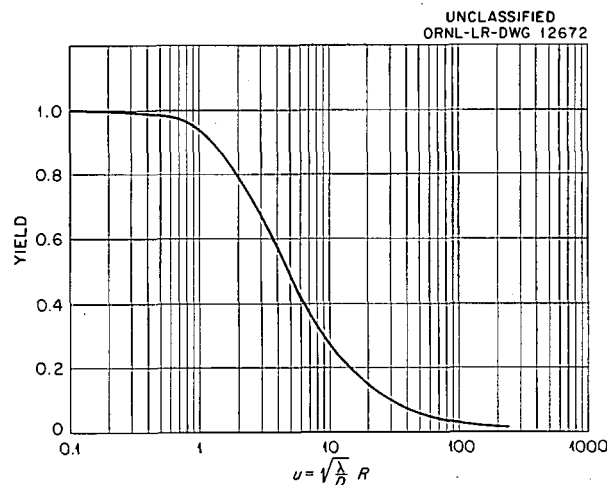


Fig. 2. Theoretical Yield  $Y(u)$  for Ion-Exchange Separation of Diffusing Radioactive Species (Decay Constant  $\lambda$ ) from Single Resin Sphere (Radius  $R$ ) with Diffusion Coefficient  $D$  Under Conditions of Rapid Flow.  $Y(u)$  is plotted as a function of the dimensionless parameter  $u = \sqrt{\frac{\lambda}{D}} R$ .

The theoretical yield for the separation may be calculated if the diffusion coefficient,  $D$ , of the Pb<sup>207m</sup> species formed in the resin phase is known. Since Pb(II) is the more stable oxidation state of lead, it is reasonable to assume that Pb(II) (chloride complexes) is formed in the resin on decay of Bi<sup>207</sup>. Separate elution experiments were therefore carried out to determine the rate of diffusion of Pb(II) in the same resin with separated Pb<sup>210</sup> (22-year RaD) being used as tracer. Daughter Bi<sup>210</sup> activity was first removed from the Pb<sup>210</sup> tracer, by anion-exchange methods described earlier,<sup>4</sup> and the purified Pb<sup>210</sup> in

<sup>4</sup>F. Nelson and K. A. Kraus, *J. Am. Chem. Soc.* 76, 5916 (1954).

0.5 M HCl was equilibrated with resin for several hours before carrying out rapid-elution experiments. The results of a typical elution experiment with  $Pb^{210}$  are shown in Fig. 3. It can be seen that the plot of log counting rate of the resin corrected for room background and a small  $Bi^{210}$  background vs time is approximately linear. The average half time for removal from three separate experiments was  $11.0 \pm 0.3$  sec. According to diffusion theory, the concentration of diffusing species in the resin decreases as  $e^{-\lambda_r t}$ , where  $\lambda_r = D\pi^2/R^2$ , after an initial transient effect associated with the decay of higher diffusion modes has died out. From the slope of the curve of Fig. 3,  $\lambda_r$  was calculated to be  $0.063 \text{ sec}^{-1}$ , corresponding to a diffusion coefficient,  $D$ , of  $Pb(II)$  in the resin of  $7.8 \times 10^{-8} \text{ cm}^2/\text{sec}$ . From  $u = \sqrt{(\lambda/D)} R$ , the decay constant for  $Pb^{207m}$ ,  $\lambda = 0.845 \text{ sec}$ , and  $R = 3.5 \times 10^{-3} \text{ cm}$ , a value  $u = 12.1$  is calculated. The yield corresponding to  $u = 12.1$  (Fig. 2) is 22.7%. The observed experimental yield of 18.3% is in fair agreement with this value. The discrepancy might be associated with the formation to some extent of a different lead oxidation state or metastable chemical species of  $Pb(II)$  which diffuses out of the resin more slowly. Lead(IV), for example, if formed initially in the decay process, might be expected to be more difficult to remove, since it absorbs strongly<sup>5</sup> from hydrochloric acid solutions.

From these results the conclusion can be drawn that ion-exchange separation of daughter activities

<sup>5</sup>Unpublished results, F. Nelson and K. A. Kraus.

having half lives even of the order of milliseconds should be possible by the present techniques.

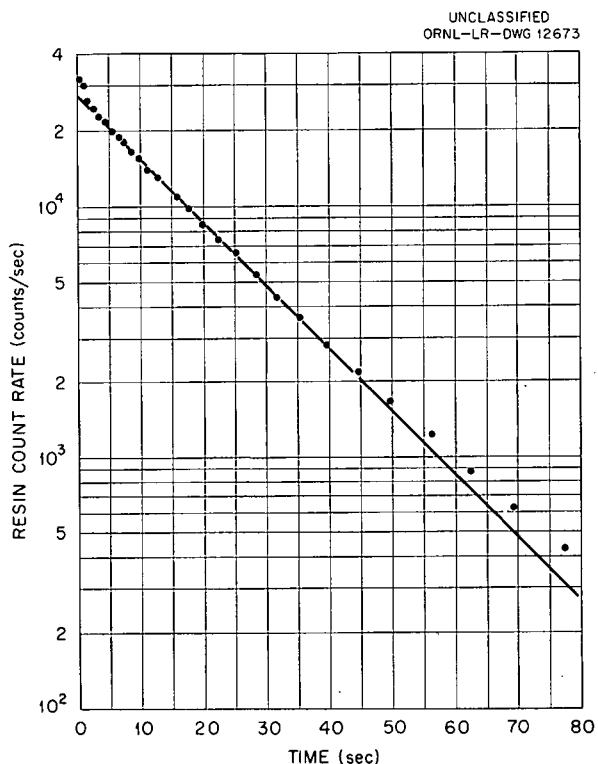


Fig. 3. Counting Rate of Resin Containing  $Pb^{210}$  (22-year RaD) in Rapid Elution Experiment (0.5 M HCl, Flow Rate 4.4 cm/sec). The decrease in counting rate is due to diffusion of  $Pb^{210}$  from the resin and subsequent removal by the liquid flow. The half time for removal was  $11.0 \pm 0.3$  sec. (Note - This is not a radioactive-decay curve.)

## EXTENSION OF PEAK EFFICIENCY OF 3 × 3 in. NaI(Tl) TO HIGH ENERGIES

N. H. Lazar

H. B. Willard

In order to determine the peak efficiency of the 3 × 3 in. NaI(Tl) crystals to 7.5 Mev, a number of gamma rays have been observed in reactions of nuclei with protons produced in the 5.5-Mv Van de Graaff generator. The ratio of the area under the full-energy peak to the total area was determined from these spectra, and this factor, when multiplied by the theoretically evaluated total efficiency, yields the peak efficiency.<sup>1</sup> Thus it was necessary to find reactions in which, primarily, only one gamma ray is obtained. The crystal, for these measurements, was placed at 90 deg to the incident beam, and essentially all scattering material was removed from its vicinity. Most of the targets were mounted on a tantalum backing, and the background was obtained with a clean tantalum foil of the same thickness, in the place of the target. Bremsstrahlung and coulomb-excited gamma rays from the tantalum were observed at low energies, and thus none of the

spectra obtained were due to the "pure" high-energy spectrum. In many instances, other peaks also appear at low energy, and they tend to distort the spectrum. These were neglected, and an arbitrary line was extrapolated down to zero energy for the determination of peak area to total area. However, excellent agreement with the previously obtained curve of peak efficiency vs energy was obtained for two gamma rays at 1.78 and 2.14 Mev (Table 1), and thus the higher energy values are probably not too badly in error. However, it is difficult to place numerical limits of uncertainty on the computed values, since they depend so severely on the extrapolation of the curve to zero energy and on possible scattering from the "snout" of the beam tube.

Figures 1 through 4 show the gamma-ray spectra obtained with a 3 × 3 in. NaI(Tl) cylinder at 9.3 cm from the targets for the reactions  $\text{Si}^{28}(p,p')\text{Si}^{28*}$ ,  $\text{Be}^9(p,\alpha)\text{Li}^6$ ,  $\text{N}^{15}(p,\alpha)\text{C}^{12}$ , and  $\text{Be}^9(p,\gamma)\text{B}^{10}$ , respectively. The results of the evaluation of peak area to total area are given in Table 1, together with the peak efficiency.

<sup>1</sup>N. H. Lazar, R. C. Davis, and P. R. Bell, *Phys. Semiann. Prog. Rep. Sept. 10, 1955*, ORNL-1975, p 72.

TABLE 1. RESULTS OF PEAK-EFFICIENCY DETERMINATIONS FOR HIGH-ENERGY GAMMA RAYS WITH 3 × 3 in. NaI(Tl) CRYSTAL

Gamma-Ray Energy (Mev)	Peak Area Total Area	Peak Efficiency, $\epsilon_p$	Reaction
1.78	0.298	0.136	$\text{Si}^{28}(p,p')\text{Si}^{28*}$
2.14	0.256	0.112	$\text{B}^{11}(p,p')\text{B}^{11*}$
3.57	0.140	0.056	$\text{Be}^9(p,\alpha)\text{Li}^6*$
4.43	0.107	0.043	$\text{N}^{15}(p,\alpha)\text{C}^{12*}$
7.48	0.062	0.025	$\text{Be}^9(p,\gamma)\text{B}^{10*}$

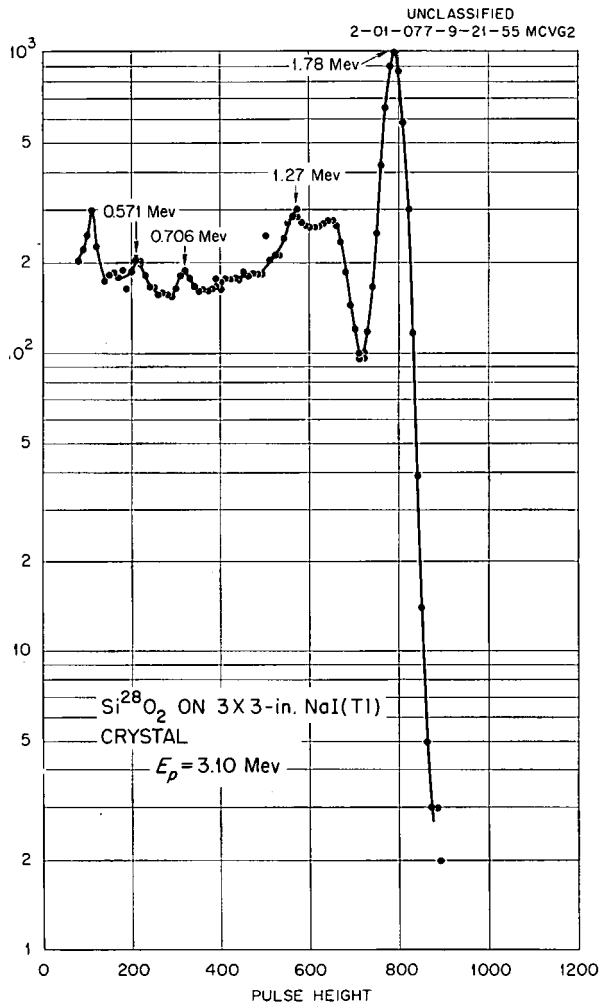


Fig. 1. Pulse-Height Spectrum of Gamma Rays from  $Si^{28}(p,p')Si^{28+}$  Reaction.

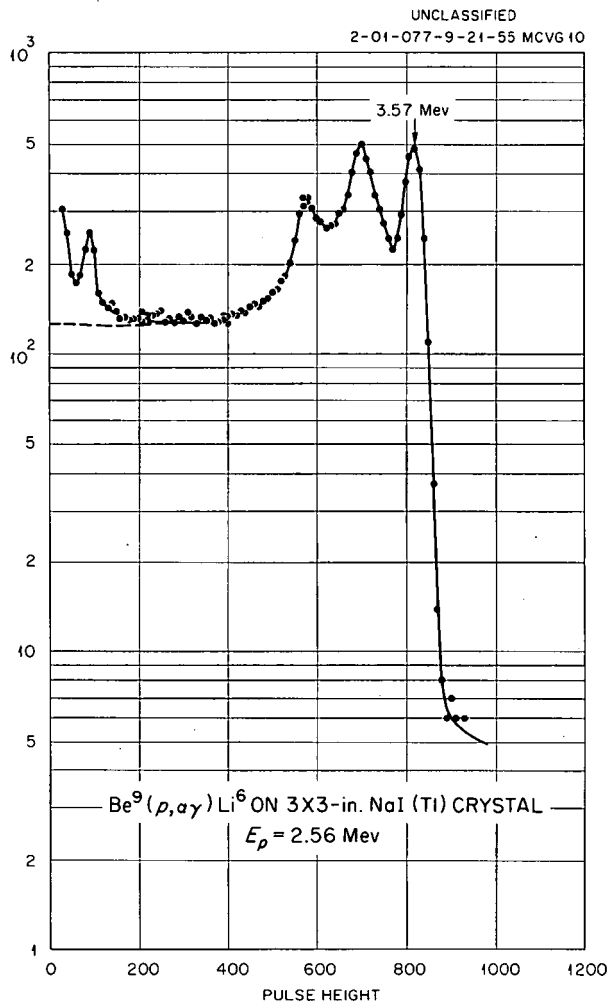


Fig. 2. Pulse-Height Spectrum of Gamma Rays from  $Be^9(p,\alpha\gamma)Li^6$  Reaction.

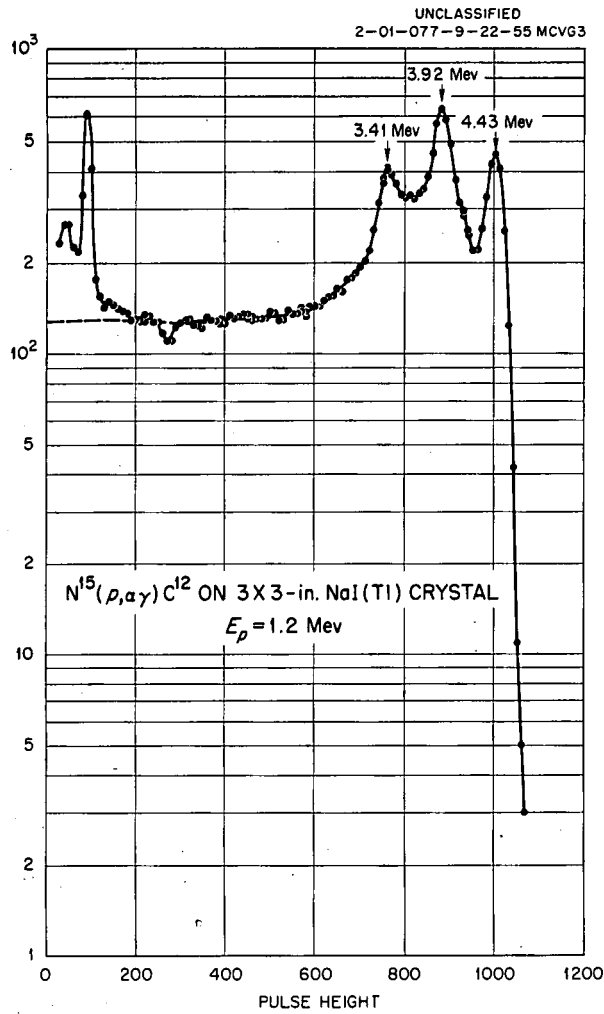


Fig. 3. Pulse-Height Spectrum of Gamma Rays from  $N^{15}(p, \alpha)\gamma C^{12}$  Reaction.

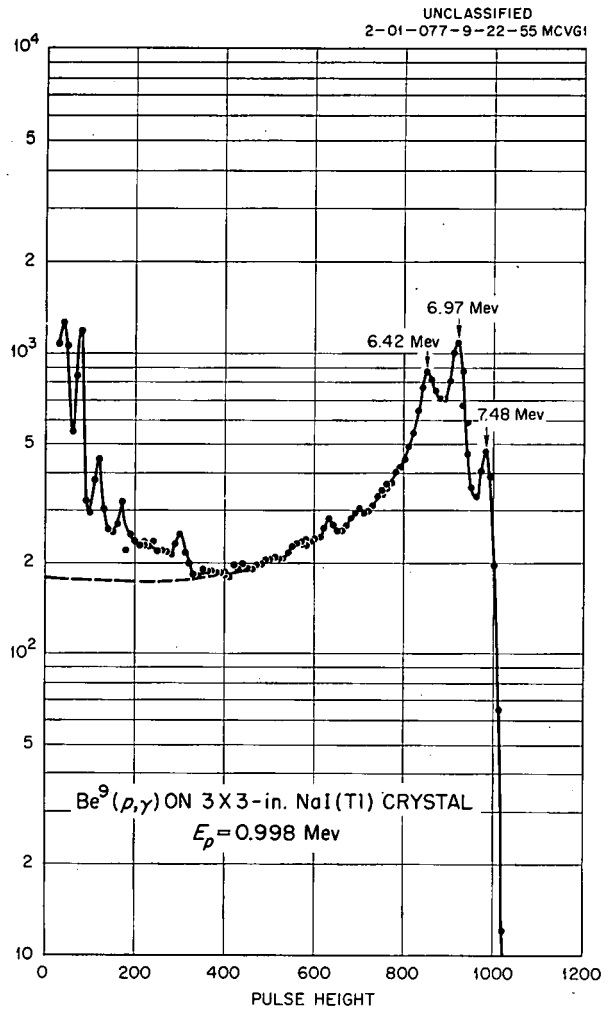


Fig. 4. Pulse-Height Spectrum of Gamma Rays from  $Be^9(p, \gamma)B^{10}$  Reaction.

## TRANSMISSION CHARACTERISTICS OF LIGHT PIPERS

C. C. Harris

P. R. Bell

## INTRODUCTION

In order to understand better the fundamental factors involved in the transmission of light from Lucite light pipers, some investigations into their properties have been carried out. The results of these investigations have stimulated interest in several other aspects of the problem, and these are being pursued.

## EXPERIMENTAL EQUIPMENT AND METHODS

The light sources for the transmission measurement were the scintillations in NaI(Tl) in response to the 661-keV gamma rays of  $\text{Cs}^{137}$ . Two  $\frac{1}{2}$ -in.-thick crystals sealed in aluminum-glass cans were used. The diameters of the crystals are  $1\frac{1}{4}$  and  $\frac{1}{2}$  in.

The Lucite for the experiments was selected from a large stock of "optical-grade Lucite, non-ultraviolet-absorbing," and only one rod was deemed of sufficient whiteness for use. The majority of the stock was definitely greenish in color. From the accepted stock, a highly polished cylinder, 3 in. in diameter and 20 in. long, was made. It was on this large piper that the majority of reflector tests were made. Following those tests, the smaller pipers,  $1\frac{1}{4}$  and  $\frac{1}{2}$  in. in diameter, were made from the big cylinder. The coupling sections described later were made from similar stock that was the nearest in quality to the stock selected for the pipers.

One photomultiplier was used for all the experiments. A Du Mont 6363 3-in. photomultiplier was selected for resolution, photosensitivity, and uniformity of photocathode. It was oriented with respect to the magnetic field of the earth, and the focus-plate potential was adjusted to secure the most uniform response as the  $1\frac{1}{4}$ -in.-dia crystal was coupled to various areas of the photocathode.

Relative transmissions were obtained by comparing the pulse height yielded by a crystal-piper combination with that yielded by the crystal coupled directly to the phototube. The pulse heights were measured with an MC3 multichannel pulse-height analyzer. In that manner comparative resolutions could also be determined. The high-voltage supply for the photomultiplier was moni-

tored with a potentiometer and checked at every measurement.

The dry reflectors chosen for study were the specular and diffuse sides of 0.0005-in. aluminum foil, an  $\alpha$ -alumina-sodium silicate spray paint, and the specular and diffuse sides of 0.0002-in. aluminum foil. (The 0.0002-in. foil is from a special roll and has been the reflectivity standard for our group for some time.) In addition, special tests were run on Tygon paint and foil reflectors optically coupled to the pipers with Dow-Corning silicone oil DC-200 and with Del cement, grade B-95 (David E. Long Corp., New York). Tests were also made with black paper over the piper or coupler, instead of a reflector.

Certain curved coupling devices were used and may be seen in Fig. 1. The largest was designed so that the angle of any light ray from the crystal strikes the wall of the coupler at an angle less than the critical angle of reflection. Its profile approximates a section of a logarithmic spiral. The other large-diameter coupler has straight walls slightly less steep than the critical angle. For the  $1\frac{1}{4}$ -in.-dia piper a paraboloid was constructed so that the crystal is coupled on in the plate of the *latus rectum*. A similar paraboloid section was made on the end of several  $\frac{1}{2}$ -in.-dia pipers.

The coupling medium used in the majority of the cases was DC-200 silicone oil, except where mineral oil was used to join sections of piper to each other.

## DISCUSSION OF RESULTS

Some of the properties of the critical-angle couplers used may be seen in Fig. 2. It is to be noted that they are of no particular value as crystal-to-phototube couplers, and it is also to be noted that the use of various reflectors does not vary their transmission greatly. The improvement when using a reflector is perhaps due to increased chances of recapturing the light which initially reflects from the coupler-tube or the coupler-piper interface. The best reflector tested was the sprayed  $\alpha$ -alumina paint, perhaps because of its diffuse nature, but more probably because it is by far the brightest of the reflectors used.

However, Figs. 3 and 4 show the improvement in the transmission of a long piper due to using the coupler. These figures show that use of a coupler minimizes the difference in reflector, if wall polish is very good. Further experimentation is planned to determine quantitatively the effect of wall polish in these cases. It may also be seen that the specular side of 0.0005-in. aluminum foil, which gives the best transmission when dry, is very poor when optically coupled to the wall of the piper. Figure 3 gives also a direct comparison of several reflectors. Figure 5 shows the poor reflectivity of Tygon paint for the scintillations of sodium iodide. In addition, a 6-in.-long by 1/2-in.-dia light piper was wrapped in specular 0.0005-in. aluminum foil, which was coupled to the piper by Del cement, grade B-95. The relative transmission of such a piper was 12% compared with 52% when the reflector was the same foil, dry wrapped.

When the piper was cut down to 1 1/4-in. in diameter, it was found that the parabolic coupler caused a significant increase in transmission, as is seen in Fig. 6.

The data of Fig. 7 were obtained by three matched pairs of 1/2-in.-dia pipers, 2, 6, and 12 in. long. One piper of each pair was necked down on one

end, as is seen in the smallest object in Fig. 1. The space around the paraboloid and the unused face of the crystal were packed with  $\alpha$ -alumina. It was hoped that the coupling section would increase the transmission, but it appears that such improvement would occur at greater lengths only. Experimentation is continuing in this case in an attempt to improve the response of probing medical counters.

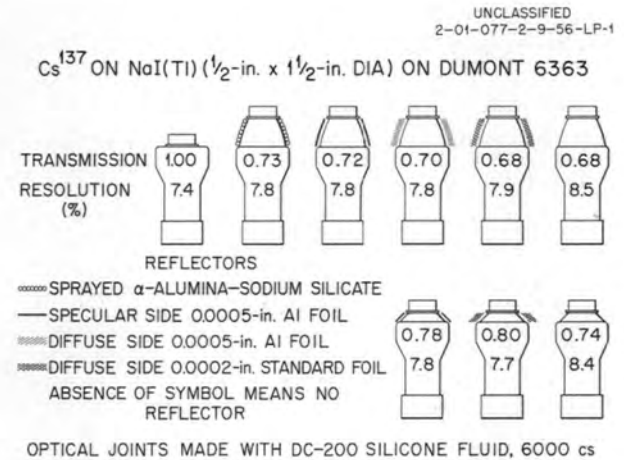


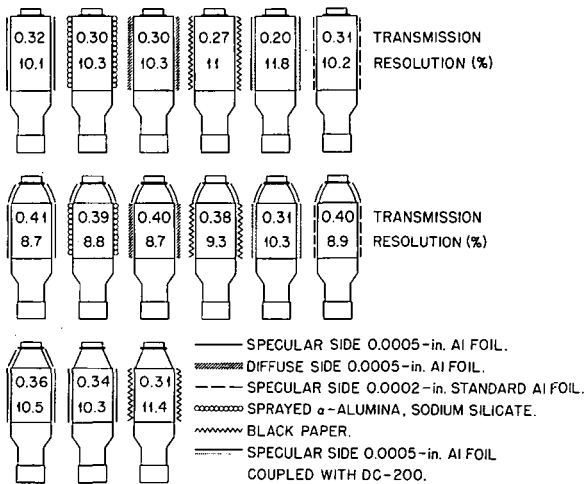
Fig. 2. Relative Transmission and Resolution for Two Critical-Angle Light Pipers.



Fig. 1. Coupling Devices.

PHYSICS PROGRESS REPORT

UNCLASSIFIED  
2-01-077-2-14-56-LP-2



REFERENCE RESOLUTION, CRYSTAL ON TUBE, 7.4%  $Cs^{137}$  ON NaI(Tl) ( $\frac{1}{2}$ -in. x  $\frac{1}{2}$ -in.-DIA) ON DUMONT 6363. OPTICAL JOINTS MADE WITH DC-200.

Fig. 3. Relative Transmission and Resolution for a 3-in.-dia, 20-in.-long Lucite Light Piper, with and without Critical-Angle Couplers with Various Piper Reflectors.

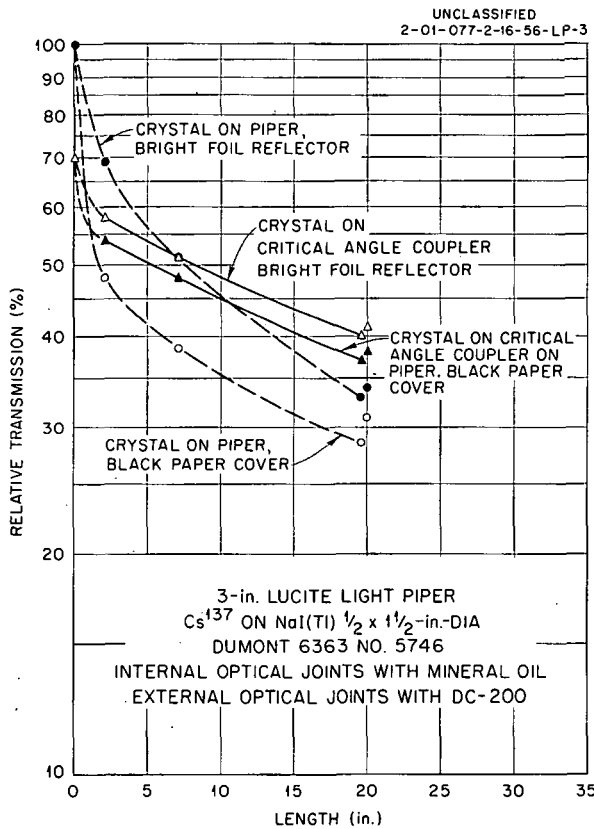


Fig. 4. Relative Transmission vs Piper Length for a 3-in. Lucite Light Piper.

UNCLASSIFIED  
2-01-077-2-16-56-LP-4

$Cs^{137}$  ON NaI(Tl) ON DUMONT 6363.  
REFERENCE: CRYSTAL ON TUBE FACE.

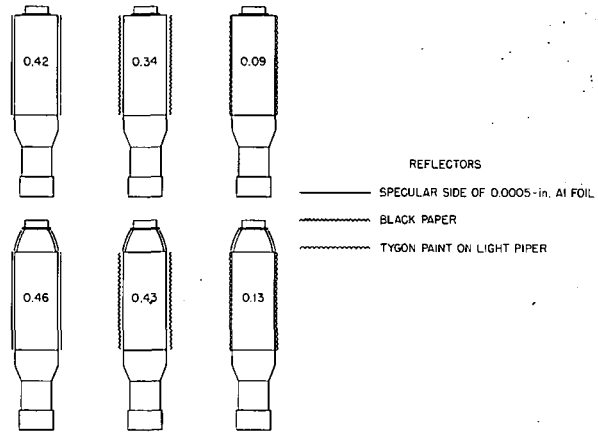


Fig. 5. Relative Transmission of a 3-in.-dia, 12-in.-long Lucite Light Piper.

UNCLASSIFIED  
2-01-077-2-20-56-LP-5

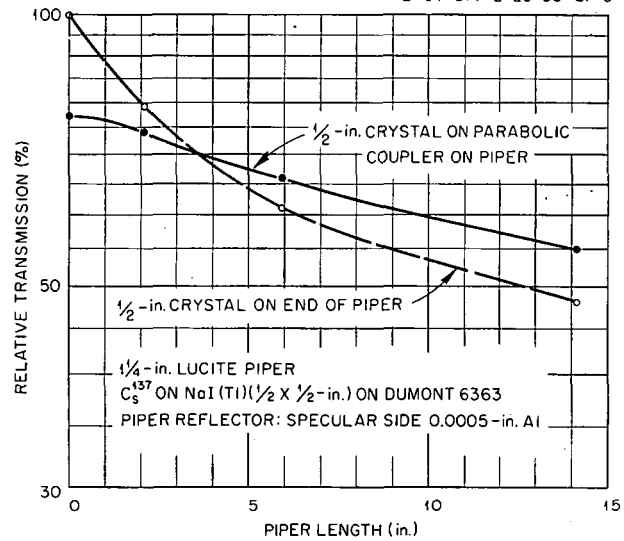


Fig. 6. Relative Transmission vs Piper Length for a 1 1/2-in.-dia Lucite Piper.

CONCLUSIONS

On the basis of experimental evidence so far, it is believed that the following conclusions may be drawn:

1. For long pipers, where a piper larger than the crystal may be used, a coupling section (log spiral or parabolic) improves transmission and lowers the apparent attenuation. The attenuation approaches exponential only with great piper length

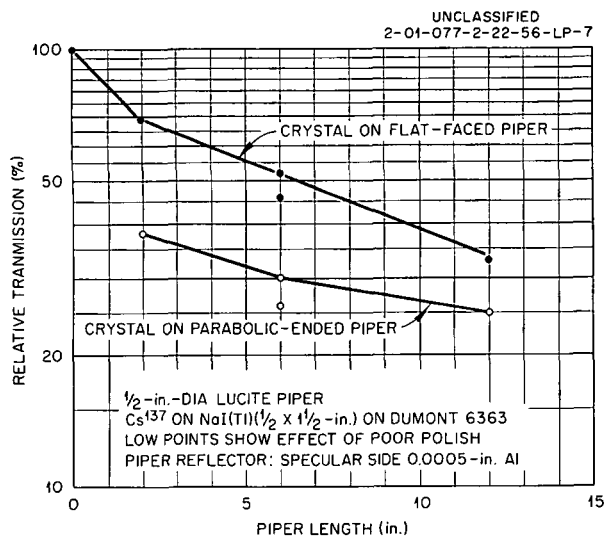


Fig. 7. Relative Transmission vs Piper Length for a 1/2-in.-dia Lucite Piper.

and does not appear wholly due to absorption in the Lucite.

2. The polish of the side walls of the piper should be as nearly perfect as possible.

3. If the polish is good and a coupling section is used, then dry reflectors, from the best to the poorest, make little difference in transmission.

4. The reflector for the coupling section makes little difference, from best to none. The best tested was  $\alpha$ -alumina paint, with specular foil nearly as good.

5. For the side reflector, specular foil appears best, but the diffuse side of foil, because of its brightness, is nearly as good. Optically coupled foil and Tygon paint are very poor. (Accidental coupling of foil at the ends due to coupling medium running in between foil and piper can decrease transmission greatly.)

6. The smaller diameter pipers appear to be extremely critical of surface polish and reflector. The length-to-diameter ratio is probably important here.

### ELECTROSTATIC LENS FOR THE 3-Mv VAN de GRAAFF

C. H. Johnson

J. P. Judish

An electrostatic lens incorporating a unipotential lens has been installed at the high-voltage terminal of the 3-Mv Van de Graaff to reduce magnification and aberrations. The unipotential lens was designed by Parker and King<sup>1</sup> for a pulsed source. It was chosen for low aberrations from the data of Liebmann<sup>2</sup> and is used for focusing with and without beam pulsing.

Figure 1 is the compound lens. Ions from the source canal are focused by the unipotential lens into the field produced by the main lens voltage  $V_1$  across the gap  $K_1$ . An image is formed in the field region for all  $V_1$ . This image is the object for the lens at the accelerator tube entrance.

A beam envelope is drawn nearly to scale in Fig. 1 to illustrate the lens action.

The condition for focus of a beam beyond the tube exit may be written as  $L_2 = L_2(P_2, K_2, D_2, N_2)$ , where

- $L_2$  = distance from the tube exit to target,
- $P_2$  = distance from object to tube entrance,
- $K_2$  = tube length,
- $D_2$  = tube diameter at entrance,
- $N_2$  = ratio of ion energies at entrance and exit to tube.

Here  $P_2 = 8.7$  in. and  $K_2 = 57$  in. One finds from explicit formulas by Elkind<sup>3</sup> that at  $L_2 = 100$  and 150 in.,  $N_2 = 52$  and 49, respectively. At a fixed unipotential and probe voltage, the main lens voltage was varied to focus at  $L_2 = 100$  and 150 in. for several accelerator voltages. Figure 2 shows

<sup>1</sup>V. E. Parker and R. F. King, *Phys. Semiann. Prog. Rep. Sept. 10, 1955, ORNL-1975*, p 65.

<sup>2</sup>G. Liebmann, *Proc. Phys. Soc.* 62B, 213 (1949).

<sup>3</sup>M. M. Elkind, *Rev. Sci. Instr.* 24, 129 (1953).

UNCLASSIFIED  
ORNL-LR-DWG 12678

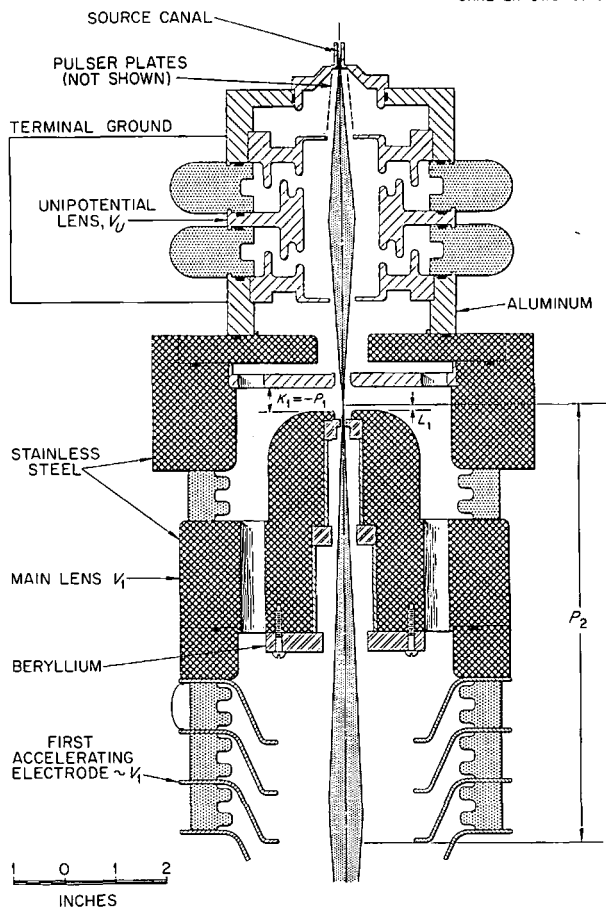


Fig. 1. Electrostatic Lens Assembly for 3-Mv Van de Graaff. The beam envelope illustrates how ions from the source canal are focused by the unipotential lens into the field region across  $K_1$  and thence are accelerated into the accelerator tube. The unipotential lens voltage  $V_u$  is proportional to probe voltage, and the main lens voltage  $V_1$  is proportional to accelerator tube voltage. The assembly is stainless steel with a beryllium liner to minimize x rays. The positions of deflector plates for beam pulsing are indicated.

the observed focus conditions; the  $N_2$  ratios for the two curves are 49 and 45 and are in good agreement with theory.

An iris diaphragm was placed at  $L_2 = 150$  in., and the focused beam transmitted to a Faraday cup was measured as a function of aperture diameter at several accelerating voltages from 0.38 to 2.47 Mv. Figure 3 shows these data.

UNCLASSIFIED  
ORNL-LR-DWG 12674

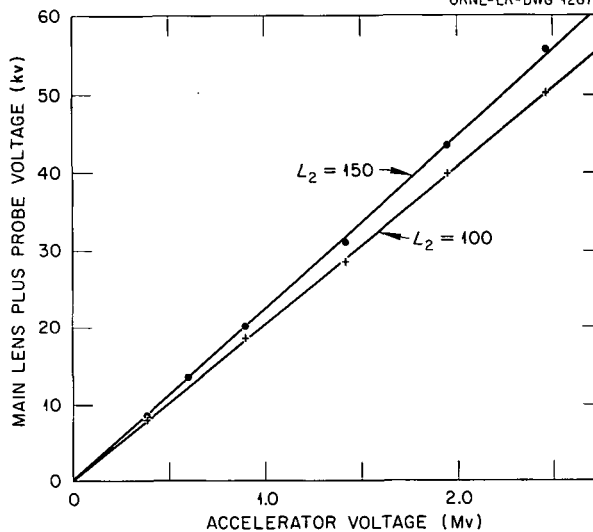


Fig. 2. The Main Lens Plus Probe Voltage for Focus at Two Target Distances vs Accelerator Tube Voltage. The ratios of the voltages for the two curves are constants and agree in absolute value with the theory.

The 90% line in Fig. 3 gives the beam diameters for 90% transmission. The over-all magnification was defined arbitrarily as the ratio of the diameter for 90% transmission to nine-tenths of the source-canal diameter ( $0.9 \times 0.04$  in.). Figure 4 is the magnification thus defined as a function of the accelerator voltage. The unipotential lens has magnification near unity, and the tube magnification for  $L_2 = 150$  in. is 5.8 according to Elkind. The fact that the observed magnification is generally less than  $1 \times 5.8$  probably results from a converging action at the entrance to the field across  $K_1$ . The magnification produced by this converging lens was calculated by assuming that the unipotential lens image was at the lower end of  $K_1$ . The final over-all magnification was multiplied by an arbitrary factor (2.25) in Fig. 4 to illustrate the agreement in energy dependence of this curve with experiment.

The discrepancy in magnitude is attributed to aberrations which must be present, even though the lenses were chosen for small aberrations. The magnification appears to increase with the age of the ion source; this probably results from a more divergent beam and greater aberrations. Used ion sources have a silicate deposit on the wall of the source canal, which could become charged and cause large beam divergence.

An additional feature of this lens is its construction of stainless steel with a beryllium "cone" to stop back-streaming electrons. The

x-ray background is about 50 times less with this structure than with the previous all-aluminum lens. The Van de Graaff has operated momentarily with an analyzed 3.5-Mev proton beam. This increase in voltage is attributed partly to the reduction in x rays and partly to the refinished interior wall of the Van de Graaff tank.

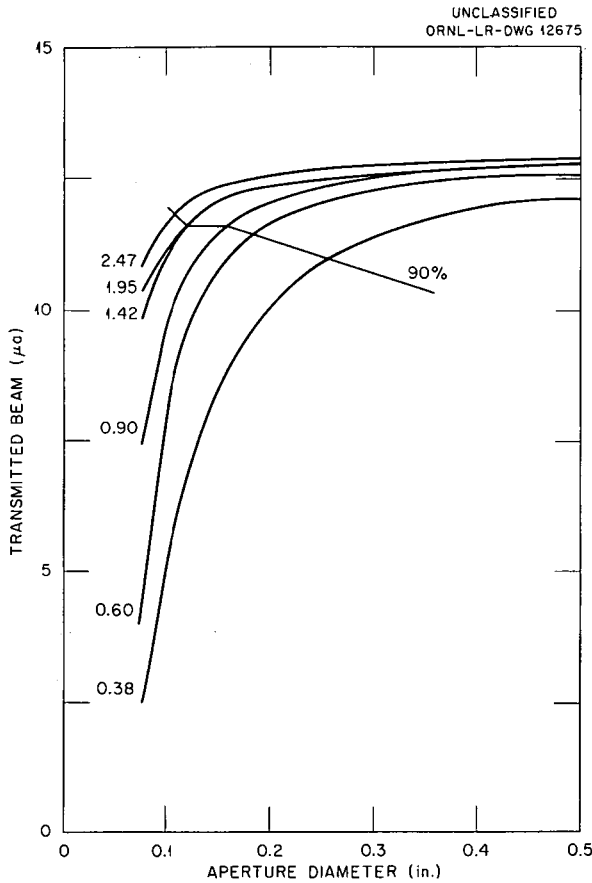


Fig. 3. The Beam Transmitted Through an Aperture Placed 150 in. from the Tube Exit vs Aperture Diameter for Accelerator Tube Voltage from 0.38 to 2.47 Mv. The 90% line indicates the diameter for transmission of 90% of the total beam.

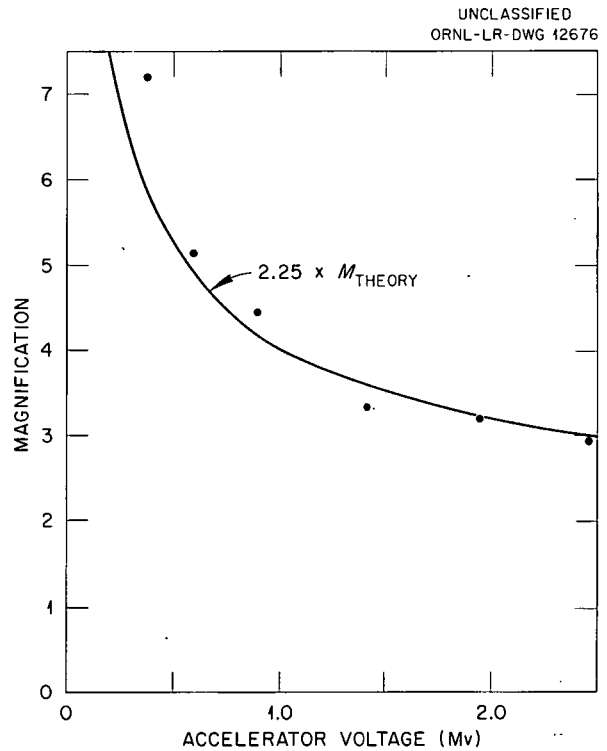


Fig. 4. Magnification vs Accelerator Voltage. Magnification is arbitrarily defined as the ratio of beam diameter for 90% of the beam to nine-tenths of the source-canal diameter. The theoretical curve gives the correct energy dependence but must be multiplied by 2.25 to agree in absolute value.

LIFE TESTS OF FILAMENTARY SUBMINIATURE TUBES

C. C. Harris

P. R. Bell

Life tests have begun to show definite indications of the optimum filament voltage of filamentary subminiature tubes at given emission currents.

Three tests are in operation. The first consists of 192 CK5854's in scalars, 22 CK5854's as register amplifiers, and 22 1AG4's as interrogated scaler drivers. These have operated for approximately 7500 hr, and three CK5854's have failed. One of these failures was the low-emission failure of a register amplifier at about 300 hr. The second was a low-emission failure of a scaler tube at 6000 hr, and the third was the previously reported "whisker" failure.<sup>1</sup>

The second test, as previously reported,<sup>2</sup> consists of 50 nonselected CK5854's operating continuously conducting at scaler conditions (0.5-ma plate current). Although 25 tubes are being operated at a filament voltage of 1.25 v and 25 at 1.35 v, both groups are tested at 1.3 and 1.1 v. The amount of rise of plate voltage (see Fig. 1) as the filament voltage is reduced is a

<sup>1</sup>G. G. Kelley, P. R. Bell, and C. C. Harris, *Phys. Semiann. Prog. Rep. Sept. 10, 1955, ORNL-1975, p 102.*

<sup>2</sup>C. C. Harris, P. R. Bell, and G. G. Kelley, *Phys. Semiann. Prog. Rep. Sept. 10, 1955, ORNL-1975, p 103.*

UNCLASSIFIED  
2-01-077-LT-1

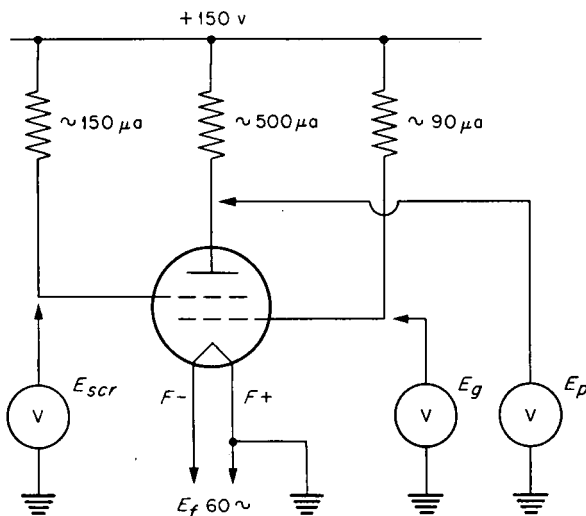


Fig. 1. Life-Test Conditions, 1AG4 and CK5854.

measure of the lack of emission reserve at the tube and of approaching failure. The amounts of adjustment made by grid and screen voltages are also valuable measures of tube quality and reserve. Figure 2 shows histograms of number of tubes vs plate voltage and shows the quality of each group at a normal and a reduced filament voltage. At

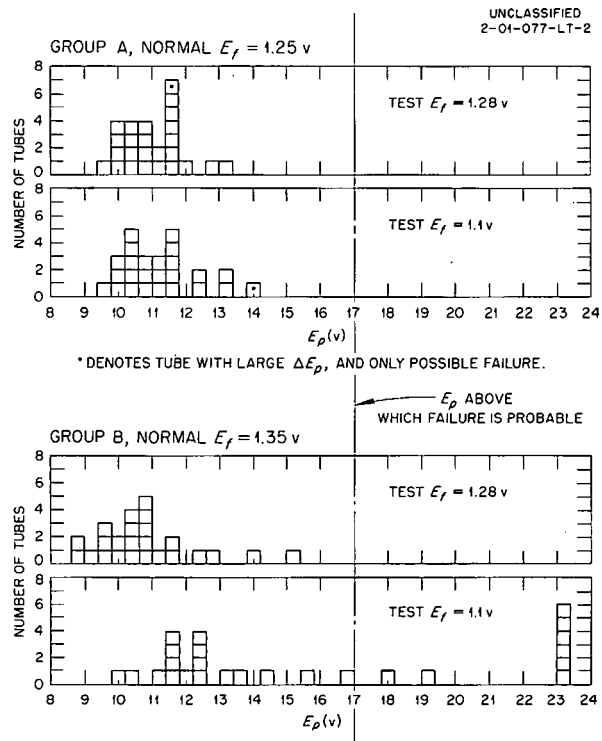


Fig. 2. Number of Tubes vs  $E_p$ , CK5854, 15,000 hr, Continuously On. Each block represents one tube.

15,000 hr and  $E_f = 1.3$  v, tubes in both groups are of sufficient quality to operate in scales of 16. The 1.25-v group shows only one possible failure at  $E_f = 1.1$  v, while the 1.35-v group shows eight probable and two possible failures. This would indicate that, for this particular emission current, longer life will be obtained at the lower filament voltage (1.25 v). This corroborates the tests and experiences of the manufacturer, which indicate that for each emission current there is an optimum filament voltage (higher than nominal voltage for

high emission and lower than nominal for low emission or cutoff conditions).

The optimum-filament-voltage evidence is strengthened greatly in the findings of the third test. One-hundred twenty nonselected 1AG4 type of tubes are on test at scaler conditions in groups of 40 at  $E_f = 1.3, 1.1,$  and  $1.2$  v. The group at  $1.2$  v was run for the first 6800 hr at  $0.9$  v. The tubes were tested for 10,700 hr at  $E_f = 1.2$  and  $0.96$  v (see Fig. 3). It is seen that the  $1.1$ -v group shows the best over-all group quality at  $1.2$  v and shows the least shift as the filament voltage is reduced to  $0.96$  v. Hence it may be concluded that, under these emission conditions,  $E_f = 1.1$  v is a better operating condition than  $E_f = 1.3$  v, and is slightly better than the  $0.9$  v for 6800 hr followed by  $1.2$  v for 4000 hr. An interesting point is that the histograms shown for 10,700 hr are almost identical to those for 8250 hr. This indicates that these tubes, especially the  $1.1$ -v group, will have exceedingly long life.

These results may be summarized as follows:

1. 214 CK5854's and 22 1AG4's operated for 7500 hr, with 3 failures: total, 2,760,000 tube hours.
2. 50 CK5854's operated for 15,000 hr, with no failures: total, 750,000 tube hours.
3. 120 1AG4's operated for 10,700 hr, with no failures: total, 1,274,000 tube hours; grand total, 4,780,000 tube hours with three failures, or 1,590,000 tube hours per failure.

Filamentary tubes of the miniature type 3A4, which are being used for register drivers, do not show these long-life qualities. Tube life of only 2000 hr is common. The causes are not yet known,

but cathode-interface faults are indicated, especially in view of the fact that this tube has a nickel filament — as contrasted with tungsten for the subminiatures — and is operated normally cut off. Investigation to determine how the life may be improved is being continued.

UNCLASSIFIED  
2-01-077-LT-3

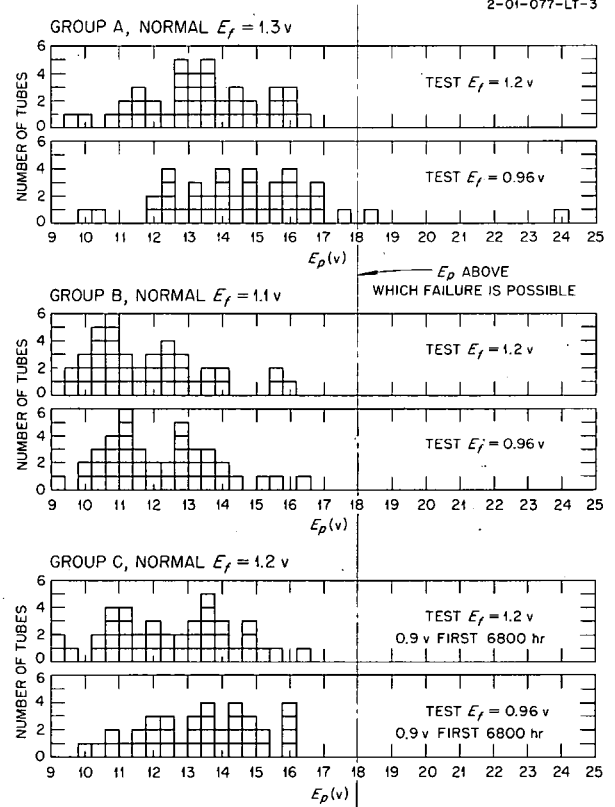


Fig. 3. Number of Tubes vs  $E_p$ , 1AG4, 10,700 hr at Scaler Conditions, 50% Plate Duty Cycle.